Universidade de Aveiro
Ano 2015

Departamento de Geociências

U.PORTO
FACULDADE DE CIÊNCIAS
UNIVERSIDADE DO PORTO

Departamento de Geociências, Ambiente eOrdenamento do Território

Frans Joost Michel Boogert

Avaliação da recuperação da vegetação após incêndio : um estudo de caso em Calde , região central de Portugal

Evaluation of vegetation recovery after fire: a case study in Calde, central region of Portugal

Universidade de Aveiro
Ano 2015

Departamento de Geociências

Departamento de Geociências, Ambiente eOrdenamento do Território

Frans Joost Michel Boogert

Avaliação da recuperação da vegetação após incêndio : um estudo de caso em Calde , região central de Portugal

Evaluation of vegetation recovery after fire: a case study in Calde, central region of Portugal

Dissertação apresentada à Universidade de Aveiro para cumprimento dos requisitos necessários à obtenção do grau de Mestre em Geomateriais e Recursos Geológicos realizada sob a orientação científica da Doutora Luísa Maria Gomes Pereira, Professora Coordenadora da Escola Superior de Tecnologia e Gestão de Águeda da Universidade de Aveiro e co-orientação do Doutor Jan Jacob Keizer, investigador do Centro de Estudos do Ambiente e do Mar (CESAM), do Departamento de Ambiente e Ordenamento da Universidade de Aveiro.

Tese desenvolvida no âmbito do projeto CASCADE "CASCADECAtastrophic Shifts in drylands: how CAn we prevent ecosystem DEgradation?" (Grant Agreement 283068), financiado pela União Europeia através do Sétimo Programa Quadro, Tema ENV.2011.2.1.4-2.

To Filipa and Félix without whom I would never have found the motivation to finish.

o júri

presidente

Prof. Doutor Fernando Almeida
Professor Associado da Universidade de Aveiro

Prof. Doutora Ana Cláudia Teodoro
Professora Auxiliar da Faculdade de Ciências da Universidade do Porto

Prof. Doutor José Alberto Gonçalves
Professor Auxiliar da Faculdade de Ciências da Universidade do Porto

Prof. Doutora Luísa Pereira
Professora Coordenadora da Escola Superior de Tecnologia e Gestão de Águeda da Universidade de Aveiro

Acknowledgements

Hereby I would like to express my thanks to my friends and colleagues from CESAM who have thought me a lot and have always been ready to help me, especially thanks to Martinho and Diana.

Other thanks go to my colleagues from GeoAtributo, Carlos and Andre, for their help with creating the orthophoto and their patience explaining me the processes involved.

In addition I would like to thank Luisa and Jacob for their expertise in Remote Sensing and Environmental sciences and guiding me, which I know must not have been easy.

Lastly I would like to thank my parents, Tin and Peter.
Because of them I learned to never do things the easy way
and their support means a lot to me.

palavras-chave

Deteção Remota; UAV; indíce de vegetação; recuperação; fogos florestais; monotorização.

resumo

A Deteção Remota tem sido utilizada durante décadas com novas aplicações a surgirem constantemente. Com este estudo pretende-se demonstrar o uso da Deteção Remota no campo da monotorização da recuperação de vegetação em áreas ardidas e o valor acrescentado da elevada resolução espacial dos dados utilizados. Para o efeito, foi feita a análise de áreas ardidas na freguesia de Calde, região central de Portugal, depois do incêndio florestal no verão de 2012, usando imagens *Landsat* 7 e 8 assim como uma ortofoto produzida com imagens adquiridas por um veículo aéreo não tripulado.

keywords

Remote Sensing; UAV; vegetation index; recovery; forest fires; monitoring.

abstract

Remote Sensing has been used for decades, and more and more applications are added to its repertoire. With this study we aim to show the use of Remote Sensing in the field of vegetation recovery monitoring in burned areas and the added value of data with a high spatial resolution. This was done by analysing both Landsat 7 and 8 scenes, after the forest fire of summer 2012 in the parish of Calde, in the central region of Portugal, as well as an orthophoto produced with images acquired by an unmanned aerial vehicle.

Contents

LIST OF FIGURES

LIST OF EQUATIONS

LIST OF TABLES

1. INTRODUCTION

This study was conducted within the framework of CASCADE (CAtastrophic Shifts in drylands: how CAn we prevent ecosystem DEgradation?) Project number: 283068 of the Seventh Framework Program. The project aims to understand sudden ecosystem shifts that can have a huge loss of biodiversity and ecosystem services as a consequence. One of the tools that has been proven its potential for retrieving vegetation properties at both global and local scale is Remote Sensing (MOUSIVAND, MENENTI, GORTE, & VERHOEF, 2015; VERSTRAETE, PINTY, & MYNENI, 1996).

Wildfires are a major agent of land degradation in the Mediterranean (SHAKESBY, 2011). The area that is burned yearly has been on average 100.000 ha in Portugal (MALVAR, PRATS, NUNES, & KEIZER, 2011). There has been a steady increase of wild fires in the past decades. One probable cause is the abandonment of agricultural land. The land is not cleared which leads to more fuel during the dry summer months (FAO, 2001).

With the objective of CASCADE being the detection of tipping points in ecosystems it has become of interest to monitor vegetation with several means. The project contemplates extensive field work, which is an intensive but reliable way of collecting data. Remote sensing might be an adequate alternative or complementary data collection tool to the field work as Landsat data are continuous and freely available through the United States Geological Survey (USGS). This study will explore the possibilities of vegetation monitoring for the Portuguese CASCADE study area, *Calde*, situated in the central region of Portugal.

This thesis addresses, in addition to the introduction, the state of the art of vegetation monitoring (section 2), the problem formulation, in section 3 that contains the statement of problem, the study area and data, the objectives and the resources in terms of software, the developed methodology to attain the objectives (section 4), with its implementation in section 5, the presentation and discussion of the results (section 6) and, in section 7, the conclusions. This thesis also contains 5 appendices with further information on data and methods and the bibliography.

2. STATE OF THE ART OF VEGETATION MONITORING.

This section contains a resume on vegetation indices and analysis techniques used in relation to vegetation recovery monitoring and burned vegetation. The list is in no way complete but mentions the most commonly used indices and techniques for these purposes.

2.1 VEGETATION INDICES

Remote Sensing and temporal analysis of vegetation have not always been common practice. With the development of planes and photographic cameras the term aerial photography was introduced. It was not until the 1960´s that the term Remote Sensing was coined as new technologies became available and the field became more professional. The first Remote Sensing satellites where launched in 1959 by the USA (United States of America) to spy on the Russians. As with most emerging technologies the first applications where military. Between the 1960's to 70's Remote Sensing shifted from air planes to satellites (FOWLER, 2013; KEVIN C. RUFFNER, 1995).

In 1972 Landsat 1 (ERTS-1) was launched and was described as the first step in merging space and Remote Sensing technologies for the monitoring and managing of earth's resources (WILLIAMS JR. & CARTER, 1976). From this moment on, the applications for Remote Sensing increased and, for example, monitoring of air pollution was introduced (BRIMBLECOMBE & DAVIES, 1978) and detecting and characterizing changes in vegetation has become more common (DEFRIES, HANSEN, TOWNSHEND, JANETOS, & LOVELAND, 2000).

On the moment of writing this thesis, the Landsat program has reached its 8th iteration and the applications vary from crop monitoring to disaster management. The most commonly stated advantage of Remote Sensing is the ability of collecting temporal measurements without the use of traditional field based methods. The application of Remote Sensing for forest and post-fire monitoring has been studied for some time and Remote Sensing is considered a useful tool to obtain temporal data for large extents of time and areas (CASADY & MARSH, 2010; RAVI, BADDOCK, ZOBECK, & HARTMAN, 2012; VAN LEEUWEN et al., 2010). Looking at the widespread use of Remote Sensing and the high temporal frequency with which measurements are taken it is clear its potential is great for monitoring.

In the area of vegetation monitoring countless measures, named indices, have been developed for different types of vegetation, diseases, fungi, stresses and sensors. For the

scope of the study only indices that can be applied to the Landsat 7 and 8 imagery have been considered.

One of the earliest developed indices is the simple ratio index. It was developed in 1968 to assess the color of growing turf and is thus the first described index for vegetation monitoring (BIRTH & MCVEY, 1968). The index is based on the red (630 to 690 nanometer) and the near infrared (770 to 900 nanometer) wavelengths. Equation 1 shows how the index is calculated, the bigger the difference between the near infrared and the red the bigger the SR value and the healthier the vegetation. From its introduction in 1968 the index has been used for many applications including biomass, chlorophyll content, green ratio, leaf area index, leaf mass per area, nitrogen content and phytomass estimations as well as for disease mapping and general vegetation monitoring purposes (CALDERÓN, NAVAS-CORTÉS, LUCENA, & ZARCO-TEJADA, 2013; EDIRIWEERA, PATHIRANA, DANAHER, & NICHOLS, 2014; LEMAIRE et al., 2008; O'CONNELL, BYRD, & KELLY, 2014; PINTY & VERSTRAETE, 1992; SIMS & GAMON, 2002; VESCOVO & GIANELLE, 2008; VINCINI, FRAZZI, & D'ALESSIO, 2006; XIAO, ZHAO, ZHOU, & GONG, 2014).

Equation 1: Simple ratio (BIRTH & MCVEY, 1968)

$$SR = \frac{NIR}{RED}$$

With the importance of the difference between the red and the near infrared, named the red edge, in vegetation monitoring recognized by scientists development started on new ways to use this information. In 1982 the difference vegetation index or DVI was introduced (WIEGAND & RICHARDSON, 1982). The DVI is solely based on the difference between the red and the near infrared wavelengths. The difference is calculated by deducting the red from the near infrared wavelength as shown in Equation 2. The range of DVI values for healthy vegetation falls between 2 to 8. The index has been used in cover estimation, leaf area index estimation and general vegetation monitoring (BAUGH & GROENEVELD, 2006; ELVIDGE & CHEN, 1995; WIEGAND & RICHARDSON, 1982).

Equation 2: Difference vegetation index (WIEGAND & RICHARDSON, 1982)

$$DVI = NIR - RED$$

Also based on the red edge is the most well-known index, the normalized difference vegetation index or NDVI. What makes the NDVI different from the SR and DVI is that it normalizes the difference between the red and the near infrared wavelength. This is

effectively done by combining the SR and DVI into Equation 3. The result gives NDVI values between -1 and 1. The greener the surface the higher the NDVI will be with healthy vegetation having values between 0.3 and 0.8 while bare soils have NDVI values between 0.2 and 0.3.With its earliest mention in 1974 the NDVI has been in use for 40 years (ROUSE, HAAS, SCHEEL, & DEERING, 1974) and is popular to this day. It´s most common application is vegetation monitoring and cover estimations (BARRY, STONE, & MOHAMMED, 2008; BAUGH & GROENEVELD, 2006; ELVIDGE & CHEN, 1995; GITELSON, KAUFMAN, STARK, & RUNDQUIST, 2002; GITELSON, 2004). In addition it has been used for plant health indicators like biomass, leaf area index, carotenoid content, chlorophyll content, nitrogen content, leaf water potential and stomatal conductance (BERJÓN, CACHORRO, ZARCO-TEJADA, & FRUTOS, 2013; NUMATA et al., 2007; PIMSTEIN, KARNIELI, BANSAL, & BONFIL, 2011; RAMA RAO, GARG, GHOSH, & DADHWAL, 2007; ZARCO-TEJADA et al., 2013). Other physical parameters have also been measured with the NDVI including tree height and crown volume (NUMATA et al., 2007; SCHLERF, ATZBERGER, & HILL, 2005). On top of all these vegetation properties the index has also been used for species distinction, disease mapping and burn severity estimations (CALDERÓN, MONTES-BORREGO, LANDA, NAVAS-CORTÉS, & ZARCO-TEJADA, 2014; EPTING, VERBYLA, & SORBEL, 2005; GALVÃO, FORMAGGIO, & TISOT, 2005). All these applications make it one of the most used and widely applied indices.

Equation 3: Normalized difference vegetation index (ROUSE et al., 1974)

$$NDVI = \frac{NIR - RED}{NIR + RED}$$

Shortly after the NDVI was introduced the green NDVI was developed. This variant on the NDVI is based on the same normalization principle but uses a green wavelength (520 to 600 nanometer) instead of the red one. This was done because green is more closely associated with chlorophyll content (DATT, 1999). This gives a different insight in the state of the vegetation in question. Because of this green NDVI is better known for its use in biomass estimations (EDIRIWEERA et al., 2014). Other chemically related uses are carotenoid, nitrogen, potassium and phosphorus content estimations (DATT, 1998; PIMSTEIN et al., 2011). On top of this the green NDVI is often used for cover and greenness estimations (GITELSON et al., 2002; VESCOVO & GIANELLE, 2008). Equation 4 shows how the green NDVI is calculated, just as the NDVI it has a range of -1 to 1 and the healthier the vegetation the higher the green NDVI value will be.

Equation 4: green normalized difference vegetation index (DATT, 1998)

$$NDVI(Green) = \frac{NIR - GREEN}{NIR + GREEN}$$

Aside from the NDVI based indices researchers found that the influence of the soil on vegetation indices was quite disturbing and thus somehow soil characteristics needed to be incorporated. With lower fractions of vegetation the soil characteristics become more prevalent and can obscure the vegetation characteristics that one wants to measure. In 1977 this led to the development of the perpendicular vegetation index (RICHARDSON & WEIGAND, 1977). The index is able to reduce the influence of bare soils by including a soil line. The soil line is a relationship between bare soil reflectance observed in two different bands (BARET, JACQUEMOUD, & HANOCQ, 1993) in this case between the red and near infrared. Equation 5 shows the calculations where *a* is the slope of the soil line and *b* is the offset of the soil line. After its introduction in 1977, the index has been used to estimate cover percentages and leaf area index (ELVIDGE & CHEN, 1995) as well as crown volume (SCHLERF et al., 2005) and nitrogen content estimations (CAMMARANO, FITZGERALD, CASA, & BASSO, 2014) and in general vegetation monitoring (BAUGH & GROENEVELD, 2006).

Equation 5: Perpendicular vegetation index (RICHARDSON & WEIGAND, 1977)

$$PVI = \frac{NIR - a * RED - b}{\sqrt{1 + a^2}}$$

In 1988 another index was developed with the intention of reducing the bare soil influence in leaf area index estimations (CLEVERS, 1988, 1989, 1991). The weighted difference vegetation index or WDVI is based on the same principles as the PVI but does not use a soil line. By creating a factor based on the bare soil reflectance in the red and near infrared wavelengths (*S),* the bare soil properties of the Landsat scene are incorporated into the index as seen in Equation 6. In addition the WDVI has been successfully applied to estimate nitrogen content (CAMMARANO et al., 2014) and for vegetation monitoring purposes with low amounts of cover (BAUGH & GROENEVELD, 2006).

Equation 6: Weighted difference vegetation index (CLEVERS, 1988)

$$WDVI = NIR - \frac{S_{NIR}}{S_{RED}} * RED$$

In 1988 another index was introduced to take soil reflectance influence into account. This was the soil adjusted vegetation index or SAVI, shown in Equation 7 (A. R. HUETE, 1988). Instead of adding a soil line or bare soil reflectance into the equation the correction factor *L* was introduced. The problem the author wished to tackle was the different reflection behavior of wet soils. The study showed that by introducing factor *L* to the NDVI the effect of wet soils was effectively reduced (A. R. HUETE, 1988). For most vegetation densities the *L* factor is 0.5 (BARET & GUYOT, 1991) but studies have shown that for different soil types adjusted *L* factors can give better results. The index has most commonly been used for vegetation monitoring and cover estimations (BAUGH & GROENEVELD, 2006; ELVIDGE & CHEN, 1995). In addition it has been used to estimate the leaf area index (EPIPHANIO & HUETE, 1992; PETTORELLI et al., 2005; RONDEAUX, STEVEN, & BARET, 1996) and burn severity (EPTING et al., 2005).

Equation 7: Soil adjusted vegetation index (A. R. HUETE, 1988)

$$SAVI = \frac{NIR - RED}{NIR + RED + L}(1 + L)$$

To reduce the somewhat considered arbitrariness of the *L* factor, the SAVI index was altered (BARET, GUYOT, & Major, 1989). By introducing a soil line into the index and describing a relationship between a soil and vegetation line the influence of bare soils in vegetation sparse areas was reduced (BARET & GUYOT, 1991). Equation 8 describes the TSAVI calculation where *a* and *b* are the slope and the offset of the soil line and *X* is the negative abscissa of point *S.* Point *S* is a point on the soil line that corresponds to the vegetation line and is described as the value 0.8. Equation 8 shows how the TSAVI is calculated and where the soil line and *X* factor come into play. Initially it was developed to increase the accuracy of leaf area index estimations (BARET & GUYOT, 1991) but it has been used in cover estimations, crown volume estimation and other vegetation monitoring purposes as well (BAUGH & GROENEVELD, 2006; ELVIDGE & CHEN, 1995; RONDEAUX et al., 1996; SCHLERF et al., 2005).

Equation 8: Transformed soil adjusted vegetation index (BARET et al., 1989)

$$TSAVI = \frac{a(NIR - aRED - b)}{aNIR + RED - ab + X * (1 + a^2)}$$

With the lack modern processing power another index was designed in 1990 with the purpose of reducing processing time in NDVI calculations (CRIPPEN, 1990). This is the infrared percentage vegetation index or IPVI. The index behaves similar to the NDVI (CRIPPEN, 1990) but the range is from 0 to 1. The theory behind it is that the amount of calculations by pixel is reduced by one. Equation 9 shows the calculations needed to calculate the IPVI and the relationship it has with the NDVI. With a similar behavior as NDVI the index is applicable in the same areas (BAUGH & GROENEVELD, 2006), however with increased computing power available the NDVI is still the more prevalent vegetation index.

Equation 9: Infrared percentage vegetation index (CRIPPEN, 1990)

$$IPVI = \frac{NIR}{NIR + RED} = \frac{1}{2}(NDVI + 1)$$

In 1991 the normalized burn ratio was introduced as a tool to map burned areas (GARCÍA & CASELLES, 1991). From its inception many studies have been conducted and slight alterations have been adopted but the most common way to calculate the NBR can be seen in Equation 10. It is based on the difference between the difference between the near infrared and the short-wave infrared (2090 to 2350 nanometers) wavelengths, with a multiplication factor of a 1000 to enhance the range and make it easier to interpret. One of the most known adaptations is the dNBR (difference normalized burn ratio) that is described in Equation 11 where the difference between the pre-fire and post-fire situations is calculated (VAN WAGTENDONK, ROOT, & KEY, 2004). This method has mainly been used to delineate burned areas as the difference between the burned and the unburned is made visible but it has also been used to keep track of vegetation recovery after fire (IRELAND & PETROPOULOS, 2015; LENTILE et al., 2006). In addition to this the NBR has also been used to asses burn severity (COCKE, FULÉ, & CROUSE, 2005; EPTING et al., 2005; ESCUIN, NAVARRO, & FERNÁNDEZ, 2008) and forest change after fire (WIMBERLY & REILLY, 1997).

Equation 10: Normalized burn ratio (GARCÍA & CASELLES, 1991)

$$NBR = 1000 * \frac{NIR - SWIR\ 2}{NIR + SWIR\ 2}$$

Equation 11: Difference normalized burn ratio (VAN WAGTENDONK et al., 2004)

$$dNBR = NBR_{pre} - NBR_{post}$$

In 1992 a new variant of the NDVI was introduced. The index was designed to reduce the influences of the atmosphere on the NDVI (Y.J. KAUFMAN & TANRE, 1992) and introduces a blue wavelength (450 to 520 nanometers). This was the atmospherically resistant index or ARVI. Equation 12 shows the adapted NDVI calculations. The range of values are between -1 and 1 with green vegetation between 0.20 and 0.80, which is similar to the NDVI. The authors advise the use of the index in areas with high aerosol content for best results (YORAM J. KAUFMAN & TANRÉ, 1994). The most common applications are species detection (FAN, FU, ZHANG, & WU, 2015) and vegetation monitoring (BAUGH & GROENEVELD, 2006).

Equation 12: Atmospherically resistant vegetation index (Y.J. KAUFMAN & TANRE, 1992)

$$ARVI = \frac{NIR - (2 * RED - BLUE)}{NIR + (2 * RED - BLUE)}$$

In the same year another index was developed with a reduced influence of atmospheric conditions, the global environment monitoring index or GEMI (PINTY & VERSTRAETE, 1992). The index is successful in negation of atmospheric effect and behaves similar to the NDVI but, as is seen in Equation 13, it is more intricate (RONDEAUX et al., 1996). The index as used to estimate soil moisture content and showed the same correlations with different sensors indicating it is good to use in multiple platforms (CUNDILL, VAN DER WERFF, & VAN DER MEIJDE, 2015). Other uses are the estimation of the leaf area index (RONDEAUX et al., 1996).

Equation 13: Global environment monitoring index (PINTY & VERSTRAETE, 1992)

$$GEMI = \frac{2(NIR^2 - RED^2) + 1.5NIR + 0.5RED}{NIR + RED + 0.5} * \left(1 - 0.25 * \frac{2(NIR^2 - RED^2) + 1.5NIR + 0.5RED}{NIR + RED + 0.5}\right) - \frac{RED - 0.125}{1 - RED}$$

In 1994 a second adjustment was made to the SAVI in another attempt to remove the arbitrary *L* factor (QI, CHEHBOUNI, HUETE, KERR, & SOROOSHIAN, 1994). The authors felt the *L* factor to be limiting the range of the SAVI index and aimed to replace the *L* factor with a self-adjusting one (QI et al., 1994). This resulted in the modified soil adjusted vegetation index or MSAVI. Equation 14 shows the resulting calculation for the index without

L factor. In the study the authors found that MSAVI had a greater dynamic range response than the SAVI as well as a lower soil influence. This led the index to be used in vegetation sparse areas and with its main purpose being leaf area index estimation (HABOUDANE, MILLER, PATTEY, ZARCO-TEJADA, & STRACHAN, 2004; RONDEAUX et al., 1996). In addition it has also been applied to burn severity estimations (EPTING et al., 2005), vegetation monitoring (BAUGH & GROENEVELD, 2006) and estimating nitrogen content (CAMMARANO et al., 2014).

Equation 14: Modified soil adjusted vegetation index (QI et al., 1994)

$$MSAVI = \frac{2NIR + 1 - \sqrt{(2NIR + 1)^2 - 8(NIR - RED)}}{2}$$

After this another revision was made to the SAVI in 1996. This index expanded on the previous work done on TSAVI and MSAVI to further reduce the impact of bare soil in the index (RONDEAUX et al., 1996). This resulted into the optimized soil adjusted vegetation index or OSAVI. Equation 15 shows the value 1.5 as a correction factor in the index. In literature values have been used varying from absent to 1.5 (BARRY et al., 2008; HABOUDANE, MILLER, TREMBLAY, ZARCO-TEJADA, & DEXTRAZE, 2002; QI et al., 1994; RONDEAUX et al., 1996; YANG, 2012). The index has been used in the estimation of leaf area index values (RONDEAUX et al., 1996), the estimation of chlorophyll content (HABOUDANE et al., 2002; XIAO et al., 2014) and the mapping of disease (CALDERÓN et al., 2013).

Equation 15: Optimized soil adjusted vegetation index (RONDEAUX et al., 1996)

$$OSAVI = \frac{1.5 * (NIR - RED)}{(NIR + RED + 0.16)}$$

In 1996 another variant of the NDVI was introduced. This index is however not based on the red edge as the NDVI is but on the difference between near infrared and the short-wave infrared. The normalized difference water index or NDWI was developed to detect moisture in vegetation (GAO, 1996). The author explains that the index provides information that cannot be derived from the NDVI but it does not manage to negate the influence of bare soil on the index resulting in lower values in vegetation sparse areas. Equation 16 shows the calculations necessary to get the NDWI. The range of heathy vegetation falls between -0.1 and 0.4. The NDWI has since successfully been used to estimate vegetation moisture content and water stress (GU, BROWN, VERDIN, & WARDLOW, 2007; MORENO

et al., 2014). Other documented uses are the estimation of leaf structure deterioration (LIU, HUANG, PU, & WANG, 2014), leaf area index and crown volume estimation (SCHLERF et al., 2005), burn severity estimation (EPTING et al., 2005) and species distinction (GALVÃO et al., 2005).

Equation 16: Normalized difference water index (GAO, 1996)

$$NDWI = \frac{NIR - SWIR}{NIR + SWIR}$$

In the year 2000 an index was introduced to increase the detection of high leaf area index values that would be lost when the NDVI would be used. The index was added as a stock Landsat product and is called the enhanced vegetation index or EVI. The EVI is based on the same principles as the NDVI but adds the blue wavelength to reduce atmospheric effects as well as 2 factors, *C*1 and *C*2, a gain factor, that equals 1 (A. HUETE et al., 2002). Equation 17 shows where these factors are added. In the equation *C*1 equals 6, *C*2 equals 7.5 and *L* equals 1. The range of the EVI is between -1 and 1 and healthy vegetation has a range between 0.20 and 0.80. The most common use for the EVI is the estimation of the leaf area index (A. HUETE et al., 2002; PETTORELLI et al., 2005; WANG, ADIKU, & TENHUNEN, 2005). The index has also successfully been used to estimate nitrogen content (CAMMARANO et al., 2014) and the monitoring of vegetation (ALEXANDRE, 2011; BAUGH & GROENEVELD, 2006).

Equation 17: Enhanced vegetation index (A. HUETE et al., 2002)

$$EVI = \frac{NIR - RED}{NIR + (C1 * RED) - (C2 * BLUE) + L} * (1 + L)$$

With the ARVI successfully incorporating the atmospheric effect into the index the visible atmospherically resistant vegetation index or VARI was developed in 2002 (GITELSON et al., 2002). By replacing the near infrared with the green wavelength, as shown in Equation 18, estimations of cover (GITELSON et al., 2002) became more accurate even with varying atmospheric conditions. In addition the index has been used in biomass estimation, leaf area index estimations and nitrogen content estimations (CAMMARANO et al., 2014).

Equation 18: Visible atmospherically resistant index (GITELSON et al., 2002)

$$VARI = \frac{GREEN - RED}{GREEN + RED - BLUE}$$

2.2 ANALYSIS TECHNIQUES

With the rise of global environmental awareness more attention has been given to temporal analysis during the past decade (TURNER et al., 2007). The data collected for this study contains both spatial and temporal elements, with the spatial element being the different burned areas and their physical location and the temporal element being the acquired Landsat and UAV scenes. Though quite some studies over the past decade use both spatial and temporal data, their advances in analysis have been separate (BIVAND, PEBESMA, & GÓMEZ-RUBIO, 2008). Spatial temporal data often appears conditionally (SCHABENBERGER & GOTWAY, 2004) meaning that in most cases the data can be analyzed either spatially or temporally. Looking at the acquired data from this perspective it is possible to simplify the analysis and decide which aspect is of more interest to the study. In this case the spatial aspect are the different treatments, control, one time burned and four times burned. Though these have a spatial aspect they can be considered an attribute or as a separate population during analysis.

The analysis is therefore based solely on the temporal aspect of the data to assess the recovery and the comparison of the several vegetation indices applied. For these analysis three methods are considered. The vertex method, the multivariate method and the vegetation index condition method.

2.2.1 Vertex method

The vertex method is, as the name implies, based on the analysis of vertices. This is achieved by creating scatter plots of vegetation index values over time (ALATORRE, BEGUERÍA, & VICENTE-SERRANO, 2011; COHEN, YANG, & KENNEDY, 2010; YAN et al., 2014). The gained vertices can be used to see trends and to make estimations for the future. This is often done by creating regression lines where the angle and the offset of the regression line tells whether or not the vegetation index value is changing over time. One common problem with this is that data are not always comparable, for instance summer is not comparable to winter. Based on the goal different data are plotted. If seasonality is analysed data from all seasons are plotted while for the analysis of peak vegetation cover only July can be used to show temporal changes. This is because if all data are plotted it can mask seasonal changes. For example, 30 years of rainfall data in India show an increase in yearly rainfall in Odisha while there is a significant decrease for rainfall in the winter, potentially endangering agricultural activity (SAHU & KHARE, 2015).

2.2.2 Multivariate method

Though a multivariate approach can be added to the vertex method the method described here is different in the sense that it needs more information than the vertex approach. It requires a time series of the used vegetation index and several types of field information. In this case one wants to know which of several field factors has more influence on the vegetation index. This approach is commonly used in vegetation and land use classification. The procedure compares plots and/or field data to spectral imagery of those plots taken at several times (BROOK & KENKEL, 2002). Multivariate techniques include cluster analysis, principle component analysis, correspondence analysis, multiple discriminant analysis and redundancy analysis.

2.2.3 Vegetation condition index

The vegetation condition index is a normalization procedure that facilitates the use of different vegetation indices. The procedure normalizes index values using the current index value and introducing an index minimum and maximum that have been found during the period of observation as seen in Equation 19 (QUIRING & GANESH, 2010; TSIROS, DOMENIKIOTIS, SPILIOTOPOULOS, & DALEZIOS, 2004). The analysis assumes that the index minimum and maximum indicate the worst and best state of the vegetation during the observed period thus the higher the value the healthier the vegetation state.

Equation 19: Vegetation condition index (TSIROS et al., 2004)

$$VCI = \frac{VI_i - VI_{min}}{VI_{max} - VI_{min}}$$

3. PROBLEM FORMULATION

This section addresses the statement of the problem, the objectives of this work, the description of the study area and the data, and the resources used in terms of software.

3.1 PROBLEM STATEMENT

The effects of fire on Mediterranean ecosystems have been studied for a considerable time. However, these effects have not been related in a clear manner with the occurrence of so-called tipping points, i.e. moments at which an abrupt and irreversible change in ecosystem state takes place. The CASCADE project is studying fire-induced tipping points in two of its case study sites, which includes the *Calde* site in central region of Portugal. More specifically, CASCADE is analyzing if recurrent fires lead to the occurrence of tipping points in pine stands. To this end, CASCADE is comparing soil nutrient and vegetation dynamics after single and multiple wildfires, including by means of a manipulative rainfall exclusion experiment simulating prolonged drought during the initial phases of post-fire soil and vegetation recovery. As an add-on to the CASCADE work, the present study is using satellite imagery to compare vegetation recovery following single and recurrent wildfires, under the hypothesis that the occurrence of or proximity to a tipping point is indicated by a slower or less complete recovery.

The monitoring of vegetation after fire may use vegetation indices each designed for different vegetation, soils and atmospheric conditions. Therefore it is imperative to know which index works best to study vegetation recovery after fire.

A second issue is the spatial resolution, in terms of the pixel size, of the imagery that needs to be used. Is the resolution sufficient to extract the required information? And if so, when the study areas have a small size, if compared to the image pixel size, are the number of pixels covering those study areas enough to derive the required information? For example, when using Landsat, the imagery has a spatial resolution of 900 m^2 while the larger studied burned area is 20450 m^2. This means that the studied areas are covered by a small number of satellite measurements. Therefore, it is reasonable to try to encounter other expedite ways of collecting images that may overcome that limitation. This implies that the images have to have a higher resolution. An alternative is thus the acquisition of images with an unmanned aerial vehicle (UAV). The information acquired from these images may also complement that of the satellite images.

3.2 STUDY AREA AND DATA

The study area, Figure 1, is located in the district of *Viseu*, parish of *Calde*, in the central region of Portugal where wild fire is a major agent of land degradation (SHAKESBY, 2011). The central region of Portugal is characterized by ecosystems with dense vegetation covers which accumulate biomass during the summer dry period (FERREIRA, COELHO, BOULET, & LOPES, 2005). While wildfires are a natural occurring phenomenon in the Mediterranean (NAVEH, 1990) the last decades have not only shown an increase in the number of wildfires but also a significant increase of the areas burned in such instances (PEREIRA, CARREIRAS, SILVA, & VASCONCELOS, 2006). This might be attributed to agricultural abandonment and the accumulation of biomass prior to the dry period (FERREIRA et al., 2005). The area has a Mediterranean climate and is prone to summer droughts (FERREIRA et al., 2005).

The vegetation in the study site consists of pine plantations. The fire of 2012 gave rise to a new opportunity for the measurement of tipping points in ecosystems and in order to choose the best study sites the fire history of the area was obtained from the *Instituto Geográfico do Exército*. This resulted in Figure 2 where the burn history of the area is mapped and shows the fire frequency. The areas chosen for monitoring, situated on slopes oriented to south and south-west (Figure 1), are the control, C1, C2 and C3, which are unburned (since 1978), the semi-degraded, SD1, SD2 and SD3, which were burned once (in 2012) and the degraded, D1, D2, D3 and D4 which were burned four times (1978, 1985, 2005 and 2012). The areas were delineated in the field with the help of a handheld GPS (Global Positioning System).

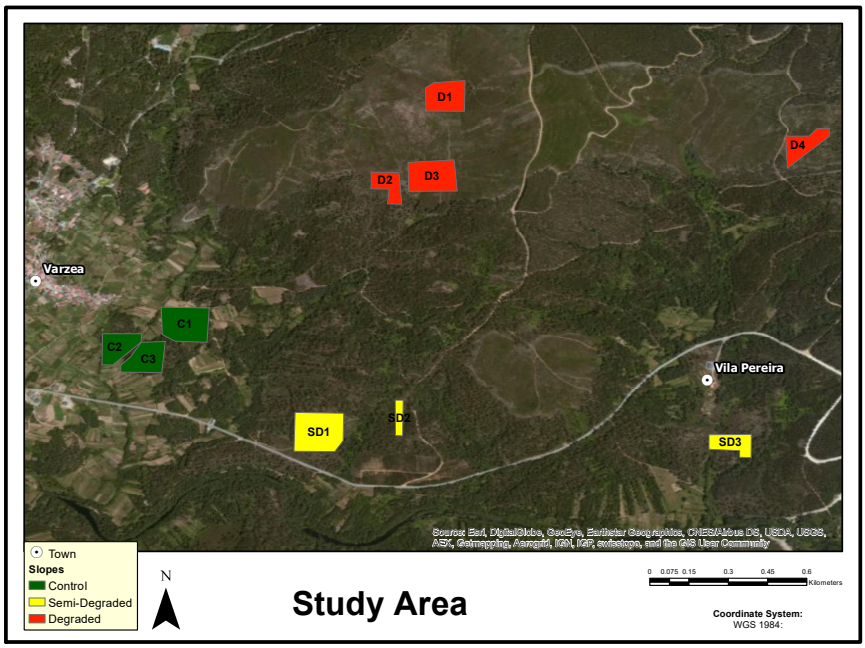

Figure 1: Study area overview

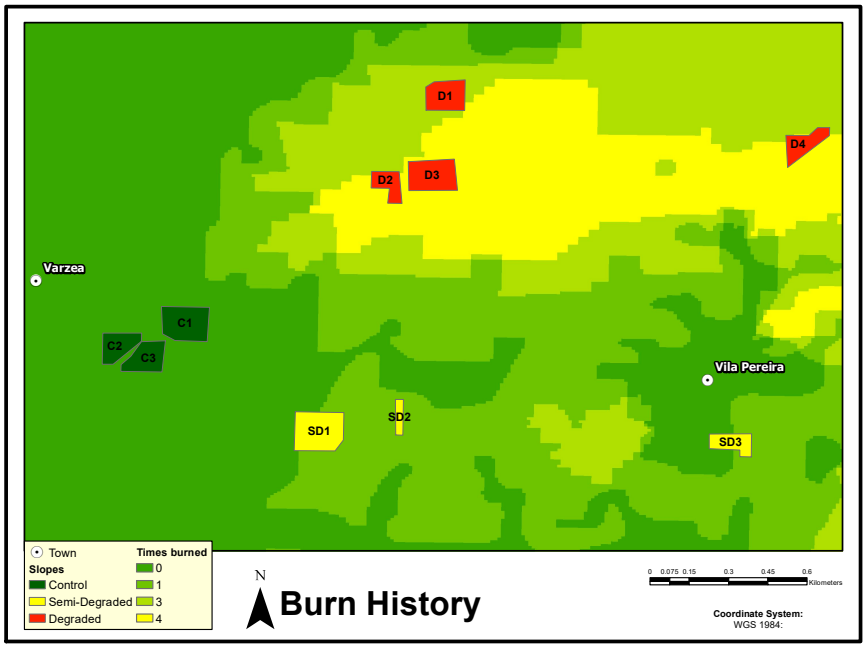

Figure 2: Burn history of Calde

The data used in this work were acquired in three different ways. First by field observations that were conducted on regular basis within the framework of the project CASCADE. These are used as reference data and are shown in Table 1. The data were

collected for all areas except for D4, during the first, second and third year after the fire of 2012 with a total of 7 sampling days and a total of 15 556 observations The observations of the control areas have been excluded as they represent the ground cover while the corresponding images show pine trees. The observations in Table 1 were made by placing a grid over a predefined square meter (3 per area, one in the lower, middle and upper part) and taking a photograph from the top. The grid divides the square in 100 sections that are then visually inspected for the presence of vegetation cover.

Table 1: Field data vegetation cover % for degraded and semi-degraded areas

DATE	D1	D2	D3	SD1	SD2	SD3
17/10/2012	0	0	0	0	0	0
19/12/2012	0	-	0	0.333333	0	0
20/02/2013	1	0	0	0.33557	0	0
06/11/2013	27.42475	4.697987	17.30104	8.754209	-	5
22/01/2014	37.33333	6.666667	31.66667	13	44.33333	4.333333
09/04/2014	44.33333	12.70903	47	31	53.66667	10
25/06/2014	62.58503	23.66667	56.90236	53.33333	71	22.97297

Secondly by the use of Landsat 7 and 8 satellite imagery. In total 125 Landsat 7 scenes and 99 Landsat 8 scenes, with a pixel size of 30 m, have been analysed. The images were acquired from the United States Geological Survey (USGS) earth explorer interface provided by the Landsat program. The Landsat 7 satellite imagery reports from January 2012 to July 2015 and the Landsat 8 reports from April 2013 to August 2015. This coincides with periods before (April 2012 to August 2012) and after the fire of 2012 (September 2012 to August 2015). The Landsat imagery has the WGS 1984 UTM zone 29 N coordinate system. In APPENDIX A, Table 10 and Table 11 give an overview of the Landsat scenes used. Figure 3 shows the wavelength ranges for Landsat 7 and Landsat 8. The more important differences are that all bands are narrower for Landsat 8 with the biggest differences in the near infrared and mid infrared range, as seen in Figure 3.

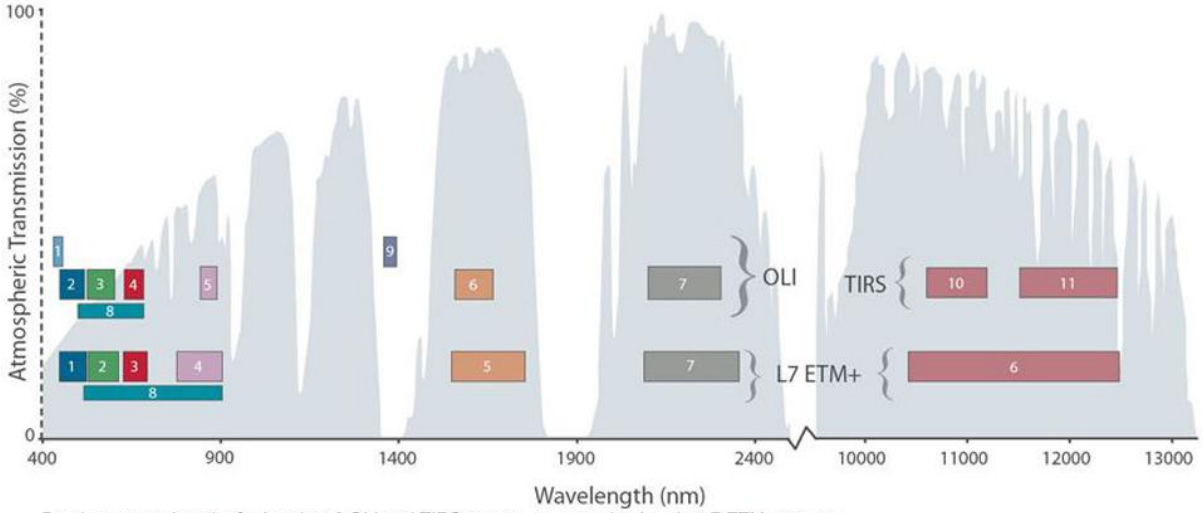

Figure 3: USGS Landsat band designations (NASA, 2015)

The third dataset is an orthophoto, Figure 4, of a part of the study area with a pixel size of 5 cm acquired, also within the framework of the project CASCADE, with images from a flight conducted with an ebee UAV (Unmanned Aerial Vehicle) of Sensefly ("SENSEFLY A PARROT COMPANY," 2015) on the 17th of July 2014 and the software Photoscan Pro of Agisoft (section 3.3). The exposure locations of the acquired images used to produce the orthophoto are presented in Figure 5.

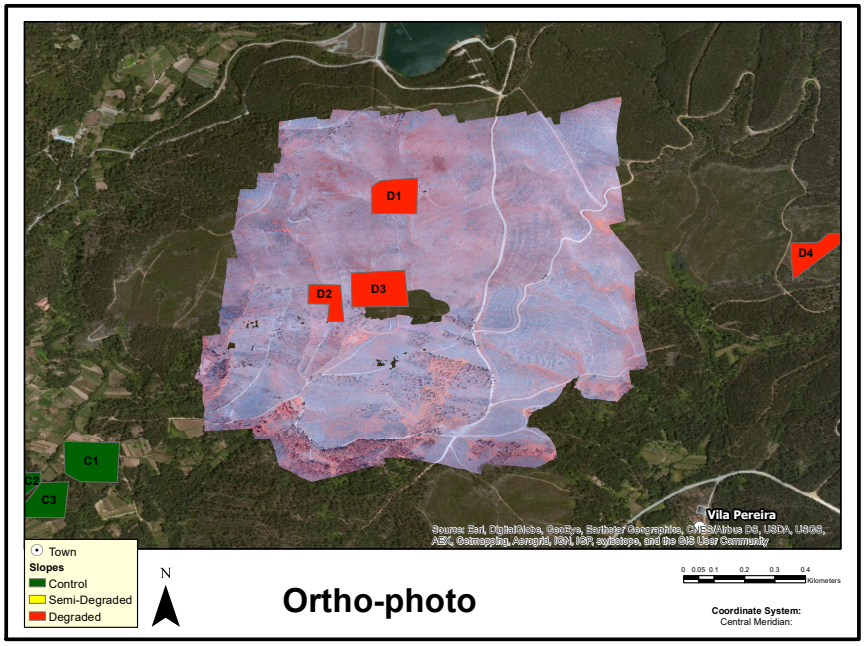

Figure 4: Orthophoto with world map backdrop

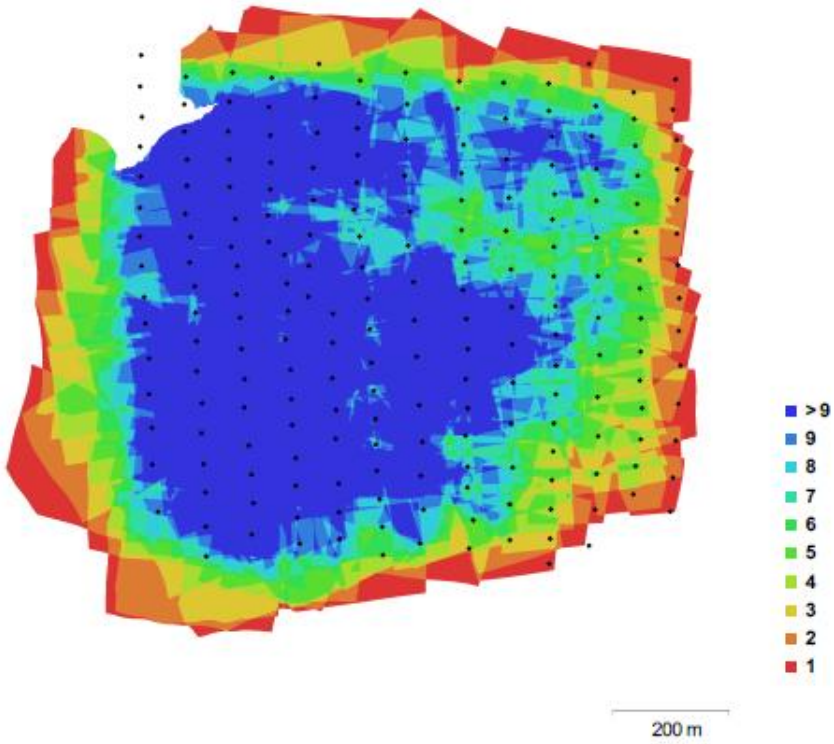

Figure 5: Camera position and image overlap

The orthophoto covers only the areas D1, D2 and D3 as seen in Figure 4. For its production control points were needed, whose coordinates in the PT-TM06 ETRS89 system were measured with the help of a geodetic GPS. Their coordinates are listed in Table 2 and their locations are presented in Figure 6.

Table 2: Ground control points used in PT-06TM ETRS89 Coordinate System

NAME	X	Y	H
PC1	122632.6	22774.64	593.057
PC2	122810.2	23153.77	586.449
PC3	122867.2	23272.72	580.427
PC4	122562.4	23221.21	560.079
PC5	122054.8	23144.22	521.537
PC6	121955.2	22841.46	489.126
PC7	121883.7	22763.12	479.026
PC8	122010.6	22802.82	492.306
PC9	122277.3	22876.15	519.717
PC10	122296.6	23007.13	513.809
PC11	122440.7	22684.08	564.539

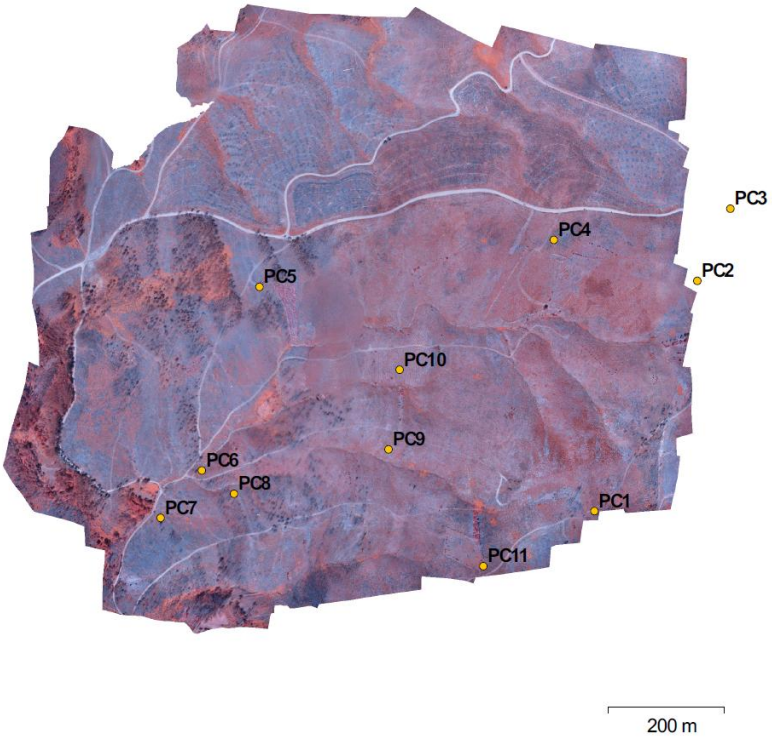

Figure 6: Ground control points used for creation of the orthophoto

3.2 OBJECTIVES

The main objective of the study is to verify if by using satellite images one can distinguish between recovery states of vegetation in areas burnt with different frequencies. Furthermore, one is interested to know if there is a slower recovery pattern for vegetation on areas with a higher burn frequency than with a lower one, with the expectation that a tipping point cloud have been reached in the higher frequency burnt area.

Other objectives are to determine which indices perform best for monitoring of vegetation growth in burned areas and if the additional use of higher spatial resolution data, as those acquired with an UAV allow one to discriminate better differences in vegetation state among areas burnt with different frequencies.

3.3 RESOURCES.

The resources needed for this study concern mainly software, since the hardware relates to a common workstation. The software comprises of Photoscan Pro by Agisoft to produce the orthophoto, as well as Arcgis 10 for visual inspection, the open source GIS (Geographic Information System) package GRASS on a Linux operating system to

compute the vegetation indices and Microsoft excel as well as Sigmaplot for statistical analysis.

4. METHODOLOGY

To attain the objectives mentioned in section 3.2 the following methodology was designed. Firstly, vegetation indices were selected and computed. As the study area does not contain any permanent patches of bare soil, indices that rely on soil lines or bare soil reflectance have been excluded. Therefore the selected vegetation indices were: SR, DVI, NDVI, NDVI green, IPVI, SAVI, OSAVI, MSAVI, NDWI, EVI, ARVI, VARI, NBR and GEMI. These vegetation indices have to be computed with reflectance values instead of the digital number (DN) that makes the images. Therefore the DN values have to be converted to reflectance values. The conversion of Landsat 7 data is based on the metadata that is provided with each scene (Landsat satellite image) and is done in two steps: from DN to spectral radiance and from spectral radiance to planetary reflection as indicated in Equation 20 and Equation 21.

Equation 20: Landsat 7 spectral radiance (NASA, 2014)

$$L_\lambda = \left(\frac{(LMAX_\lambda - LMIN_\lambda)}{QCALMAX - QCALMIN}\right) * (QCAL - QCALMIN) + LMIN_\lambda$$

Where:

L_λ	= Spectral Radiance at the sensor´s aperture in watts/(m^2 * ster* µm).
$QCAL$	= the quantized calibrated pixel value in DN.
$LMAX_\lambda$	= the spectral radiance that is scaled to QCALMAX in watts/(m^2 * ster * µm).
$LMIN_\lambda$	= the spectral radiance that is scaled to QCALMIN in watts/(m^2 * ster * µm).
$QCALMAX$	= the maximum quantized calibrated pixel value (corresponding to $LMAX_\lambda$).
$QCALMIN$	= the maximum quantized calibrated pixel value (corresponding to $LMIN_\lambda$).

Equation 21: Landsat 7 planetary reflectance (NASA, 2014)

$$\rho_p = \frac{\pi * L_\lambda * d^2}{ESUN_\lambda * cos\theta_s}$$

Where:

ρ_p	= Unitless planetary reflectance.
L_λ	= Spectral radiance at sensor´s aperture.
d	= Earth-Sun distance in astronomical units.
$ESUN_\lambda$	= Mean solar exoatmospheric irradiances.
θ_s	= Solar zenith angle in degrees.

The procedure for Landsat 8 is quite similar but is simplified and only needs one conversion step to convert to reflectance, Equation 22. Though the result is named differently as top of atmosphere (TOA) planetary spectral reflectance.

Equation 22: Landsat 8 TOA planetary reflectance (NASA, 2015)

$$\rho_\lambda = \frac{M_\rho * QCAL + A_\rho}{\sin\theta}$$

Where:

ρ_λ	= top of atmosphere planetary spectral reflectance, unitless.
M_ρ	= reflectance multiplicative scaling factor for the band.
$QCAL$	= the quantized calibrated pixel value in DN.
A_ρ	= reflectance additive scaling factor for the band.
θ	= solar elevation angle.

After the conversion from DN to planetary reflectance the vegetation indices were calculated. This was done using an automated approach to calculate all vegetation indices for a scene in one go using GRASS. By using masks, made with the delineation lines produced in the field for the study areas (section 3.2), vegetation indices were computed for each pixel. This process is described in Appendix B. After this step all values were imported into excel. In this way each scene provides, per area, a set of vegetation index values associated to each pixel. These values are needed further in the seasonality study, to estimate vegetation index values per area (mean values) needed for the vegetation recovery analysis, for the vegetation indices performance assessment and to compare the vegetation index values computed with an orthophoto with those computed with the Landsat images.

For the assessment of the performance of the vegetation indices a Pearson correlation test was applied by using the Landsat 7 and 8 scenes acquired closest to the field sampling dates. The Pearson product moment correlation coefficient will tell us if there is a positive, negative or no correlation between the field data and the vegetation index values. There is no rigid criterion but, in general, a positive correlation is a Pearsons value higher than 0.7 and a negative one is smaller than -0.7. The closer the value is to 1 or -1 the stronger the correlation is. With this, the indices with the stronger correlations can be selected for the vegetation recovery analysis.

The vegetation recovery analysis is usually done by comparing the obtained vegetation index values to a previous or healthy state (QUIRING & GANESH, 2010; TSIROS et al., 2004). This is however not possible in this case as the vegetation in the

healthy control sites is pine and the vegetation burned in the studied areas (SD and D) was also pine. Pine plantations have a growth cycle of about 25-30 years and thus it is impossible to see this recovery in such a short time.

Instead we looked at the changing of the vegetation index values over time by taking an average value per month per area of interest (SD and D). These values, one per area per month, were plotted and a trend line computed. A linear trend line was chosen as it is unlikely that in this short period (almost three years) a new equilibrium would be reached. By comparing the slopes and offsets of the linear trend lines from the different areas one can say which area is recovering faster and whether burn frequency has an influence on recovery speed.

The trend lines is influenced by seasonality and therefore that should be taken into account. This was done by recognizing seasonal patterns for which the vegetation indices of the pixels within the control areas were used. With these vegetation indices, average and maximum and minimum values were computed per set of images of control areas acquired in the same months. The patterns were then recognized by visually inspecting the plots made with the referred average and maximum and minimum values against the months of all the years.

To compare vegetation index values computed with an orthophoto with those computed with the Landsat images first it was computed the mean, the first and third quartiles, and the maximum and minimum values of the vegetation indices within an area (D because it is the only area of interest present in the orthophoto). Second, by using those data, plotted in the form of boxplots, we recognized, by visual inspection the similarities and dissimilarities of those vegetation indices. Care should be taken to use only those vegetation index that are not much affected by using digital numbers instead of reflectance. This is because there was no way to convert the digital numbers of the orthophoto to reflectance values. Furthermore, not all the indices can be computed for the orthophoto only contains the red, green and near infrared wavelengths. Therefore only the vegetation indices IPVI, NDVI, NDVI green, OSAVI, SAVI and SR were computed.

5. IMPLEMENTATION.

This section addresses the creation of scripts used to process the satellite images and calculate the vegetation indices, as well as the production of the orthophoto.

5.1 PRE-PROCESSING OF THE SATELLITE IMAGES

The pre-processing of the data was done in GRASS (Geographical Resources Analysis Support System) due to its compatibility with bash programming and easy adaptation of tools provided by the open source GRASS community. As both Landsat 7 and 8 have a different number of bands and data structure two scripts have been written with slightly different steps for cloud detection and the conversion of the DN value (digital number) to reflectance (Section 4).

The above mentioned process is simplified by the use of some tools in GRASS that are specially designed for Landsat imagery. These are i.landsat.toar and i.landsat.acca.

i.landsat.toar can handle multiple satellite sensors (from Landsat 1 to 8) and is designed to calculate top of atmosphere radiance or reflectance. By loading the metadata file the tool knows which calibration values to apply in the conversion formula.

i.landsat.acca is designed to apply the automatic cloud cover assessment algorithm (IRISH, BARKER, GOWARD, & ARVIDSON, 2006). When applying the ACCA the assumption is made that there are no ice-sheets in the image. This because the algorithm assumes the landmass to have a higher temperature than the clouds when detecting cloud cover. As the study area is located in the central region of Portugal we can assume the ACCA will deliver reasonable results.

For the Landsat 8 images the ACCA does not have to be applied since the USGS provides a quality assurance value for each pixel from which cloud cover can be derived. These quality assurance values are described in Table 3.

Table 3: Landsat 8 Quality Assurance bits table (NASA, 2015)

16-bit Landsat 8 QA Band – Read bits from RIGHT to LEFT <- starting with bit 0

BIT	15	14	13	12	11	10	9	8	7	6	5	4	3	2	1	0
Description	Cloud confidence		Cirrus confidence		Snow/ice confidence		Reserved for vegetation confidence		Cloud shadow confidence		Water confidence		Reserved	Terrain occlusion	Dropped frame	Designated fill

The application of the quality assurance band is not as straigth forward as the i.landsat.toar or i.landsat.acca tools. Instead a mask is created using the converted 16bit value of 1100000000000000 which is based on bit number 14 and 15 from Table 3. This results in the value 49152 which can then be looked up in the quality assurance band image.

For the calculation of the vegetation indices the GRASS tool r.mapcalc is used. The tool a spatial calculator and is one of the main features in GRASS

For further information please refer to APPENDIX B. It contains a step by step guide of the processing of the Landsat scenes in GRASS and a short explanation on other tools used within the GRASS opensource GIS package.

5.2 PRODUCTION OF THE ORTHOPHOTO

For the creation of the orthophoto the software Agisoft Photoscan Pro was used to process the images taken with the Sensefly ebee UAV. By using the images and ground control points, Table 2, Photoscan Pro applies image matching and bundle adjustment algorithms to produce a point cloud. From the point cloud it produces a Digital Surface Model (DSM) in TIN format, Figure 7.With this DSM, the images and parameters estimated from the bundle adjustment the orthophoto is produced with a pixel size of 5 cm covering an area of 1 km^2.

The camera on the Ebee UAV was an adapted Canon PowerShot ELPH 110 HS that record the green, red and infrared wavelengths. Because of the adaptation, the red and green bands of the image are tainted with near infrared radiation. Therefore, for the vegetation index calculations the near infrared values have to be removed from the red

and green bands before any indices are calculated. Due to constraints when acquiring the images, no white calibration surface was placed in the field. This means that the vegetation indices obtained from the orthophoto are not computed using reflectance values but with digital numbers which are affected by several factors, like the sun azimuth and height as well as atmospheric conditions. Therefore, the comparison between the vegetation indices values computed with the help of the orthophoto and those of the satellite images has to be done with great care.

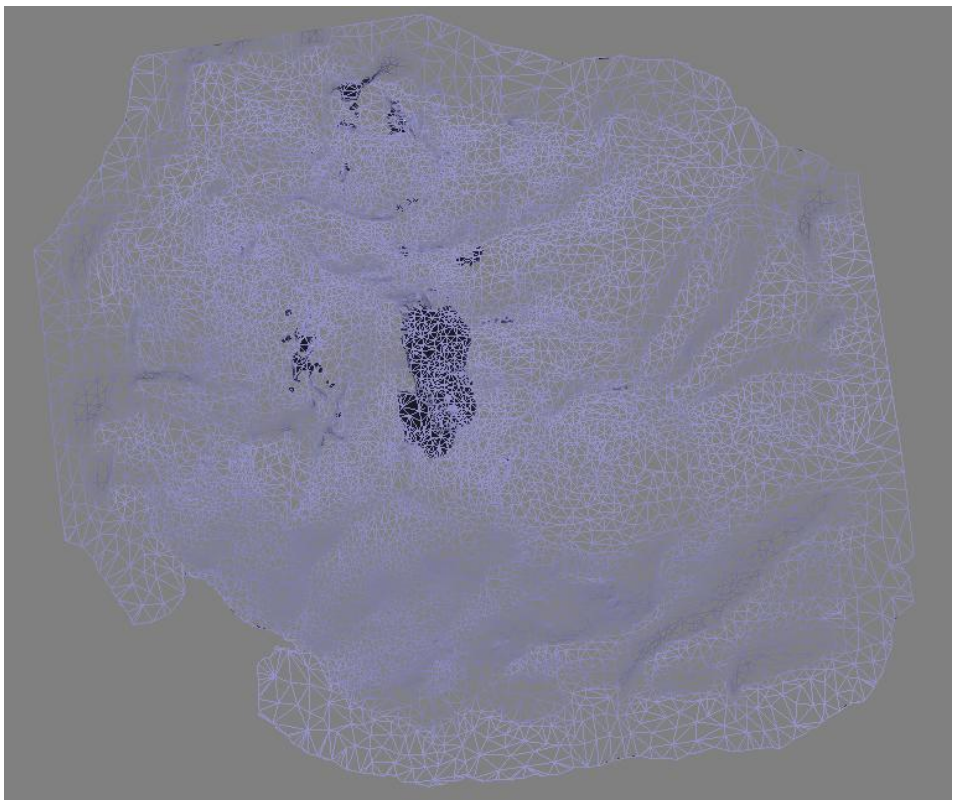

Figure 7: Digital Surface Model (DSM) in TIN format

6. PRESENTATION AND DISCUSSION OF RESULTS

6.1 VEGETATION INDEX PERFORMANCE

The assessment of the performance of the vegetation indices (chapter 4) shows that correlations can be found between those indices and the percentage of vegetation cover. Table 4 shows that the best correlations are encountered for DVI, EVI, NBR, OSAVI and SAVI while the worst correlations are found for ARVI, GEMI, MSAVI and VARI. DVI has the best correlation with an average Pearson´s R of 0.86 and second best is SAVI with an average of 0.77. These average values are computed with the 4 Pearson values (Table 4) associated with each vegetation index of an area of interest (SD and D).

Table 4: Pearson´s R between vegetation cover and indices where D is degraded and SD is semi-degraded

VEGETATION	L7 D	L7 SD	L8 D	L8 SD	AVERAGE OF ALL PEARSON´S R´S
ARVI	0.09	0.03	-0.19	0.22	0.0375
DVI	0.79	0.85	0.92	0.89	0.8625
EVI	-0.69	-0.71	1	0.83	0.1075
GEMI	-0.32	-0.5	0.31	0.27	-0.06
IPVI	0.79	0.4	0.36	0.56	0.5275
MSAVI	-0.46	-0.26	0.3	0.15	-0.0675
NBR	0.66	0.74	0.56	0.82	0.695
NDVI	0.65	0.63	0.36	0.56	0.55
NDVIG	0.52	0.6	0.61	-0.24	0.3725
NDWI	0.59	0.66	0.42	0.78	0.6125
OSAVI	0.73	0.75	0.58	0.71	0.6925
SAVI	0.76	0.8	0.72	0.79	0.7675
SR	0.72	0.72	0.42	0.64	0.625
VARI	-0.16	-0.08	-0.81	0.4	-0.1625

The analysis of performance of the vegetation indices also shows some noteworthy observations. The ARVI, EVI, MSAVI and VARI have scattered and hard to interpret values after the fire event, while EVI, IPVI, NBR, NDVI, NDVI green, NDWI, OSAVI, SAVI and SR have less scattered values after the fire event, as illustrated in the figures in appendix C. In all of these, the fire event is clearly visible and a recovery trend can be discerned in both the degraded and semi-degraded data, as demonstrated in Figure 8. Surprising is the fact that the GEMI (appendix C) shows a strong decline before the fire event, even though, the event itself and the recovery after is still visible.

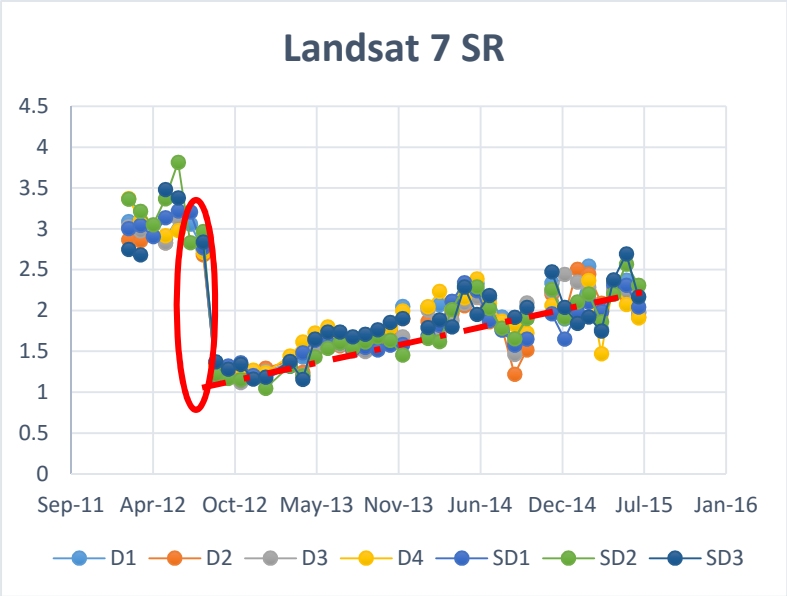

Figure 8: SR Landsat 7 plot with fire event and recovery line

The behaviour of each vegetation index is quite different when using Landsat 7 or Landsat 8 images. For demonstration purposes we will look solely at the results obtained with the NDVI. The results for the other indices can be found in APPENDIX D. Figure 9 shows the time-series of NDVI based on Landsat 7 imagery. The first drop in NDVI values indicates the fire event in summer 2012 while the third, fourth and fifth are anomalies caused by the lack of reliable data. In fact because of the size of the study areas versus the pixel size of the satellite images, as referred to in section 3.1, each area is covered by a small amount of pixels. In case of anomalies in the images, the combination of a small number of pixels with pixels partly covered with clouds may explain the sudden drop of NDVI values.

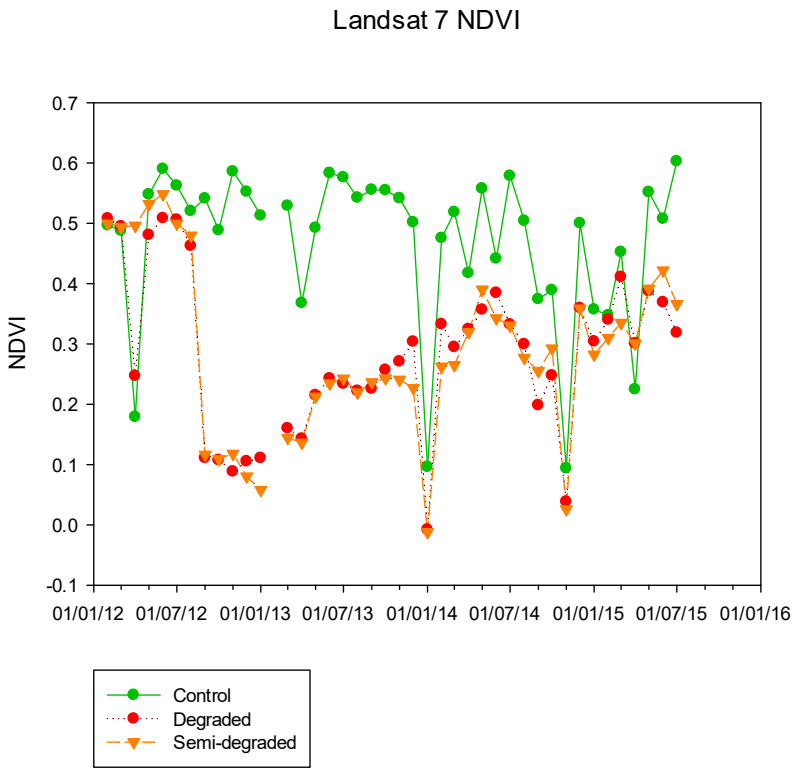

Figure 9: Landsat 7 NDVI time series where C is control, D is degraded and SD is semi-degraded (other indices are shown in APPENDIX C)

Figure 10 also shows a time-series of NDVI values but for the Landsat 8 imagery, unfortunately the Landsat 8 satellite was only launched after the summer fire of 2012 occurred and so misses the first values that would show the drop of NDVI values of semi-degraded and degraded areas. However we do see that over time the difference between the control and the semi-degraded and degraded sites decrease in both Landsat 7 and 8 time-series.

As can be seen in Figure 10 the data are hard to interpret, contrary to those of Figure 9. Throughout the years the NDVI values go up and down as an influence of the seasons. Figure 11 and Figure 12 show this seasonal variability for the NDVI. The figures show the average values of the vegetation indices for the control areas per month as well as maximum and minimum values (see seasonality study in chapter 4). Using the obtained seasonality for all indices seasonal trends may be identified and not mistaken for actual recovery. This is however done by visual inspection as described in chapter 4.

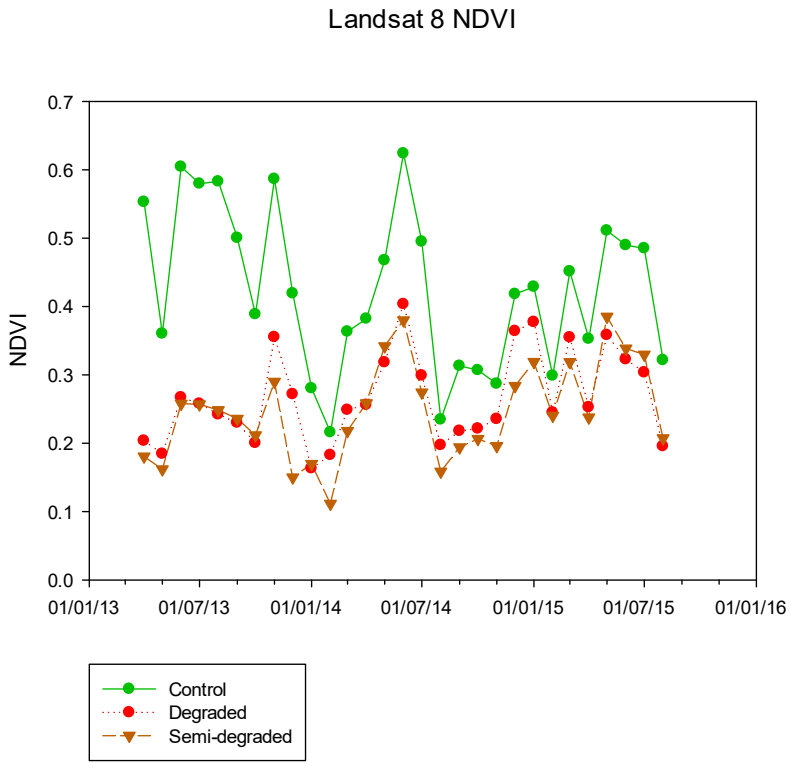

Figure 10: Landsat 8 NDVI time-series where C is control, D is degraded and SD is semi-degraded (other indices are shown in APPENDIX C)

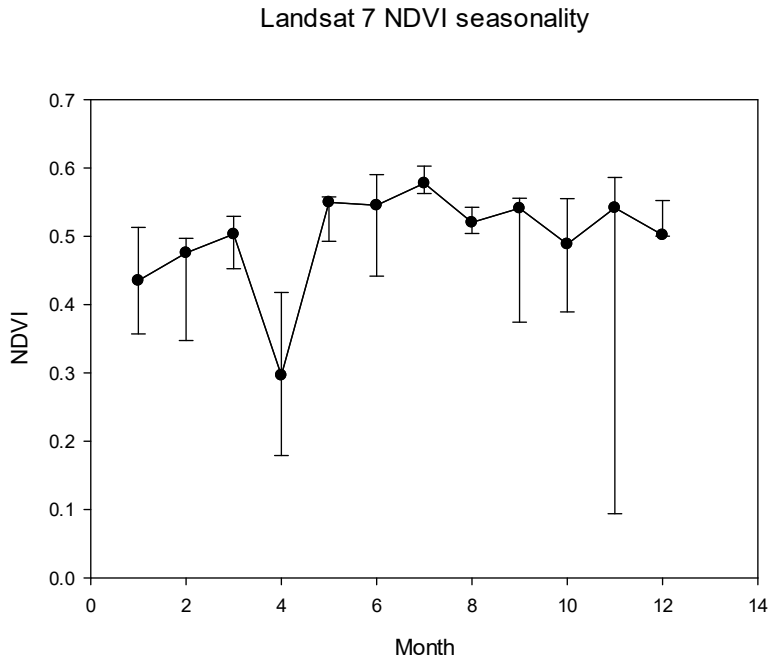

Figure 11: Landsat 7 NDVI seasonality plot of mean vegetation indices for control areas with positive and negative errors

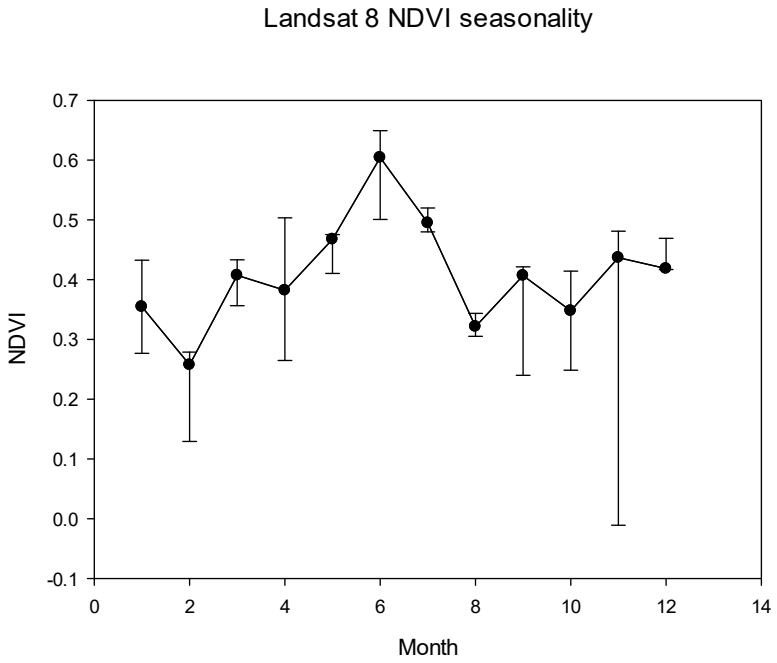

Figure 12: Landsat 8 NDVI seasonality plot of mean vegetation indices for control areas with positive and negative errors

6.2 VEGETATION RECOVERY ANALYSIS

For the recovery analysis we look solely at the DVI and SAVI indices, as they were the ones that performed best (6.1). The vegetation cover of the different areas (SD and D) are compared by comparing trend lines, as described in chapter 4. As an example, Figure 13 shows the trend lines obtained with the DVI vegetation index computed with Landsat 8 images, for the SD1 and D1 areas. As seen in that figure, the trend line for SD1 has a higher inclination than that for D1, as expected. This happens for all the other areas (Table 5). Nonetheless, when using Landsat 7 images, this does not happen, although the encountered differences do not appear significant (Table 6). This behavior was also obtained when using the SAVI index (Appendix D, where the trend lines for all the SD and D areas are also given). When comparing the regression lines, remembering that the SD areas where burned once, and D where burned four times, it can be seen that, even though there is a detectable recovery, there is no clear difference between the vegetation recovery speeds between the areas.

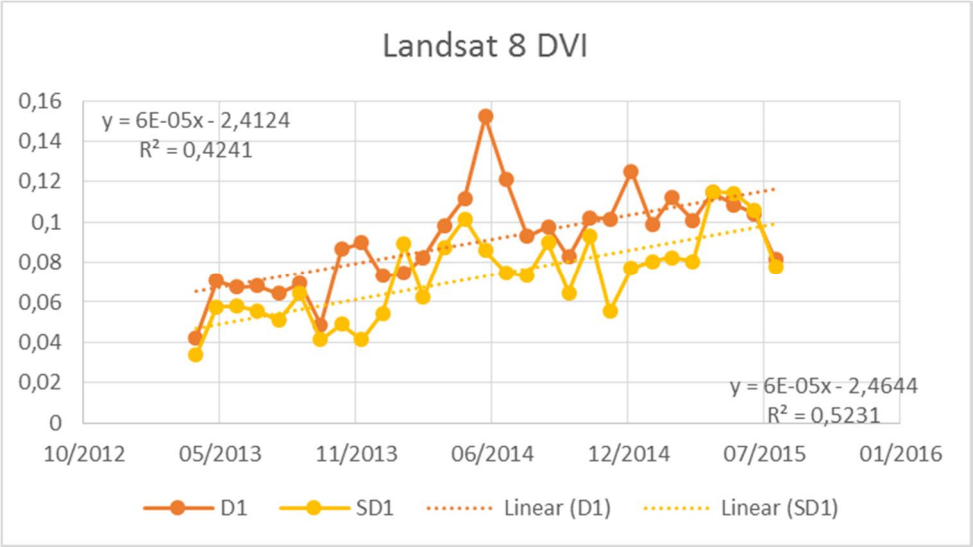

Figure 13: Trend lines for SD1 and D1 areas using DVI vegetation index computed with Landsat 8 images (the trend line parameters for SD1 are in the upper left and those of D1 are in the lower right)

Table 5: Slope and R-squares of the trend lines for SD and D areas using DVI vegetation index computed with Landsat 8 images

LANDSAT 8	SLOPE	R2
D1	0.00006	0.42
D2	0.00006	0.46
D3	0.00005	0.45
D4	0.00005	0.33
SD1	0.00006	0.52
SD2	0.00007	0.52
SD3	0.00006	0.48

Table 6: : Slope and R-squares of the trend lines for SD and D areas using DVI vegetation index computed with Landsat 7 images

LANDSAT 7	SLOPE	R2
D1	0.00010	0.73
D2	0.00009	0.81
D3	0.00009	0.83
D4	0.00006	0.45
SD1	0.00008	0.54
SD2	0.00009	0.71
SD3	0.00009	0.77

6.3 COMPARISON FROM VEGETATION INDICES FROM ORTHOPHOTO AND LANDSAT IMAGES

The comparison of the degraded areas (D) in the orthophoto with those in the Landsat 7 and 8 imagery acquired closest to the 17th of July 2014 led to Table 7, Table 8 and Table 9 where are listed the mean, the first and third quartiles, and the maximum and minimum values of the selected vegetation indices (chapter 4) within areas D1, D2 and D3 for the orthophoto, Landsat 7 and Landsat 8, respectively. These statistics are illustrated, for example for the NDVI index, in Figure 14 where it can be seen that the spread of data is smaller for the UAV data than that of the Landsat 7 data. The Landsat 8 data is however more difficult to interpret as there is a smaller number of pixels available per area and thus a smaller spread. This difference in the amount of pixels per area for the images of Landsat 7 versus Landsat 8 resulted from an inadequate usage of the GRASS software tools that due to time constraints could not be resolved. In fact, the images of Landsat 7 were resampled to a pixel size of 15 m, unintentionally. As an overview it can be said that, except for NDVI and SR the spread of the values is higher for UAV data than that of the Landsat images. The other plots for the other vegetation indices can be consulted in APPENDIX E.

Table 7: Orthophoto vegetation index statistics

	ORTHOPHOTO						
NAME	Min	Max	Q1	Q3	median	average	Count
IPVI D1	0.4671	0.8085	0.5505	0.5657	0.5580	0.5585	3905984
IPVI D2	0.5000	0.7075	0.5457	0.5582	0.5514	0.5526	2136658
IPVI D3	0.4787	0.7703	0.5488	0.5610	0.5545	0.5557	3440122
NDVI D1	-0.0659	0.6170	0.1010	0.1313	0.1159	0.1170	3905640
NDVI D2	-0.0078	0.5789	0.1013	0.1269	0.1137	0.1155	2136653
NDVI D3	-0.0426	0.5405	0.0976	0.1220	0.1091	0.1114	3440045
NDVIG D1	-0.5302	0.5385	-0.0552	0.0435	-0.0036	-0.0084	3831689
NDVIG D2	-0.3112	0.6667	-0.0263	0.0636	0.0244	0.0174	1320953
NDVIG D3	-0.3532	0.6164	0.0078	0.0726	0.0442	0.0371	3391029
OSAVI D1	-0.0987	0.9240	0.1515	0.1969	0.1738	0.1755	3905640
OSAVI D2	-0.0116	0.8660	0.1519	0.1902	0.1705	0.1732	2136653
OSAVI D3	-0.0638	0.8091	0.1463	0.1828	0.1636	0.1670	3440045
SAVI D1	-0.0985	0.9206	0.1513	0.1966	0.1736	0.1752	3905640
SAVI D2	-0.0116	0.8609	0.1518	0.1900	0.1703	0.1729	2136653
SAVI D3	-0.0637	0.8054	0.1461	0.1826	0.1634	0.1668	3440045
SR D1	0.8764	4.2222	1.2248	1.3023	1.2623	1.2675	3905984
SR D2	0.9846	3.7500	1.2255	1.2907	1.2566	1.2631	2136658
SR D3	0.9184	3.3529	1.2162	1.2778	1.2449	1.2526	3440122

Table 8: Landsat 7 vegetation index statistics

LANDSAT 7

NAME	Min	Max	Q1	Q3	median	average	Count
IPVI D1	0.6453	0.7450	0.6747	0.6987	0.6906	0.6888	62
IPVI D2	0.6435	0.6697	0.6520	0.6625	0.6572	0.6568	33
IPVI D3	0.6396	0.7058	0.6453	0.6744	0.6552	0.6603	67
NDVI D1	0.2907	0.4899	0.3494	0.3973	0.3812	0.3776	62
NDVI D2	0.2870	0.3395	0.3041	0.3250	0.3145	0.3137	33
NDVI D3	0.2793	0.4116	0.2907	0.3488	0.3103	0.3205	67
NDVIG D1	0.3158	0.4338	0.3609	0.3941	0.3682	0.3734	62
NDVIG D2	0.2919	0.3395	0.3003	0.3310	0.3045	0.3154	33
NDVIG D3	0.3103	0.3685	0.3166	0.3412	0.3250	0.3312	67
OSAVI D1	0.2808	0.4677	0.3444	0.3876	0.3662	0.3661	62
OSAVI D2	0.2747	0.3299	0.2868	0.3118	0.2991	0.3008	33
OSAVI D3	0.2780	0.3818	0.2827	0.3361	0.3002	0.3096	67
SAVI D1	0.1599	0.2645	0.1992	0.2200	0.2092	0.2090	62
SAVI D2	0.1540	0.1887	0.1603	0.1788	0.1667	0.1703	33
SAVI D3	0.1591	0.2110	0.1618	0.1900	0.1727	0.1763	67
SR D1	1.8196	2.9212	2.0739	2.3192	2.2321	2.2292	62
SR D2	1.8052	2.0278	1.8739	1.9629	1.9175	1.9157	33
SR D3	1.7751	2.3990	1.8196	2.0715	1.8999	1.9534	67

Table 9: Landsat 8 vegetation index statistics

	LANDSAT 8						
NAME	Min	Max	Q1	Q3	median	average	Count
IPVI D1	0.5493	0.5509	0.5500	0.5505	0.5504	0.5503	15
IPVI D2	0.5489	0.5499	0.5490	0.5493	0.5491	0.5492	8
IPVI D3	0.5489	0.5514	0.5497	0.5505	0.5502	0.5501	16
NDVI D1	0.0985	0.1019	0.1000	0.1009	0.1007	0.1005	15
NDVI D2	0.0977	0.0997	0.0980	0.0986	0.0982	0.0984	8
NDVI D3	0.0977	0.1029	0.0994	0.1011	0.1004	0.1003	16
NDVIG D1	0.0001	0.0031	0.0016	0.0021	0.0018	0.0018	15
NDVIG D2	0.0000	0.0018	0.0003	0.0014	0.0007	0.0008	8
NDVIG D3	-0.0013	0.0041	0.0003	0.0020	0.0015	0.0013	16
OSAVI D1	0.1239	0.1281	0.1258	0.1269	0.1266	0.1264	15
OSAVI D2	0.1230	0.1253	0.1233	0.1240	0.1236	0.1238	8
OSAVI D3	0.1228	0.1292	0.1250	0.1270	0.1262	0.1260	16
SAVI D1	0.0921	0.0954	0.0936	0.0944	0.0941	0.0940	15
SAVI D2	0.0916	0.0932	0.0918	0.0924	0.0921	0.0922	8
SAVI D3	0.0913	0.0960	0.0931	0.0944	0.0939	0.0937	16
SR D1	1.2186	1.2269	1.2223	1.2245	1.2240	1.2235	15
SR D2	1.2167	1.2216	1.2172	1.2187	1.2178	1.2183	8
SR D3	1.2166	1.2293	1.2208	1.2249	1.2232	1.2229	16

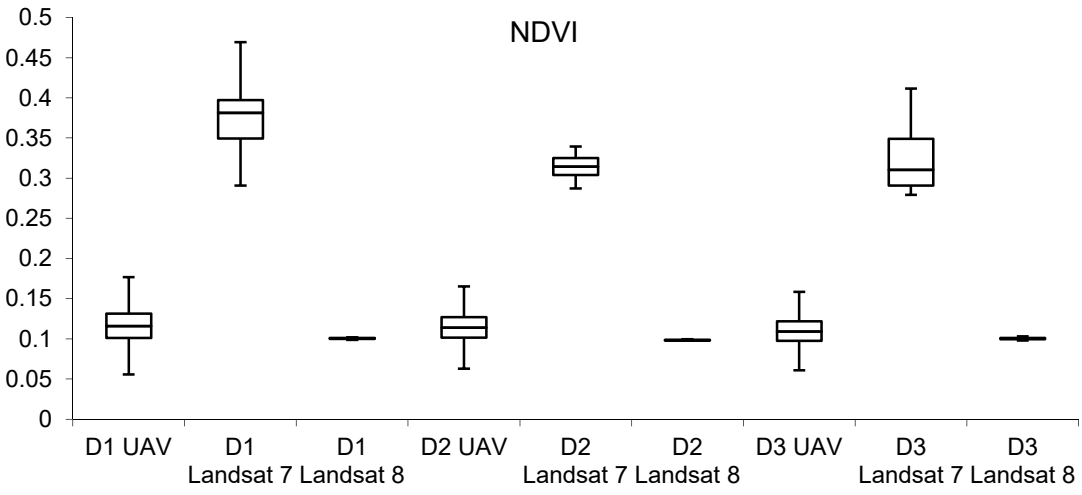

Figure 14: NDVI boxplot orthophoto and Landsat 7 and 8 comparison

7. CONCLUSIONS

The difference in Landsat 7 and 8 vegetation index values shown in Figure 9 and Figure 10 is surprising. The launch of Landsat 8 indicated the next step in remote sensing and is welcomed to ensure the Landsat Data continuity Mission and one of the main aims is to keep data comparable. One possible cause of this difference in this behaviour might be attributed to the slightly different band wavelength width used by the Landsat 8 satellite, Figure 3.

The Pearson´s R´s listed in Table 4 give a very useful indication of the applicability of the vegetation indices for the estimation of vegetation recovery. Though this is to be expected there are some that can potentially reduce the intensity of field work or be used to add information between sampling dates. For this purpose especially DVI and SAVI are recommended as they show the highest correlations with vegetation cover and show in the time-series a clear recovery trend.

The trend line analysis shows that the vegetation recovery of the higher frequently burned areas and of the lower frequently burned areas is similar. We expected that the lower frequently burned areas would recover faster but, perhaps the time span is too short to take such a conclusion.

For the comparison of the orthophoto to the Landsat imagery the following can be said. There is a clear increase in the measurement range for most vegetation indices as expected. This means more differences can be seen with the higher spatial resolution. However with only one orthophoto it is difficult to make any assumptions on vegetation recovery as it is not directly comparable to the Landsat imagery, due to the lack of radiometric calibration and thus of surface reflectance. It is however clear that some events not perceived by using Landsat images, due to its low resolution, may be recovered by using UAV images due to its higher spatial resolution.

As more scenes become available, every 16 days, the seasonality calculations can be improved and, with the CASCADE project still collecting field data also the Pearson´s R´s found for vegetation cover can be improved as more scenes and field samples are collected and analysed and, in the future a possible levelling-off of the recovering vegetation might be witnessed. When this happens we can determine whether or not a tipping point has been reached.

8. APPENDIX A: LANDSAT SCENES OVERVIEW

This appendix contains an overview of the Landsat 7 and 8 scenes used and how many pixel values have been obtained from each scene for each area.

Table 10: Landsat 7 overview with obtained pixel count per area

Landsat 7										
Date	**C1**	**C2**	**C3**	**D1**	**D2**	**D3**	**D4**	**SD1**	**SD2**	**SD3**
02/02/2012	53	43	52	53	33	53	41	53	18	36
11/02/2012	53	43	52	53	27	53	41	53	18	36
18/02/2012	53	43	52	53	33	53	41	53	18	36
27/02/2012	53	43	52	53	11	53	41	36	18	36
05/03/2012	53	43	52	53	33	53	41	53	18	36
14/03/2012	53	23	11	53	-	-	41	-	-	-
21/03/2012	53	43	52	53	33	53	36	53	18	36
06/04/2012	53	8	14	53	33	53	2	-	-	-
15/04/2012	-	-	-	-	33	37	-	53	2	-
24/05/2012	8	11	30	12	33	53	18	53	18	10
25/06/2012	53	43	52	53	-	17	41	-	12	36
11/07/2012	53	39	52	53	-	-	-	53	18	-
21/08/2012	53	43	52	53	4	46	41	22	18	36
06/09/2012	53	43	52	53	-	-	41	-	4	36
13/09/2012	53	43	52	53	33	53	41	53	18	36
29/09/2012	53	43	52	53	-	31	41	8	16	36
08/10/2012	53	43	52	53	33	53	41	53	18	36
15/10/2012	53	10	8	53	33	47	41	53	2	-
31/10/2012	9	20	41	16	33	53	20	53	18	30
09/11/2012	53	43	52	53	33	53	41	53	18	36
02/12/2012	53	36	28	53	22	10	41	44	-	30
03/01/2013	53	43	52	53	4	46	41	22	18	36
01/03/2013	53	43	52	53	33	53	41	53	18	36
02/04/2013	-	43	52	-	33	53	-	-	-	-
18/04/2013	39	-	-	40	6	-	31	10	-	-
25/04/2013	9	24	31	12	33	53	18	53	18	30
04/05/2013	-	-	-	-	-	-	-	-	-	-
11/05/2013	53	43	52	53	33	53	41	53	18	36
20/05/2013	-	-	-	-	33	53	-	-	4	-
27/05/2013	7	3	45	-	33	53	-	3	12	36
05/06/2013	53	43	52	53	10	53	41	30	18	36
12/06/2013	53	43	52	53	6	-	-	-	-	-
28/06/2013	8	10	13	-	8	16	1	20	4	9
14/07/2013	-	10	13	-	8	16	1	20	4	9

30/07/2013	24	10	13	13	8	16	10	20	4	9
24/08/2013	49	-	-	48	-	-	32	1	-	-
31/08/2013	16	10	13	8	8	16	4	20	4	9
09/09/2013	53	27	11	53	-	-	41	-	-	-
16/09/2013	-	10	13	-	8	16	1	20	4	9
11/10/2013	53	43	52	53	21	53	41	52	18	36
27/10/2013	-	43	52	-	33	53	-	53	18	36
03/11/2013	24	10	13	15	8	16	11	20	4	9
12/11/2013	-	-	-	-	33	37	-	53	2	-
19/11/2013	22	10	13	12	8	16	2	20	4	-
28/11/2013	53	43	52	53	33	53	41	53	18	36
05/12/2013	16	10	13	8	8	16	4	20	4	9
14/12/2013	53	6	-	53	-	-	41	-	-	-
21/12/2013	24	10	13	15	8	16	10	20	4	9
30/12/2013	-	-	-	-	-	12	-	-	4	-
06/01/2014	-	-	-	-	-	-	-	-	-	-
15/01/2014	-	-	-	-	-	-	-	-	-	-
22/01/2014	-	8	13	-	8	16	-	20	4	9
31/01/2014	-	-	-	-	-	-	-	-	-	-
07/02/2014	-	-	-	-	-	-	-	-	-	-
16/02/2014	53	43	52	53	-	5	41	-	8	36
23/02/2014	24	10	13	15	8	16	11	20	4	9
04/03/2014	-	-	-	-	-	7	-	-	4	-
11/03/2014	24	10	13	15	8	16	11	20	4	9
20/03/2014	53	43	52	53	33	53	41	53	18	36
27/03/2014	-	-	-	-	1	-	-	2	-	-
05/04/2014	-	-	-	-	-	-	-	-	-	-
12/04/2014	24	10	13	13	8	16	10	20	4	9
21/04/2014	4	-	-	-	-	-	38	-	-	36
28/04/2014	-	-	-	-	6	7	-	3	-	-
07/05/2014	28	17	6	50	33	53	36	53	18	36
14/05/2014	24	10	13	15	8	16	11	20	4	9
23/05/2014	53	-	4	53	-	-	1	-	-	18
30/05/2014	24	6	4	-	7	4	1	14	-	3
08/06/2014	-	-	-	-	-	-	-	-	-	-
15/06/2014	24	10	13	15	8	16	11	20	4	9
24/06/2014	-	9	11	-	-	-	-	-	-	16
01/07/2014	-	-	-	-	-	-	-	-	-	-
10/07/2014	53	27	11	53	-	-	41	-	-	-
17/07/2014	23	9	13	15	-	12	11	5	4	9
26/07/2014	-	-	-	-	33	53	-	53	10	-
02/08/2014	-	-	-	-	-	-	-	-	-	-
11/08/2014	-	-	-	-	33	33	-	53	2	-

18/08/2014	-	9	13	1	8	16	1	20	4	-
27/08/2014	53	14	8	53	-	-	41	-	-	-
03/09/2014	1	-	-	-	1	-	-	-	-	-
12/09/2014	-	6	2	22	17	53	41	44	6	28
19/09/2014	2	-	-	2	-	-	1	20	3	7
05/10/2014	24	8	8	-	2	-	11	10	-	1
14/10/2014	15	-	-	7	10	-	3	-	-	-
21/10/2014	24	8	9	15	2	-	11	7	1	9
30/10/2014	53	43	52	53	-	39	41	16	16	36
06/11/2014	-	1	2	-	-	-	-	-	-	-
15/11/2014	2	-	-	5	-	-	9	-	-	-
22/11/2014	-	2	-	-	-	-	-	-	-	2
01/12/2014	35	-	-	31	6	-	25	14	-	-
08/12/2014	24	10	13	15	8	16	11	20	4	9
17/12/2014	-	-	-	-	33	37	-	53	2	-
24/12/2014	-	-	-	-	-	-	-	-	-	-
02/01/2015	17	-	-	8	-	-	3	-	-	-
09/01/2015	24	10	13	15	8	16	11	20	4	9
18/01/2015	32	-	-	8	6	-	-	10	-	-
25/01/2015	-	1	1	-	-	-	-	4	1	2
03/02/2015	-	7	18	-	-	-	-	-	-	20
10/02/2015	19	10	13	10	8	16	6	20	4	9
19/02/2015	21	43	52	8	33	53	9	53	18	36
26/02/2015	2	-	-	2	-	-	-	-	-	-
07/03/2015	53	43	52	53	33	53	41	53	18	36
14/03/2015	24	10	13	15	-	3	11	-	2	9
23/03/2015	-	9	11	-	-	-	-	-	-	16
30/03/2015	24	1	-	15	8	13	11	20	1	-
08/04/2015	-	-	-	-	-	18	-	18	4	-
15/04/2015	24	-	8	15	8	16	11	-	-	9
01/05/2015	-	-	-	-	-	2	-	-	-	-
10/05/2015	27	7	12	53	33	53	37	53	18	34
17/05/2015	24	6	5	15	7	3	11	13	-	4
26/05/2015	2	-	-	5	25	22	5	53	-	-
02/06/2015	13	2	6	11	8	16	8	20	4	1
11/06/2015	-	14	4	-	-	-	2	-	-	-
18/06/2015	18	-	3	15	8	16	10	20	3	-
27/06/2015	-	-	-	-	33	53	-	53	10	-
04/07/2015	7	10	13	-	8	16	1	20	4	9
13/07/2015	53	36	22	53	-	-	41	-	-	10
20/07/2015	24	10	13	15	8	16	10	20	4	9

Table 11: Landsat 8 overview with obtained pixel count per area

Landsat 8										
Date	**C1**	**C2**	**C3**	**D1**	**D2**	**D3**	**D4**	**SD1**	**SD2**	**SD3**
17/04/2013	24	10	13	15	8	16	11	20	4	9
12/05/2013	24	20	13	15	8	16	11	20	4	9
19/05/2013	24	10	13	15	8	16	11	20	4	9
28/05/2013	24	10	13	15	8	16	11	20	4	9
04/06/2013	24	10	13	15	8	16	11	20	4	9
13/06/2013	24	10	13	15	8	16	11	20	4	9
20/06/2013	24	10	13	15	8	16	11	20	4	9
29/06/2013	24	10	13	15	8	16	11	20	4	9
06/07/2013	24	10	13	15	8	16	11	20	4	9
15/07/2013	24	10	13	15	8	16	11	20	4	9
22/07/2013	24	10	13	15	8	16	11	20	4	9
31/07/2013	24	10	13	15	8	16	11	20	4	9
07/08/2013	24	10	13	15	8	16	11	20	4	9
16/08/2013	24	10	13	15	8	16	11	20	4	9
23/08/2013	24	10	13	15	8	16	11	20	4	9
01/09/2013	24	10	13	15	8	16	11	20	4	9
08/09/2013	24	10	13	15	8	16	11	20	4	9
17/09/2013	24	10	13	15	8	16	11	20	4	9
24/09/2013	24	10	13	15	8	16	11	20	4	9
03/10/2013	24	10	13	15	8	16	11	20	4	9
10/10/2013	24	10	13	15	8	16	11	20	4	9
26/10/2013	24	10	13	15	8	16	11	20	4	9
11/11/2013	24	10	13	15	8	16	11	20	4	9
20/11/2013	24	10	13	15	8	16	11	20	4	9
27/11/2013	24	10	13	15	8	16	11	20	4	9
06/12/2013	24	10	13	15	8	16	11	20	4	9
13/12/2013	24	10	13	15	8	16	11	20	4	9
22/12/2013	24	10	13	15	8	16	11	20	4	9
29/12/2013	24	10	13	15	8	16	11	20	4	9
23/01/2014	24	10	13	15	8	16	11	20	4	9
30/01/2014	24	10	13	15	8	16	11	20	4	9
08/02/2014	24	10	13	15	8	16	11	20	4	9
24/02/2014	24	10	13	15	8	16	11	20	4	9
12/03/2014	24	10	13	15	8	16	11	20	4	9
19/03/2014	24	10	13	15	8	16	11	20	4	9
28/03/2014	24	10	13	15	8	16	11	20	4	9
13/04/2014	24	10	13	15	8	16	11	20	4	9
20/04/2014	24	10	13	15	8	16	11	20	4	9
06/05/2014	24	10	13	15	8	16	11	20	4	9

15/05/2014	24	10	13	15	8	16	11	20	4	9
22/05/2014	24	10	13	15	8	16	11	20	4	9
31/05/2014	24	10	13	15	8	16	11	20	4	9
07/06/2014	24	10	13	15	8	16	11	20	4	9
16/06/2014	24	10	13	15	8	16	11	20	4	9
23/06/2014	24	10	13	15	8	16	11	20	4	9
02/07/2014	24	10	13	15	8	16	11	20	4	9
09/07/2014	24	10	13	15	8	16	11	20	4	9
18/07/2014	24	10	13	15	8	16	11	20	4	9
25/07/2014	24	10	13	15	8	16	11	20	4	9
03/08/2014	24	10	13	15	8	16	11	20	4	9
10/08/2014	24	10	13	15	8	16	11	20	4	9
19/08/2014	24	10	13	15	8	16	11	20	4	9
26/08/2014	24	10	13	15	8	16	11	20	4	9
04/09/2014	24	10	13	15	8	16	11	20	4	9
11/09/2014	24	10	13	15	8	16	11	20	4	9
20/09/2014	24	10	13	15	8	16	11	20	4	9
27/09/2014	24	10	13	15	8	16	11	20	4	9
06/10/2014	24	10	13	15	8	16	11	20	4	9
13/10/2014	24	10	13	15	8	16	11	20	4	9
22/10/2014	24	10	13	15	8	16	11	20	4	9
29/10/2014	24	10	13	15	8	16	11	20	4	9
07/11/2014	24	10	13	15	8	16	11	20	4	9
14/11/2014	24	10	13	15	8	16	11	20	4	9
23/11/2014	24	10	13	15	8	16	11	20	4	9
30/11/2014	24	10	13	15	8	16	11	20	4	9
09/12/2014	24	10	13	15	8	16	11	20	4	9
16/12/2014	24	10	13	15	8	16	11	20	4	9
25/12/2014	24	10	13	15	8	16	11	20	4	9
01/01/2015	24	10	13	15	8	16	11	20	4	9
10/01/2015	24	10	13	15	8	16	11	20	4	9
17/01/2015	24	10	13	15	8	16	11	20	4	9
26/01/2015	24	10	13	15	8	16	11	20	4	9
02/02/2015	24	10	13	15	8	16	11	20	4	9
11/02/2015	24	10	13	15	8	16	11	20	4	9
18/02/2015	24	10	13	15	8	16	11	20	4	9
27/02/2015	24	10	13	15	8	16	11	20	4	9
06/03/2015	24	10	13	15	8	16	11	20	4	9
15/03/2015	24	10	13	15	8	16	11	20	4	9
22/03/2015	24	10	13	15	8	16	11	20	4	9
31/03/2015	24	10	13	15	8	16	11	20	4	9
07/04/2015	24	10	13	15	8	16	11	20	4	9
16/04/2015	24	10	13	15	8	16	11	20	4	9

23/04/2015	24	10	13	15	8	16	11	20	4	9
02/05/2015	24	10	13	15	8	16	11	20	4	9
09/05/2015	24	10	13	15	8	16	11	20	4	9
18/05/2015	24	10	13	15	8	16	11	20	4	9
25/05/2015	24	10	13	15	8	16	11	20	4	9
03/06/2015	24	10	13	15	8	16	11	20	4	9
10/06/2015	24	10	13	15	8	16	11	20	4	9
19/06/2015	24	10	13	15	8	16	11	20	4	9
26/06/2015	24	10	13	15	8	16	11	20	4	9
05/07/2015	24	10	13	15	8	16	11	20	4	9
12/07/2015	24	10	13	15	8	16	11	20	4	9
21/07/2015	24	10	13	15	8	16	11	20	4	9
28/07/2015	24	10	13	15	8	16	11	20	4	9
06/08/2015	24	10	13	15	8	16	11	20	4	9
13/08/2015	24	10	13	15	8	16	11	20	4	9
22/08/2015	24	10	13	15	8	16	11	20	4	9
29/08/2015	24	10	13	15	8	16	11	20	4	9

9. APPENDIX B: GRASS STEP BY STEP PROCESSING

The processing of the data is separated into three scripts:

- Runbatch
- L7
- L8

This was done for managing purposes and reusability of the scripts.

9.1 RUNBATCH

This script is telling GRASS where the folders are with the satellite images and run either L7 or L8 for each of the satellite scenes in the folder.

```
###Parameters###

#location on Script files
loc_s=/home/username/scripts/

#Landsat scene location
loc_scene=/home/username/scenes/

#GRASS workspace location
loc_m=/home/username/GRASS_loc/

#Location of shape and raster files of study area
input=/home/username/input/

#Output location for extracted number files
OP=/home/username/output/

###user input###

#Give the name of the script to be used (L7 or L8)
echo "Give script name to be run in GRASS:"
read script

#Give name of the mapset to be used in GRASS
echo "State mapset for GRASS:"
read mapset

###Export variables###

export loc_s
export loc_scene
export input
export OP

###Run BATCH###

Do
       export file
```

```
        #run GRASS with script
        chmod u+x $loc_s$script
        grass70 $loc_m$mapset
done
```

The script is separated into three sections to keep it clear. The first section, Parameters, is used to define parameters that are static throughout the running of the script and contains location information. The second section, user input, is to enable some input to the user of the script. In this case which script has to be used and in which GRASS mapset do the calculations take place. The read command enables the user to give a value to the parameter. Using this it is easy to switch some parameters between the sections user input and parameters. The third section, export variables, exports the parameters that are now defined so that they can be accessed and called upon when GRASS is running the script. The fourth section, run BATCH, is used to run the chosen script for each Landsat scene in the designated folder.

9.2 L7

This script is designed for the use with Landsat 7 imagery. By using the parameters set by runbatch GRASS is able to apply all commands to the imagery.

```
###import boundaries###

v.in.ogr -o --overwrite --quiet $input/Boundary.shp output=Varzea_R
v.in.ogr -o --overwrite --quiet $input/C1.shp output=C1
v.in.ogr -o --overwrite --quiet $input/C2.shp output=C2
v.in.ogr -o --overwrite --quiet $input/C3.shp output=C3
v.in.ogr -o --overwrite --quiet $input/SD1.shp output=SD1
v.in.ogr -o --overwrite --quiet $input/SD2.shp output=SD2
v.in.ogr -o --overwrite --quiet $input/SD3.shp output=SD3
v.in.ogr -o --overwrite --quiet $input/D1.shp output=D1
v.in.ogr -o --overwrite --quiet $input/D2.shp output=D2
v.in.ogr -o --overwrite --quiet $input/D3.shp output=D3
v.in.ogr -o --overwrite --quiet $input/D4.shp output=D4
```

The first section of the script, import boundaries, imports the study site boundary of Calde and the separate slopes.

```
###set boundary mask###
r.mask --overwrite --quiet vector=Calde_R
```

The second section, set boundary mask, is used to limit the processing of the satellite imagery to only the study area. This is done to save on processing power and time.

```
###import data###
r.in.gdal --overwrite --quiet input=$loc_scene$(basename "$file" .tif/$(basename
"$file" .tif)´_B1.TIF´ output=S_B1
r.in.gdal --overwrite --quiet input=$loc_scene$(basename "$file" .tif/$(basename
"$file" .tif)´_B2.TIF´ output=S_B2
r.in.gdal --overwrite --quiet input=$loc_scene$(basename "$file" .tif/$(basename
"$file" .tif)´_B3.TIF´ output=S_B3
r.in.gdal --overwrite --quiet input=$loc_scene$(basename "$file" .tif/$(basename
"$file" .tif)´_B4.TIF´ output=S_B4
r.in.gdal --overwrite --quiet input=$loc_scene$(basename "$file" .tif/$(basename
"$file" .tif)´_B5.TIF´ output=S_B5
r.in.gdal --overwrite --quiet input=$loc_scene$(basename "$file" .tif/$(basename
"$file" .tif)´_B61.TIF´ output=S_B61
r.in.gdal --overwrite --quiet input=$loc_scene$(basename "$file" .tif/$(basename
"$file" .tif)´_B62.TIF´ output=S_B62
r.in.gdal --overwrite --quiet input=$loc_scene$(basename "$file" .tif/$(basename
"$file" .tif)´_B7.TIF´ output=S_B7
r.in.gdal --overwrite --quiet input=$loc_scene$(basename "$file" .tif/$(basename
"$file" .tif)´_B8.TIF´ output=S_B8
```

The third section is used to import all bands of the designated scene into GRASS. Note that there are 9 bands in total.

```
###toar convertion###
i.landsat.toar --quiet --overwrite input=S_B output=S_B.Toar
metfile=$loc_scene$(basename "$file" .tif)/$(basename "$file" .tif)´_MTL.TXT`
```

The fourth section is used to perform the conversion of DN to top of atmosphere reflection. This is done by taking the correction values that are provided by USGS with the Landsat metadata file, MTL.txt, and applying them in the conversion formulas.

```
###ACCA###
i.landsat.acca --overwrite input=S_B.Toar output=acca
r.mapcalc –o --quiet "ACCA2 = if(`acca´ > 0 , 0 , 0 )"
r.null --quiet map=ACCA2 null=1
r.mapcalc --o --quiet "ACCA_B1 = ´ACCA2´ * ´S_B.Toar1´"
r.mapcalc --o --quiet "ACCA_B2 = ´ACCA2´ * ´S_B.Toar2´"
r.mapcalc --o --quiet "ACCA_B3 = ´ACCA2´ * ´S_B.Toar3´"
r.mapcalc --o --quiet "ACCA_B4 = ´ACCA2´ * ´S_B.Toar4´"
r.mapcalc --o --quiet "ACCA_B5 = ´ACCA2´ * ´S_B.Toar5´"
```

```
r.mapcalc --o --quiet "ACCA_B61 = ´ACCA2´ * ´S_B.Toar61´"
r.mapcalc --o --quiet "ACCA_B62 = ´ACCA2´ * ´S_B.Toar62´"
r.mapcalc --o --quiet "ACCA_B7 = ´ACCA2´ * ´S_B.Toar7´"
r.mapcalc --o --quiet "ACCA_B8 = ´ACCA2´ * ´S_B.Toar8´"
```

The fifth section applies the automatic cloud detection or ACCA (IRISH et al., 2006) to the Landsat scene using the top of atmosphere reflection calculated in section four. The r.mapcalc command creates a map where cloud cover has the value 0 and the rest is considered empty. To rectify this r.null is used to change all empty cells to value one creating a cloud mask. The last r.mapcalc commands applies the calculated cloud mask to the top of atmosphere reflection bands so that only the pixels without clouds remain and the other pixels have value 0 resulting in uncalculatable indices later on.

```
###Apply VGI###
r.mapcalc --o --quiet "SR = (´ACCA_B4` / ´ACCA_B3´)"
r.mapcalc --o --quiet "DVI = (´ACCA_B4` - ´ACCA_B3`)"
r.mapcalc --o --quiet "NDVI = (´ACCA_B4` - ´ACCA_B3`) / (´ACCA_B4` + ´ACCA_B3`)"
r.mapcalc --o --quiet "NDVIG = (´ACCA_B4` - ´ACCA_B2`) / (´ACCA_B4` +
´ACCA_B2`)"
r.mapcalc --o --quiet "IPVI = ´ACCA_B4` / (´ACCA_B4` + ´ACCA_B3`)"
r.mapcalc --o --quiet "SAVI = ((´ACCA_B4` - ´ACCA_B3`) / (´ACCA_B4` + ´ACCA_B3`
+ 0.5)) * 1.5"
r.mapcalc --o --quiet "MSAVI = (2 * ´ACCA_B4` + 1 - sqrt(2 * ´ACCA_B4` + 1, 2) -
8 * (´ACCA_B4` - ´ACCA_B3`)) / 2)"
r.mapcalc --o --quiet "OSAVI = (1.5 * (´ACCA_B4` - ´ACCA_B3`)) / (´ACCA_B4` +
´ACCA_B3` + 0.16)"
r.mapcalc --o --quiet "NDWI = (´ACCA_B4` - ´ACCA_B5`) / (´ACCA_B4` + ´ACCA_B5`)"
r.mapcalc --o --quiet "EVI = ((´ACCA_B4` - ´ACCA_B3`) / (´ACCA_B4` + (6 *
´ACCA_B3`) - (7.5 * ´ACCA_B1`) + 1)) +2"
r.mapcalc --o --quiet "ARVI = (´ACCA_B4` - (2 * ´ACCA_B3` - ´ACCA_B1`)) /
(´ACCA_B4` + (2 * ´ACCA_B3` - ´ACCA_B1`))"
r.mapcalc --o --quiet "VARI = (´ACCA_B2` - ´ACCA_B3`) / (´ACCA_B2` + ´ACCA_B3` -
´ACCA_B1`)"
r.mapcalc --o --quiet "NBR = 1000 * ((´ACCA_B4` - ´ACCA_B7`) / (´ACCA_B4` +
´ACCA_B7`)"
r.mapcalc --o --quiet "GEMI = ((2 * (pow(´ACCA_B4` , 2) - pow(´ACCA_B3` , 2)) +
1.5 * ´ACCA_B4` + 0.5 * ´ACCA_B3`) / (´ACCA_B4` + ´ACCA_B3´ + 0.5)) * (1 - 0.25
* ((2 * (pow(´ACCA_B4` , 2) - pow(´ACCA_B3` , 2)) + 1.5 * ´ACCA_B4` + 0.5 *
´ACCA_B3`) / (´ACCA_B4` + ´ACCA_B3` + 0.5))) - ((´ACCA_B3` - 0.125) / (1 -
´ACCA_B3`))"
```

The sixth section applies all chosen vegetation indices. The formulas have been adapted to GRASS syntax. This step creates maps of the entire study area for all indices.

```
###Extract values###
r.mask --overwrite --quiet vector=C1

r.stats -n -1 -c --overwrite --quiet input=SR separator=pipe
output=$OP$(basename "$file" .tif)´_C1_SR´
r.stats -n -1 -c --overwrite --quiet input=DVI separator=pipe
output=$OP$(basename "$file" .tif)´_C1_DVI´
r.stats -n -1 -c --overwrite --quiet input=NDVI separator=pipe
output=$OP$(basename "$file" .tif)´_C1_NDVI´
r.stats -n -1 -c --overwrite --quiet input=NDVIG separator=pipe
output=$OP$(basename "$file" .tif)´_C1_NDVIG´
r.stats -n -1 -c --overwrite --quiet input=IPVI separator=pipe
output=$OP$(basename "$file" .tif)´_C1_IPVI´
r.stats -n -1 -c --overwrite --quiet input=SAVI separator=pipe
output=$OP$(basename "$file" .tif)´_C1_SAVI´
r.stats -n -1 -c --overwrite --quiet input=MSAVI separator=pipe
output=$OP$(basename "$file" .tif)´_C1_MSAVI´
r.stats -n -1 -c --overwrite --quiet input=OSAVI separator=pipe
output=$OP$(basename "$file" .tif)´_C1_OSAVI´
r.stats -n -1 -c --overwrite --quiet input=NDWI separator=pipe
output=$OP$(basename "$file" .tif)´_C1_NDWI´
r.stats -n -1 -c --overwrite --quiet input=EVI separator=pipe
output=$OP$(basename "$file" .tif)´_C1_EVI´
r.stats -n -1 -c --overwrite --quiet input=ARVI separator=pipe
output=$OP$(basename "$file" .tif)´_C1_ARVI´
r.stats -n -1 -c --overwrite --quiet input=VARI separator=pipe
output=$OP$(basename "$file" .tif)´_C1_VARI´
r.stats -n -1 -c --overwrite --quiet input=NBR separator=pipe
output=$OP$(basename "$file" .tif)´_C1_NBR´
r.stats -n -1 -c --overwrite --quiet input=GEMI separator=pipe
output=$OP$(basename "$file" .tif)´_C1_GEMI´


r.stats -n -1 -c --overwrite --quiet input=S_B.Toar1 separator=pipe
output=$OP$(basename "$file" .tif)´_C1_B1´
r.stats -n -1 -c --overwrite --quiet input= S_B.Toar2 separator=pipe
output=$OP$(basename "$file" .tif)´_C1_B2´
r.stats -n -1 -c --overwrite --quiet input= S_B.Toar3 separator=pipe
output=$OP$(basename "$file" .tif)´_C1_B3´
r.stats -n -1 -c --overwrite --quiet input= S_B.Toar4 separator=pipe
output=$OP$(basename "$file" .tif)´_C1_B4´
r.stats -n -1 -c --overwrite --quiet input= S_B.Toar5 separator=pipe
output=$OP$(basename "$file" .tif)´_C1_B5´
r.stats -n -1 -c --overwrite --quiet input= S_B.Toar61 separator=pipe
output=$OP$(basename "$file" .tif)´_C1_B61´
```

```
r.stats –n -1 –c --overwrite --quiet input= S_B.Toar62 separator=pipe
output=$OP$(basename "$file" .tif)´_C1_B62´
r.stats –n -1 –c --overwrite --quiet input= S_B.Toar7 separator=pipe
output=$OP$(basename "$file" .tif)´_C1_B7´
r.stats –n -1 –c --overwrite --quiet input= S_B.Toar8 separator=pipe
output=$OP$(basename "$file" .tif)´_C1_B8´
```

The seventh section extracts all values, in this case for slope C1, and saves them in an ascii file format in the output folder. This section is repeated for each slope and C1 is replaced by the slope in question. To clarify all values of the vegetation indices as well as the reflectance band values are extracted.

```
###remove temporary files###
g.remove –f --quiet type=raster name=S_B1
g.remove –f --quiet type=raster name=S_B2
g.remove –f --quiet type=raster name=S_B3
g.remove –f --quiet type=raster name=S_B4
g.remove –f --quiet type=raster name=S_B5
g.remove –f --quiet type=raster name=S_B61
g.remove –f --quiet type=raster name=S_B62
g.remove –f --quiet type=raster name=S_B7
g.remove –f --quiet type=raster name=S_B8

g.remove –f --quiet type=raster name=S_B.Toar1
g.remove –f --quiet type=raster name=S_B.Toar2
g.remove –f --quiet type=raster name=S_B.Toar3
g.remove –f --quiet type=raster name=S_B.Toar4
g.remove –f --quiet type=raster name=S_B.Toar5
g.remove –f --quiet type=raster name=S_B.Toar61
g.remove –f --quiet type=raster name=S_B.Toar62
g.remove –f --quiet type=raster name=S_B.Toar7
g.remove –f --quiet type=raster name=S_B.Toar8

g.remove –f --quiet type=raster name=S_B_Toar1
g.remove –f --quiet type=raster name=S_B_Toar2
g.remove –f --quiet type=raster name=S_B_Toar3
g.remove –f --quiet type=raster name=S_B_Toar4
g.remove –f --quiet type=raster name=S_B_Toar5
g.remove –f --quiet type=raster name=S_B_Toar61
g.remove –f --quiet type=raster name=S_B_Toar62
g.remove –f --quiet type=raster name=S_B_Toar7
g.remove –f --quiet type=raster name=S_B_Toar8
```

```
g.remove -f --quiet type=raster name=ACCA_B1
g.remove -f --quiet type=raster name=ACCA_B2
g.remove -f --quiet type=raster name=ACCA_B3
g.remove -f --quiet type=raster name=ACCA_B4
g.remove -f --quiet type=raster name=ACCA_B5
g.remove -f --quiet type=raster name=ACCA_B61
g.remove -f --quiet type=raster name=ACCA_B62
g.remove -f --quiet type=raster name=ACCA_B7
g.remove -f --quiet type=raster name=ACCA_B8

g.remove -f --quiet type=raster name=SR
g.remove -f --quiet type=raster name=DVI
g.remove -f --quiet type=raster name=NDVI
g.remove -f --quiet type=raster name=NDVIG
g.remove -f --quiet type=raster name=IPVI
g.remove -f --quiet type=raster name=SAVI
g.remove -f --quiet type=raster name=MSAVI
g.remove -f --quiet type=raster name=OSAVI
g.remove -f --quiet type=raster name=NDWI
g.remove -f --quiet type=raster name=EVI
g.remove -f --quiet type=raster name=ARVI
g.remove -f --quiet type=raster name=VARI
g.remove -f --quiet type=raster name=NBR
g.remove -f --quiet type=raster name=GEMI


g.remove -f --quiet type=raster name=acca
g.remove -f --quiet type=raster name=ACCA2
g.remove -f --quiet type=raster name=MASK
g.remove -f --quiet type=vector name=C1
g.remove -f --quiet type=vector name=C2
g.remove -f --quiet type=vector name=C3
g.remove -f --quiet type=vector name=SD1
g.remove -f --quiet type=vector name=SD2
g.remove -f --quiet type=vector name=SD3
g.remove -f --quiet type=vector name=D1
g.remove -f --quiet type=vector name=D2
g.remove -f --quiet type=vector name=D3
g.remove -f --quiet type=vector name=D4
g.remove -f --quiet type=vector name=Calde_R
```

The eighth and final section removes all redundant data that has been created.

9.3 L8

The Landsat 8 script has a similar structure but differs from the Landsat 7 script in a few areas. First difference is that there are more bands in a Landsat 8 image than in Landsat 7. Therefore in the script a few adjustments had to be made. In the sections where bands are referred to have to be adapted to include all bands and when loading the data also include the BQA band. In section six the band number have to be converted. This was done by using Table 12.

Table 12: Landsat 7 and 8 band comparison

Landsat 7	Band name	Landsat 8
-	Coastal aerosol	Band 1
Band 1	Blue	Band 2
Band 2	Green	Band 3
Band 3	Red	Band 4
Band 4	NIR	Band 5
Band 5	SWIR1	Band 6
Band 7	SWIR2	Band 7
Band 8	Panchromatic	Band 8
-	Cirrus	Band 9
Band 61	TIRS1	Band 10
Band 62	TIRS2	Band 11

Another adaption is the ACCA calculation, as the USGS already provides this information in the band quality assessment file provided with each Landsat 8 scene. Section five, ACCA, is therefore replaced with the following.

```
###Apply BQA###
r.mapcalc --o --quiet "ACCA2 = if(´BQA´ == 49152, null(), 1 )"
r.mapcalc --o --quiet "ACCA_B1 = ´ACCA2´ * ´S_B.Toar1´"
r.mapcalc --o --quiet "ACCA_B2 = ´ACCA2´ * ´S_B.Toar2´"
r.mapcalc --o --quiet "ACCA_B3 = ´ACCA2´ * ´S_B.Toar3´"
r.mapcalc --o --quiet "ACCA_B4 = ´ACCA2´ * ´S_B.Toar4´"
r.mapcalc --o --quiet "ACCA_B5 = ´ACCA2´ * ´S_B.Toar5´"
r.mapcalc --o --quiet "ACCA_B6 = ´ACCA2´ * ´S_B.Toar6´"
r.mapcalc --o --quiet "ACCA_B7 = ´ACCA2´ * ´S_B.Toar7´"
r.mapcalc --o --quiet "ACCA_B8 = ´ACCA2´ * ´S_B.Toar8´"
r.mapcalc --o --quiet "ACCA_B9 = ´ACCA2´ * ´S_B.Toar9´"
r.mapcalc --o --quiet "ACCA_B10 = ´ACCA2´ * ´S_B.Toar10´"
```

```
r.mapcalc --o --quiet "ACCA_B11 = ´ACCA2´ * ´S_B.Toar11´"
```

The value 49152 is the value for any type of cloud in the BQA band and the r.mapcalc command replaces the pixels covered with clouds with a no data value and the rest with one. So that only pixels without clouds have values.

10. APPENDIX C: GRAPHS OF THE VEGETATION INDEX VALUES COMPUTED FOR LANDSAT 7 AND 8

Appendix C contains the graphs of the vegetation index values obtained per burned area per time period, computed by using Landsat 7 images (10.1) and Landsat 8 images (10.2)

10.1 LANDSAT 7

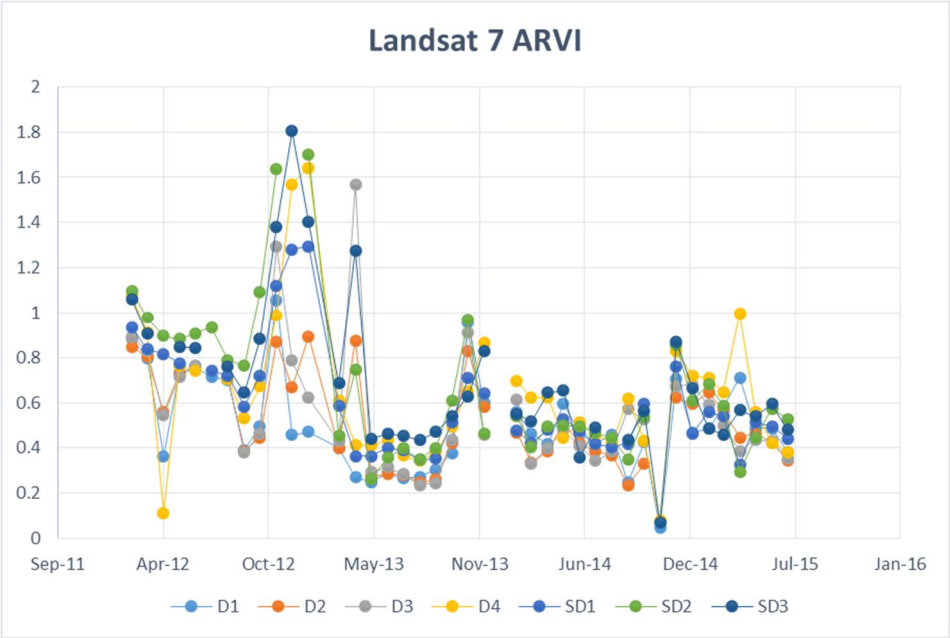

Figure 15: Landsat 7 ARVI

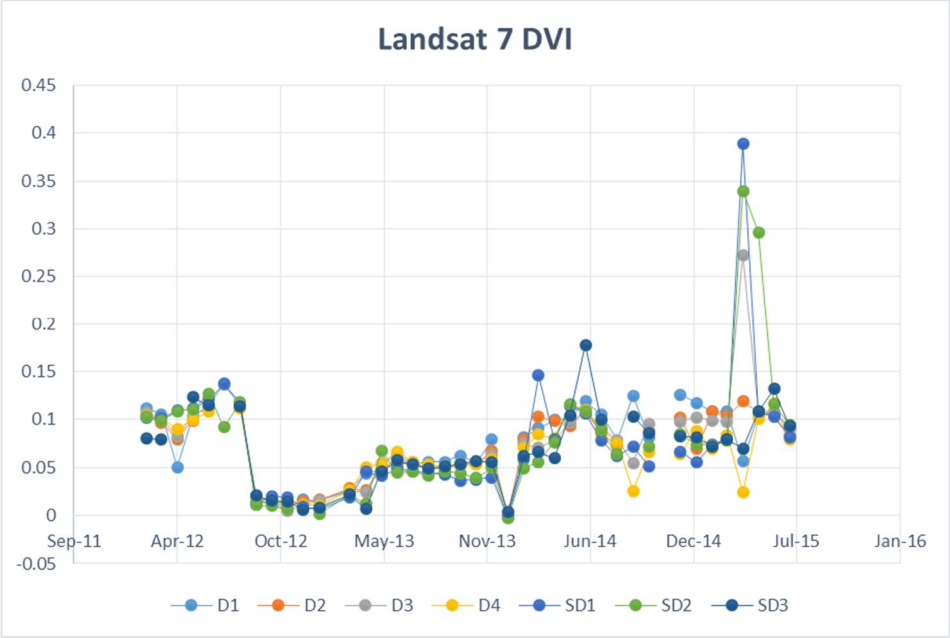

Figure 16: Landsat 7 DVI

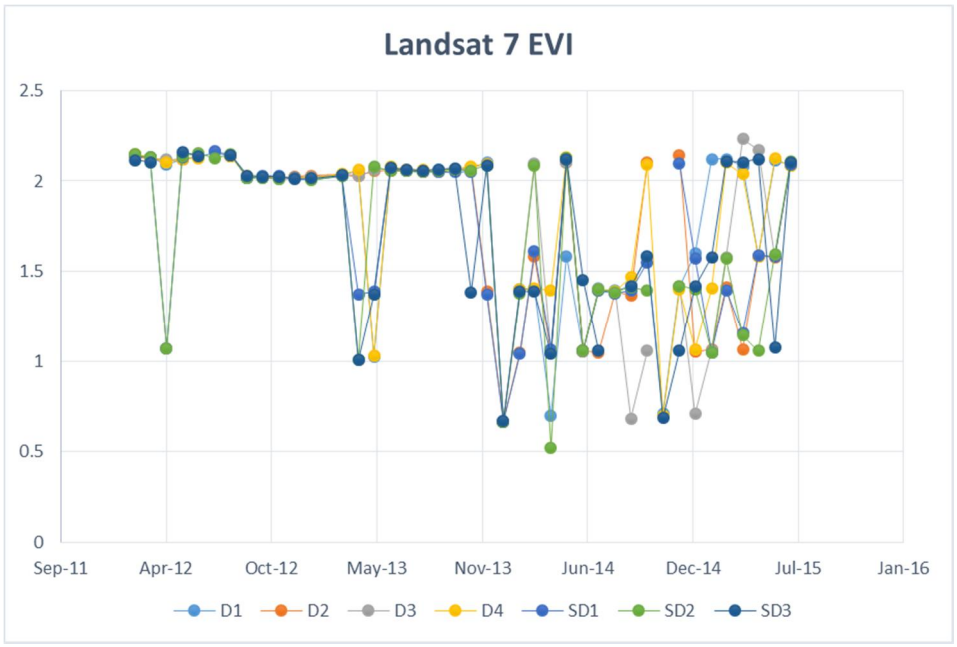

Figure 17: Landsat 7 EVI

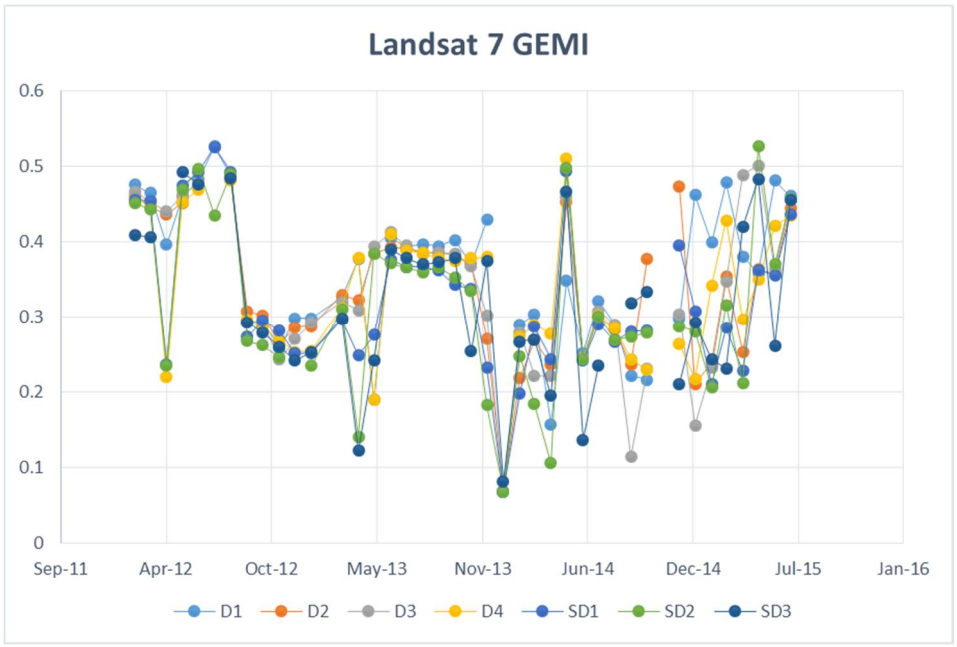

Figure 18: Landsat 7 GEMI

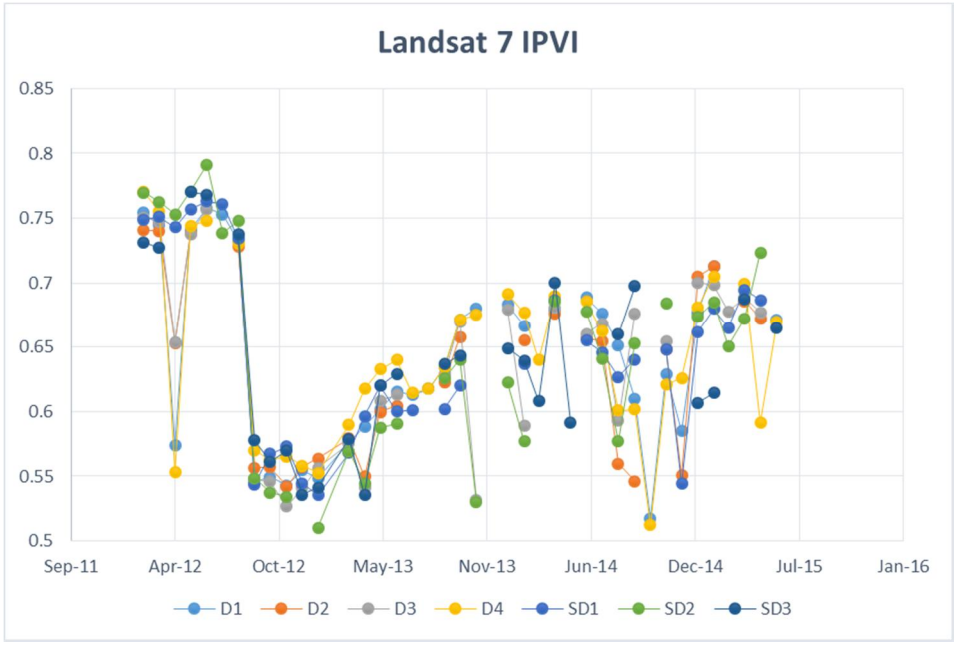

Figure 19: Landsat 7 IPVI

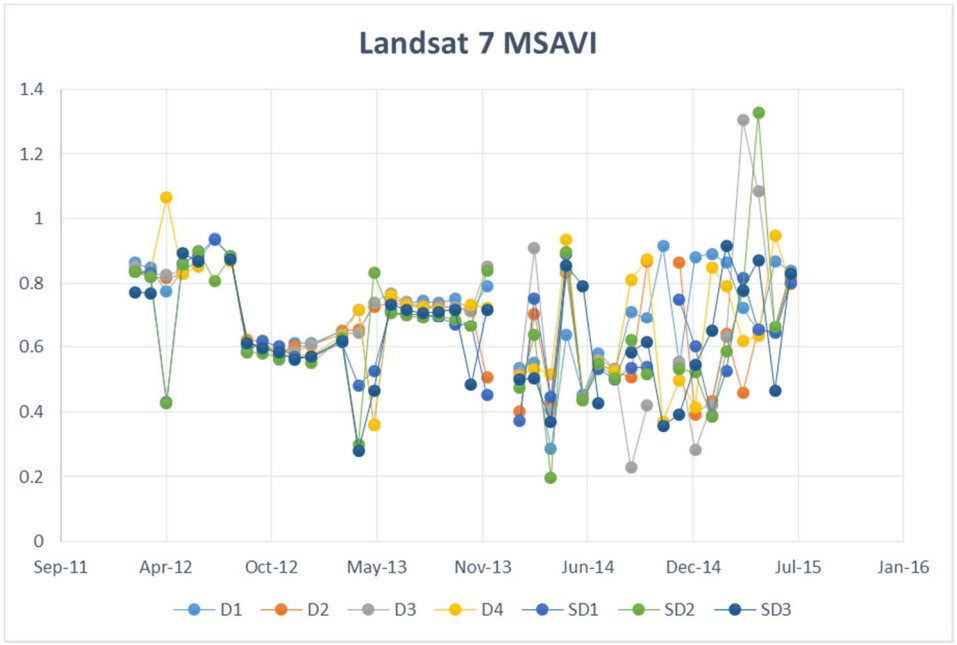

Figure 20: Landsat 7 MSAVI

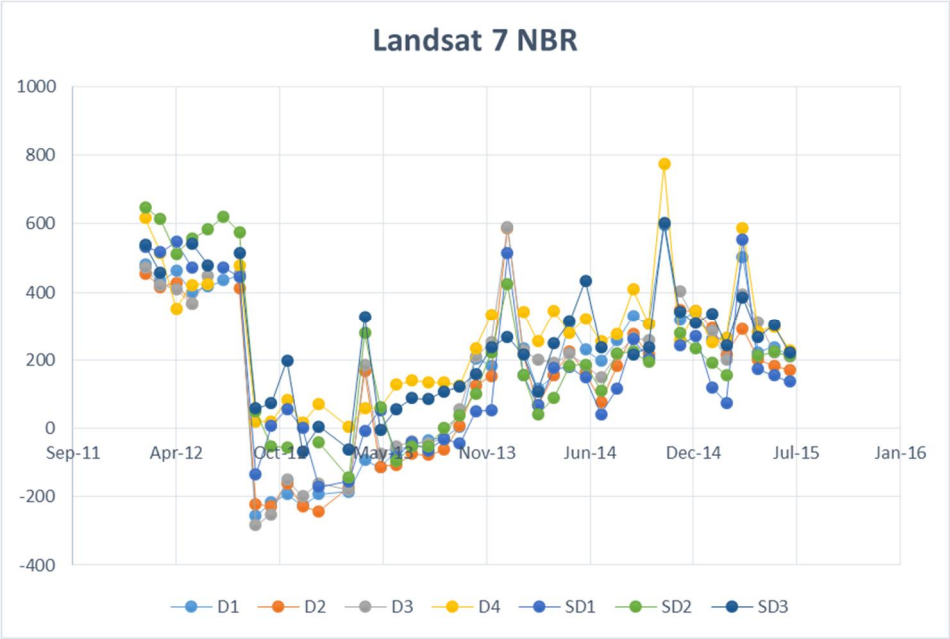

Figure 21: Landsat 7 NBR

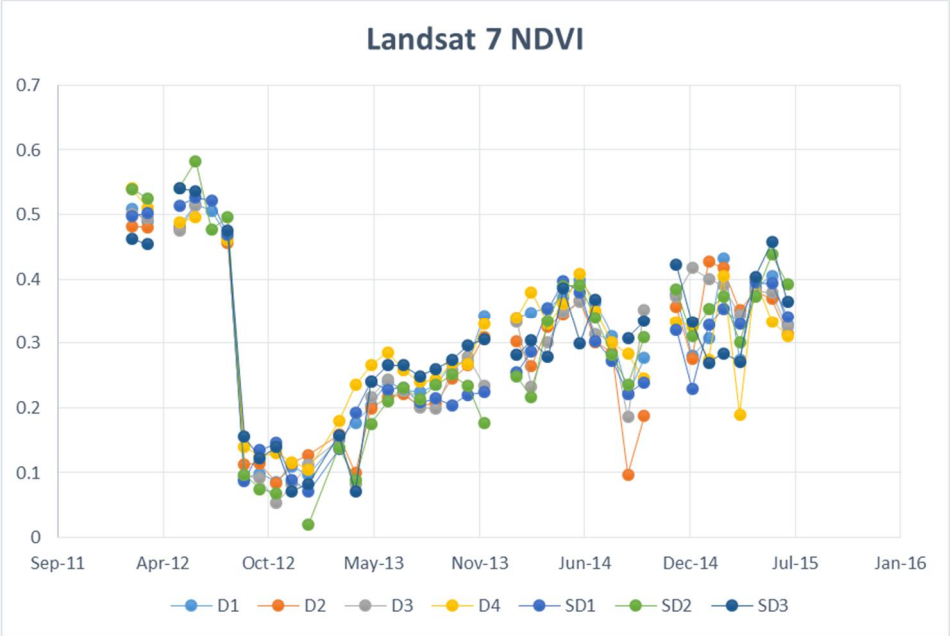

Figure 22: Landsat 7 NDVI

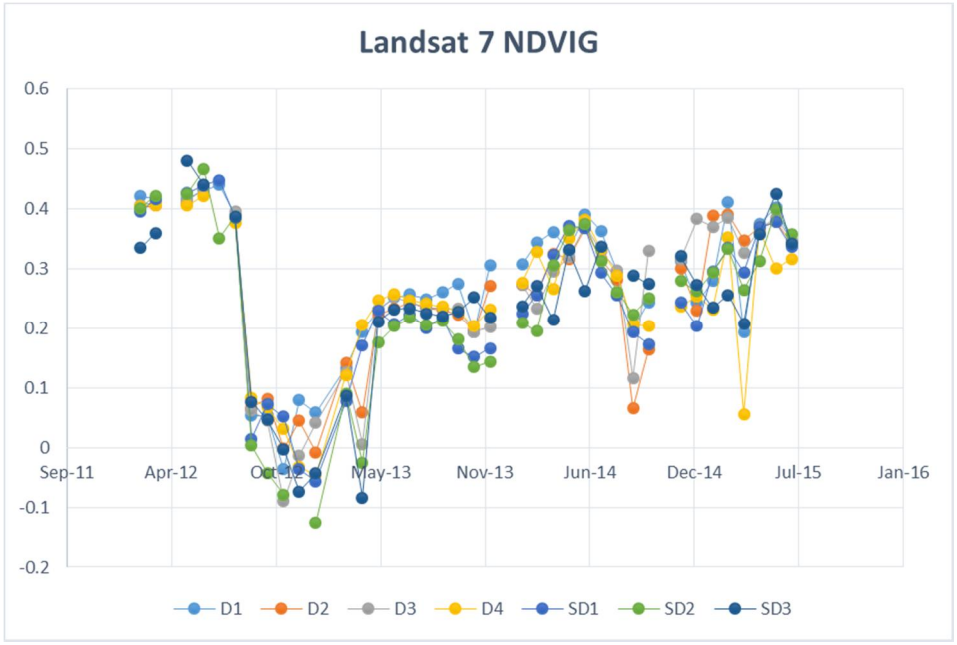

Figure 23: Landsat 7 NDVI green

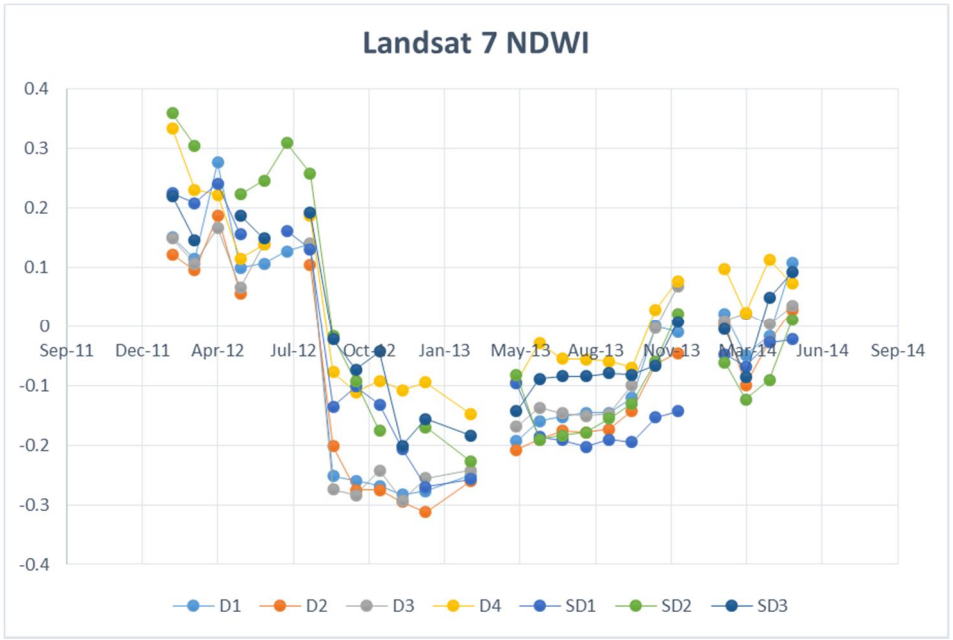

Figure 24: Landsat 7 NDWI

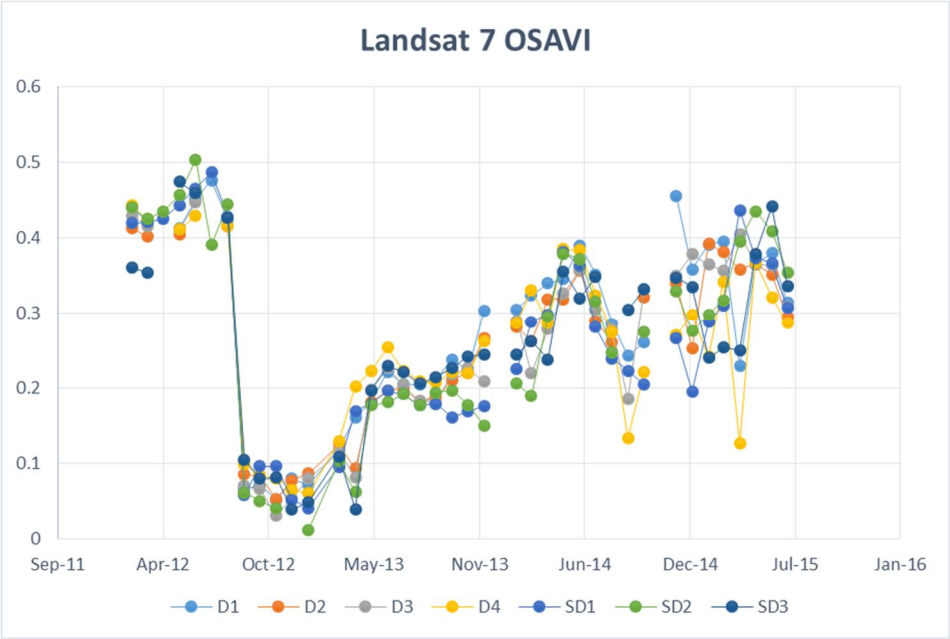

Figure 25: Landsat 7 OSAVI

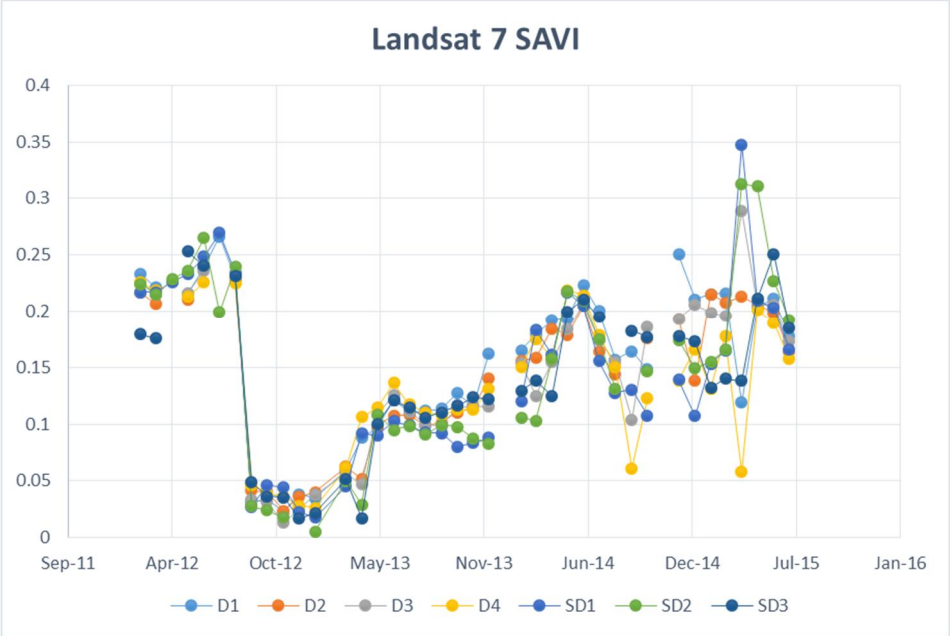

Figure 26: Landsat 7 SAVI

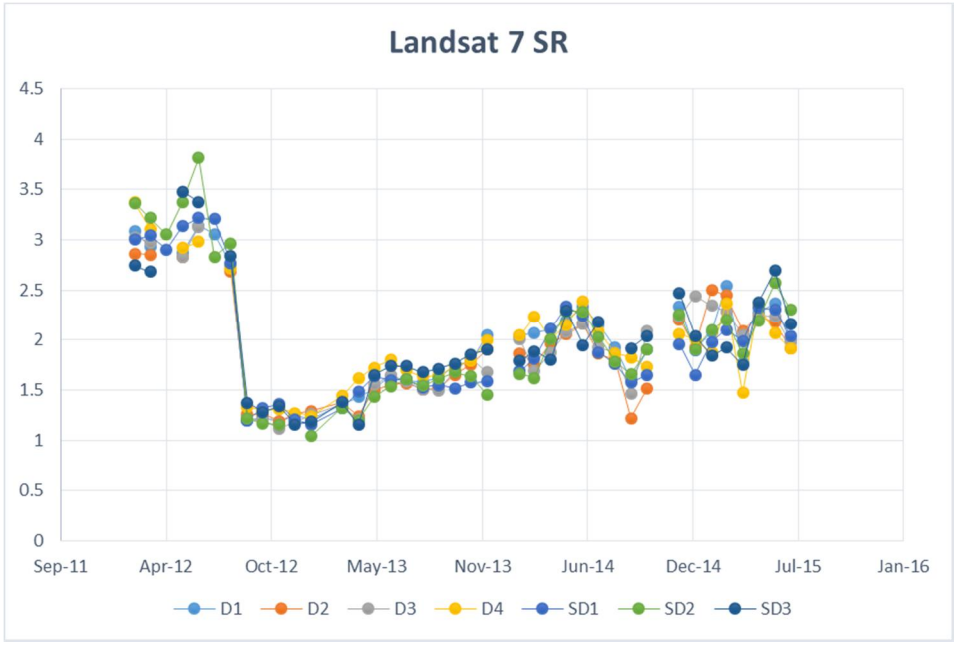

Figure 27: Landsat 7 SR

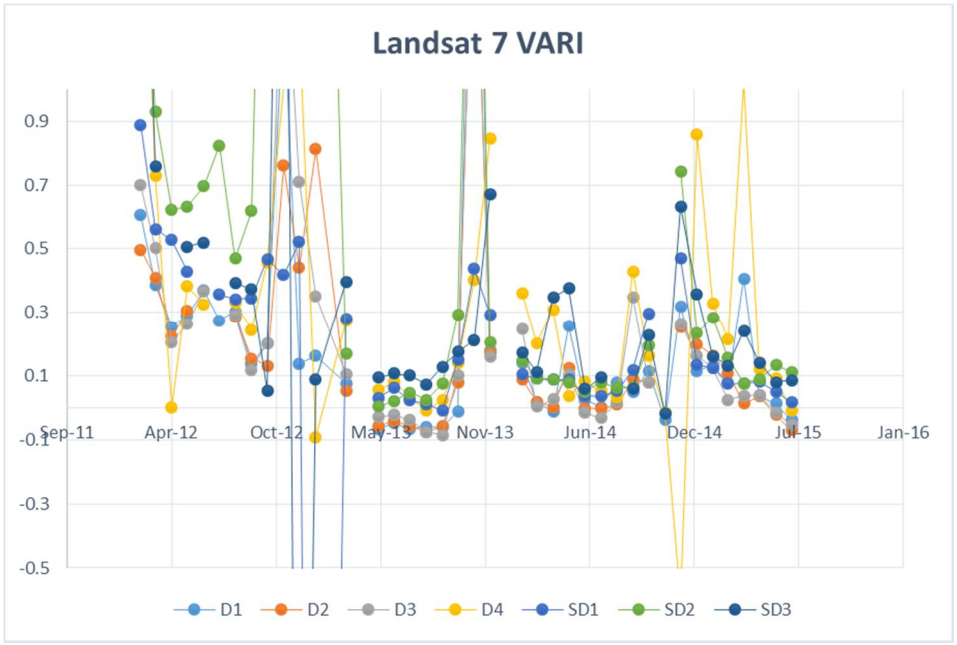

Figure 28: Landsat 7 VARI

10.2 LANDSAT 8

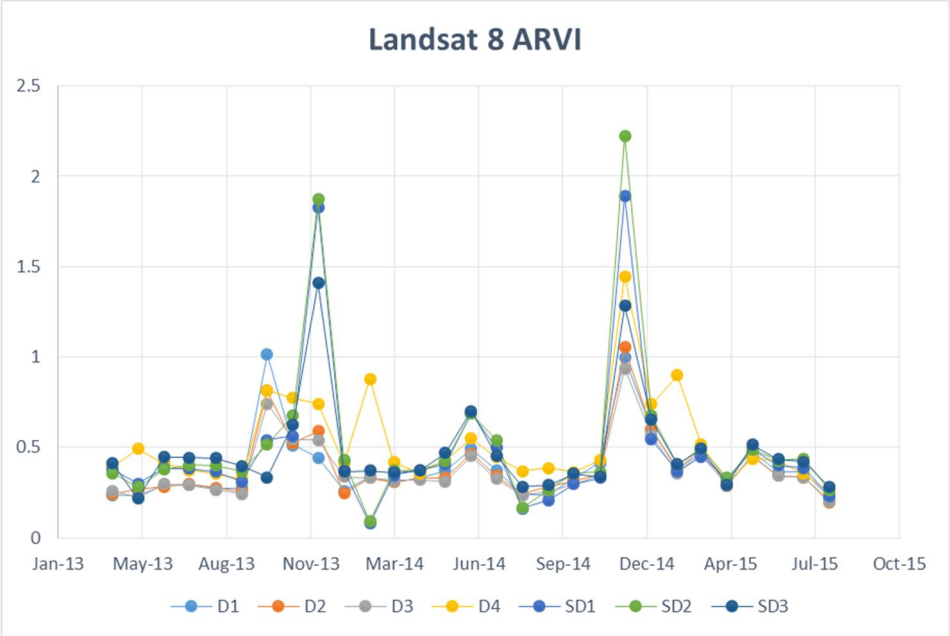

Figure 29: Landsat 8 ARVI

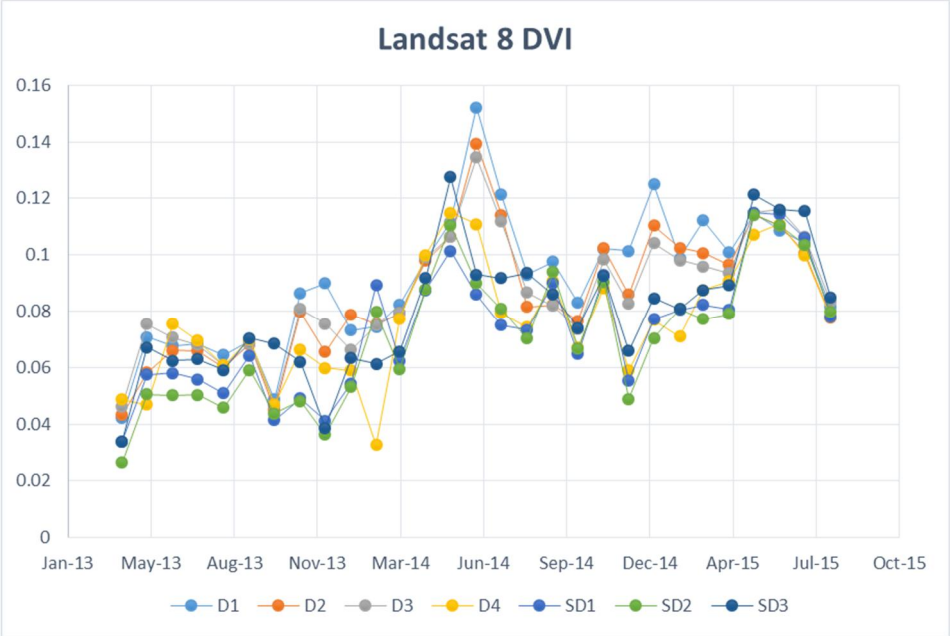

Figure 30: Landsat 8 DVI

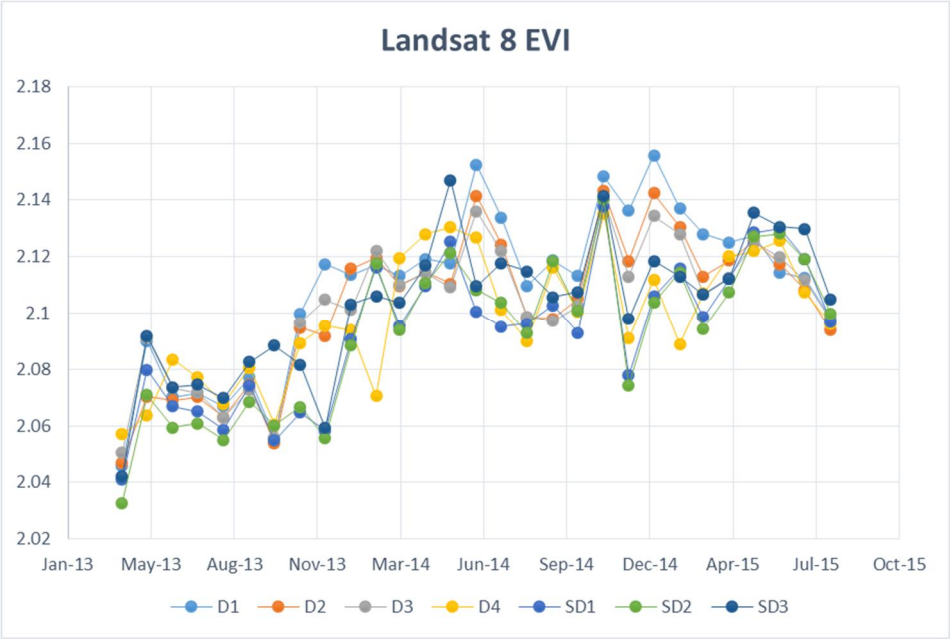

Figure 31: Landsat 8 EVI

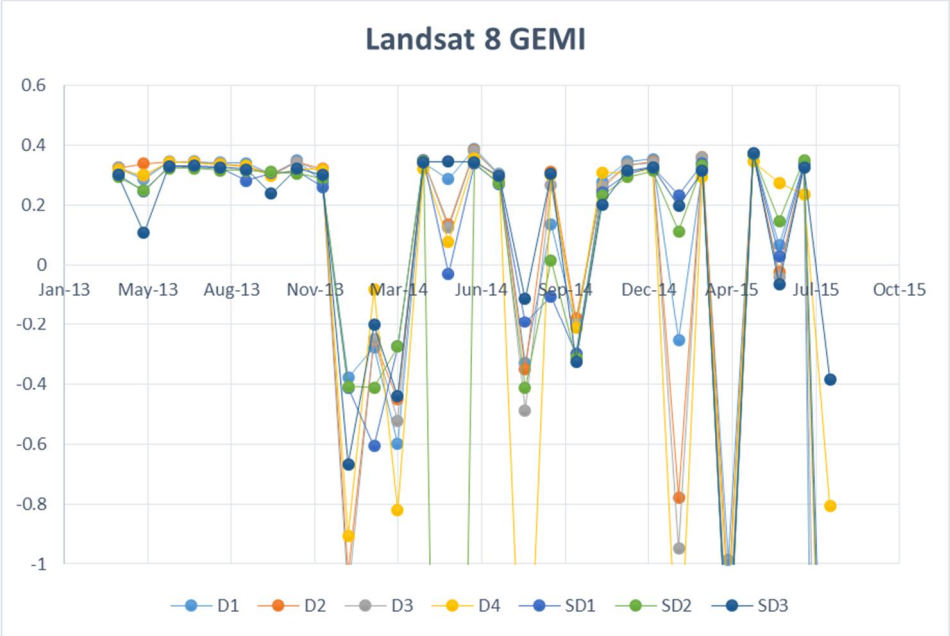

Figure 32: Landsat 8 GEMI

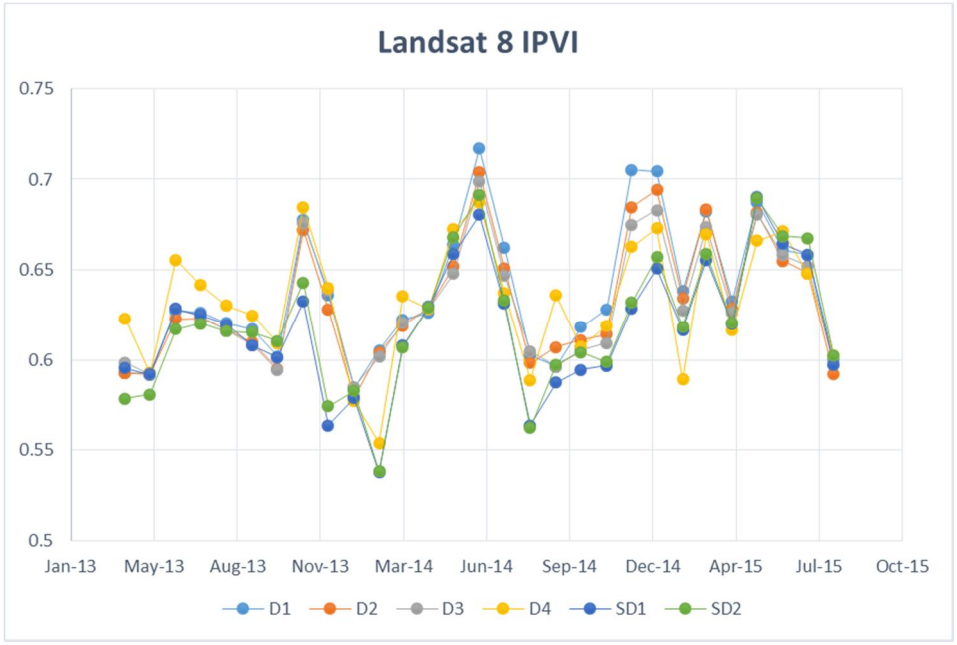

Figure 33: Landsat 8 IPVI

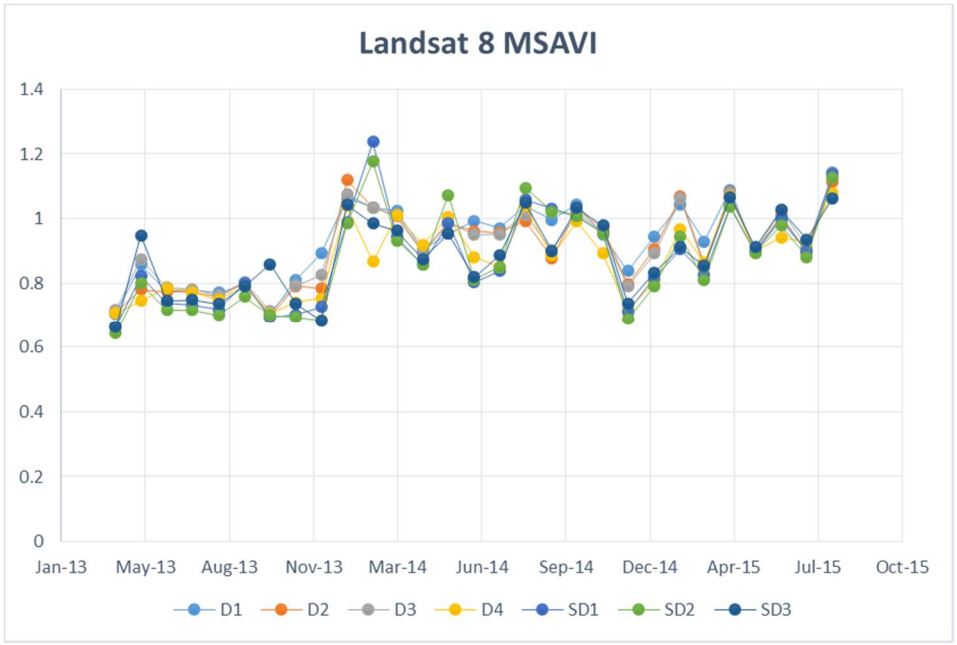

Figure 34: Landsat 8 MSAVI

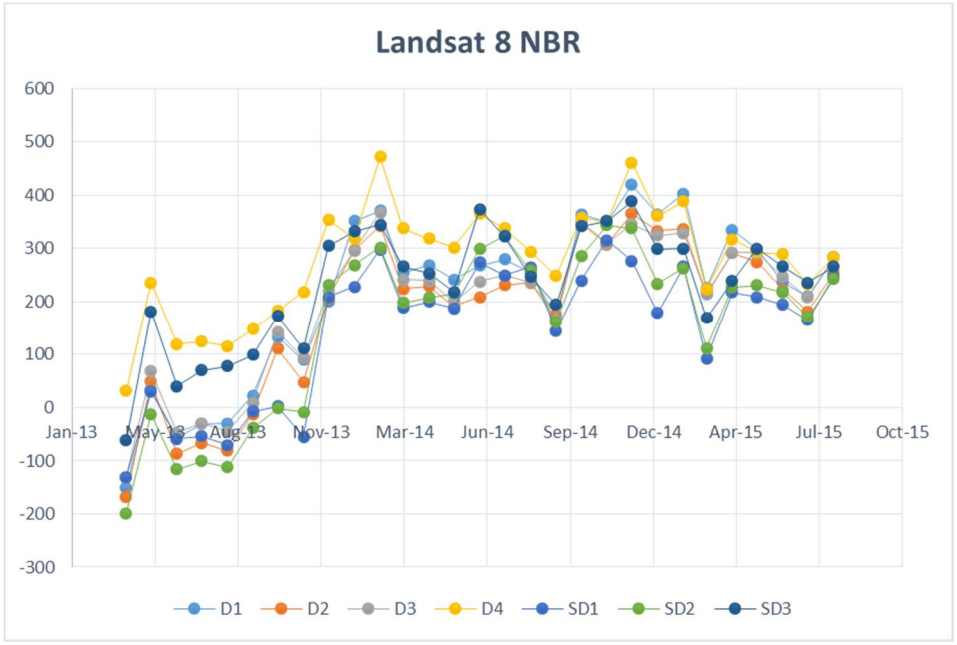

Figure 35: Landsat 8 NBR

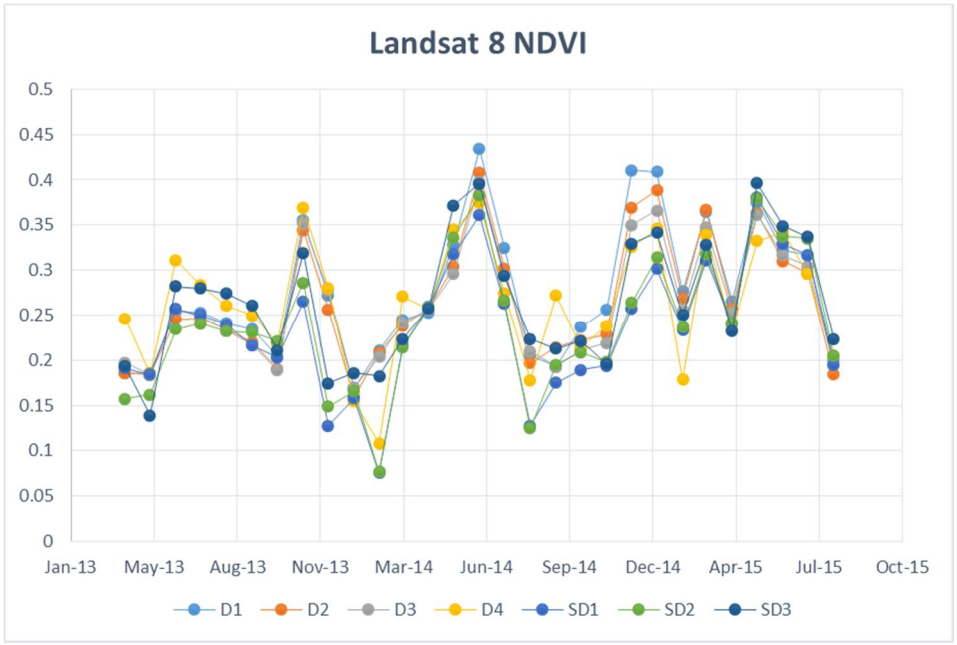

Figure 36: Landsat 8 NDVI

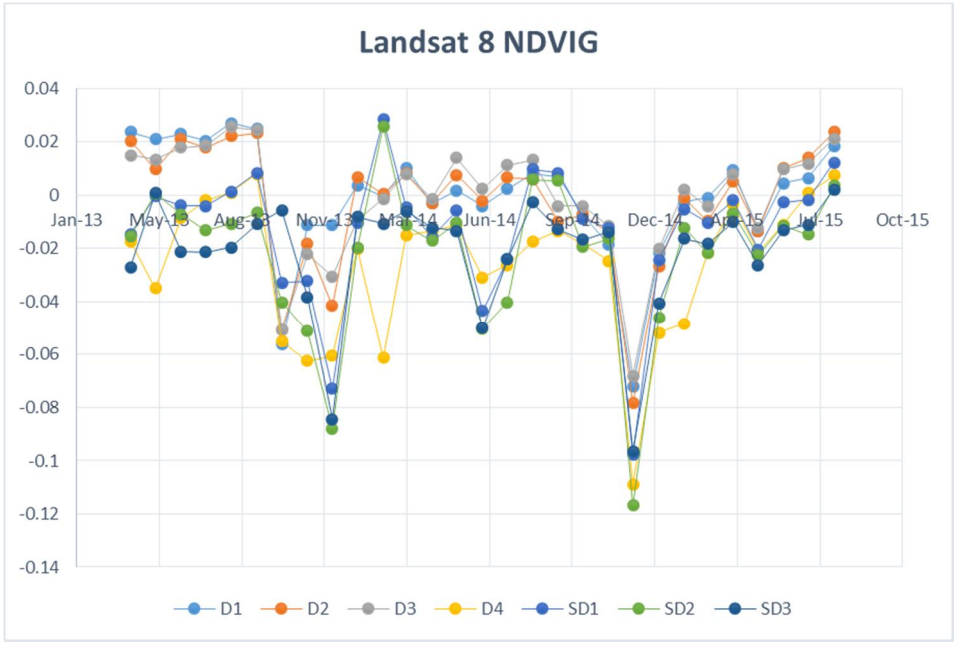

Figure 37: Landsat 8 NDVIG

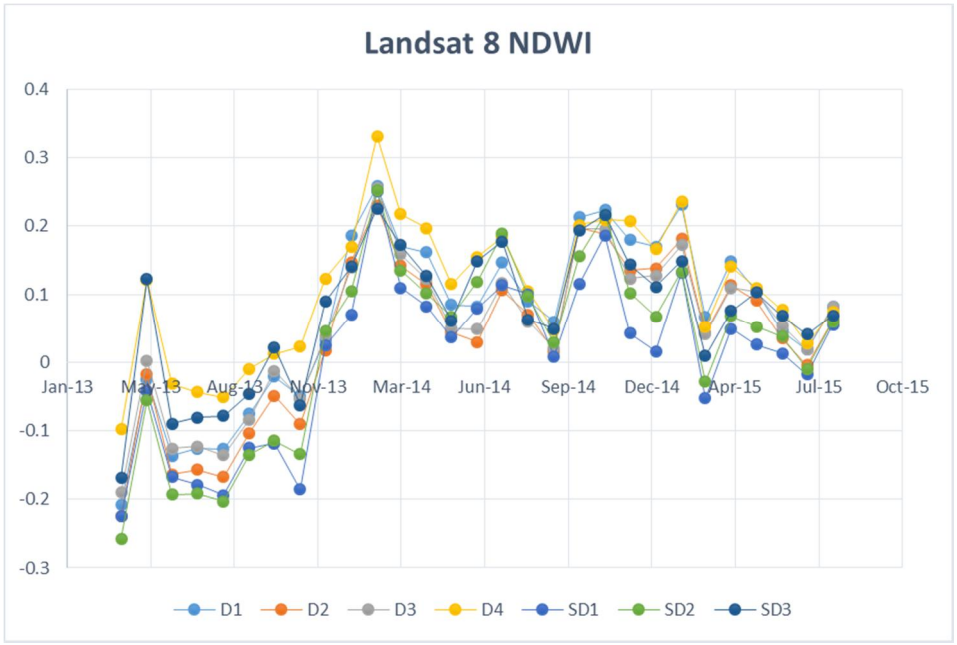

Figure 38: Landsat 8 NDWI

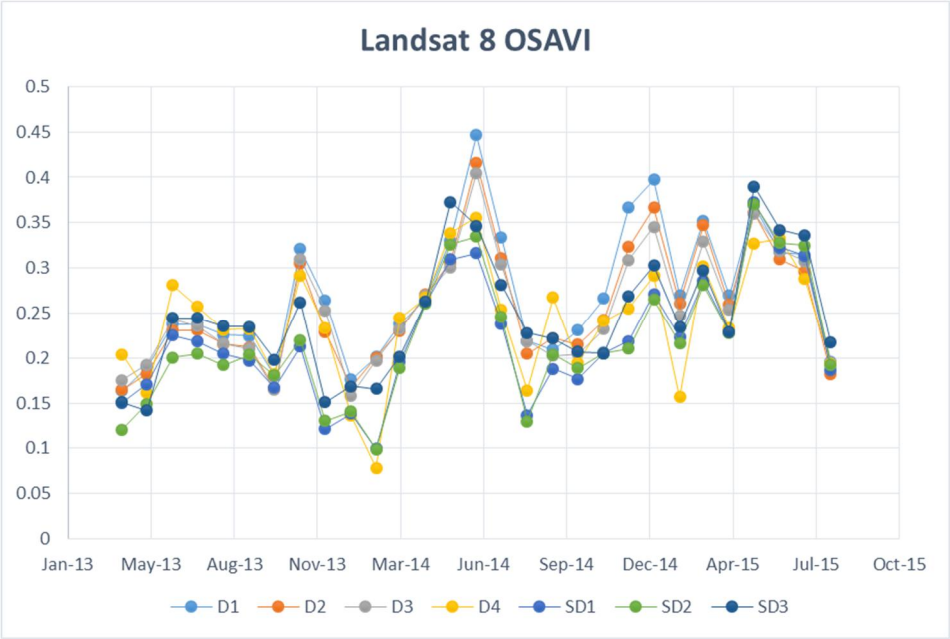

Figure 39: Landsat 8 OSAVI

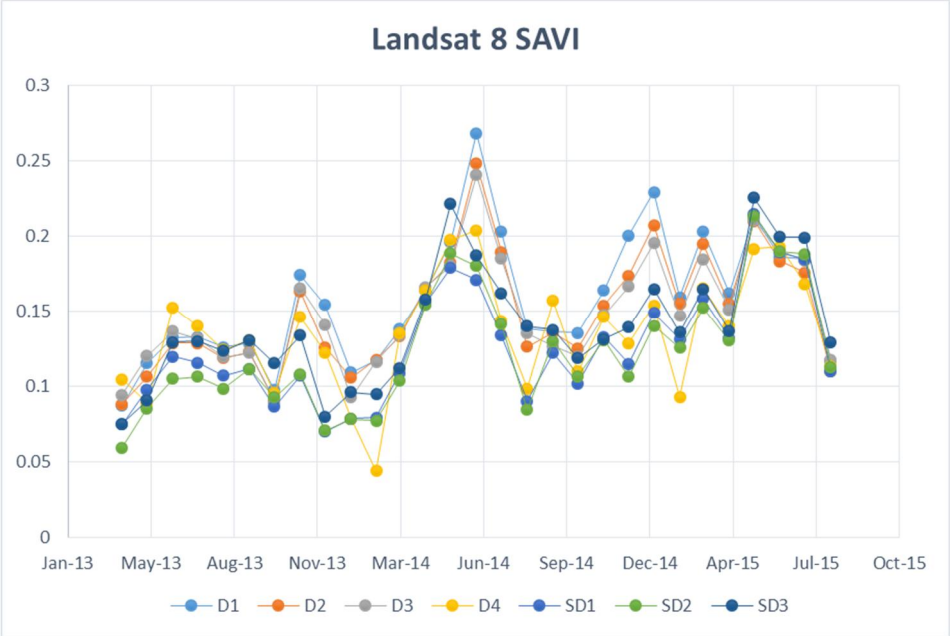

Figure 40: Landsat 8 SAVI

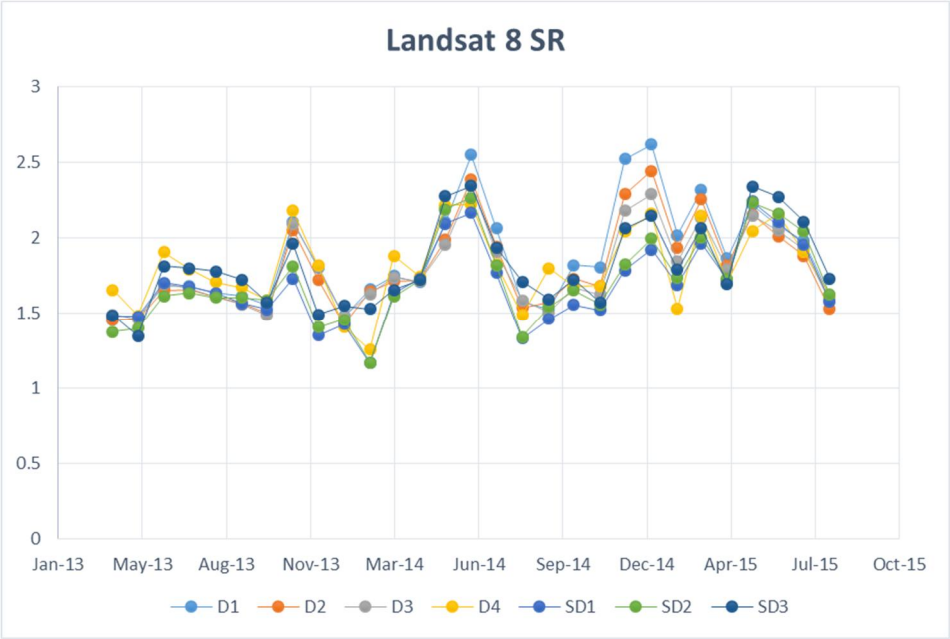

Figure 41: Landsat 8 SR

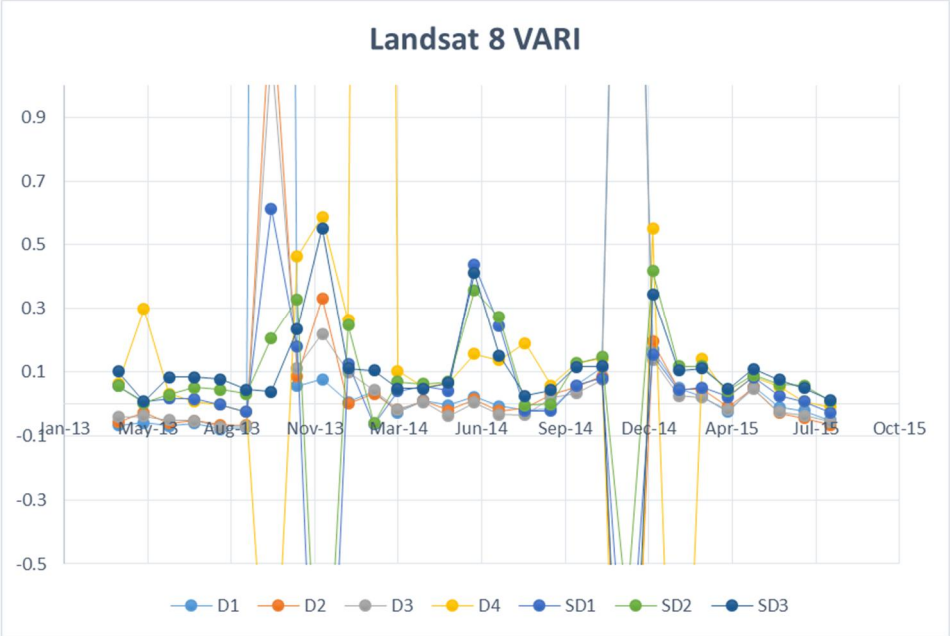

Figure 42: Landsat 8 VARI

11. APPENDIX D: VEGETATION RECOVERY GRAPHS

This section contain all DVI and SAVI recovery graphs with accompanying trends.

11.1 DVI

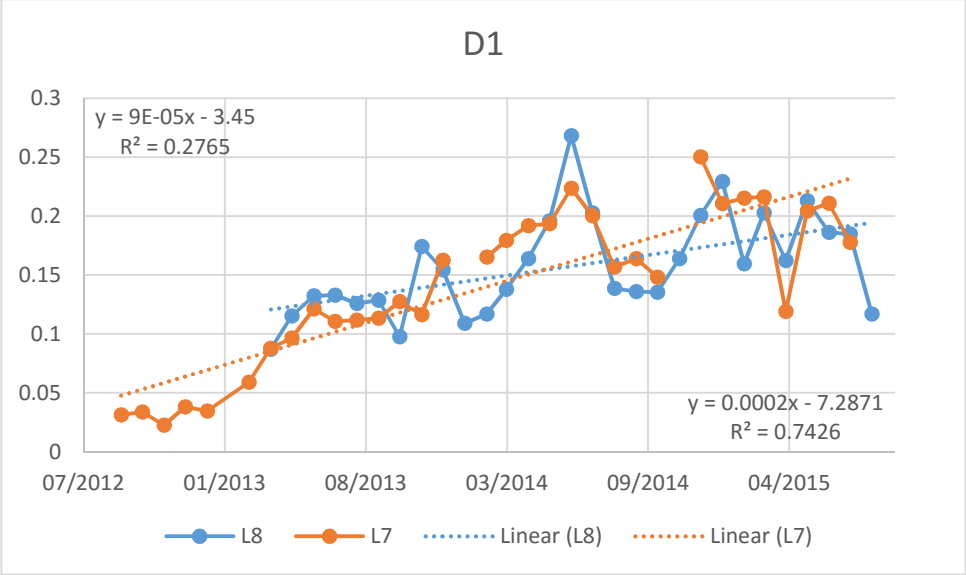

Figure 43: DVI regression slope D1

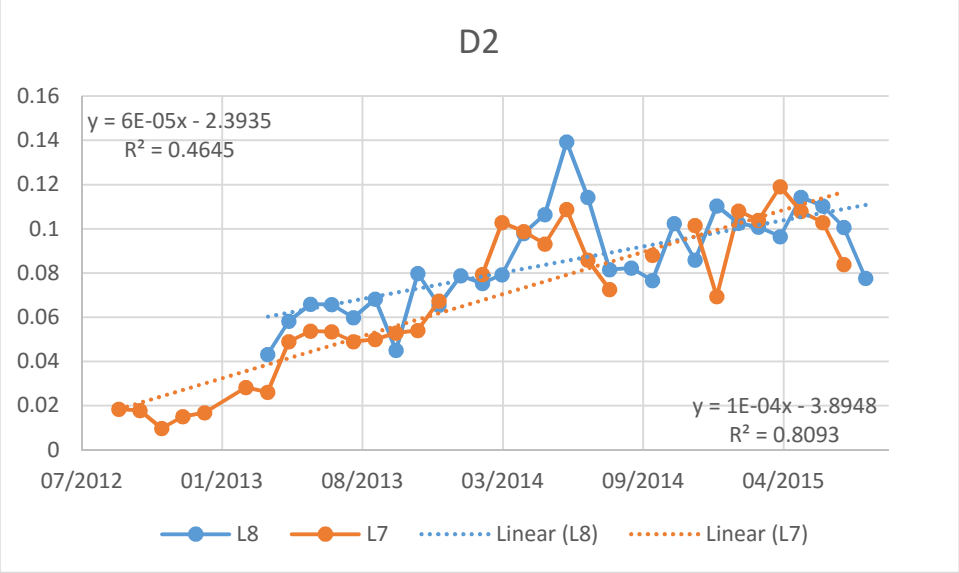

Figure 44: DVI regression slope D2

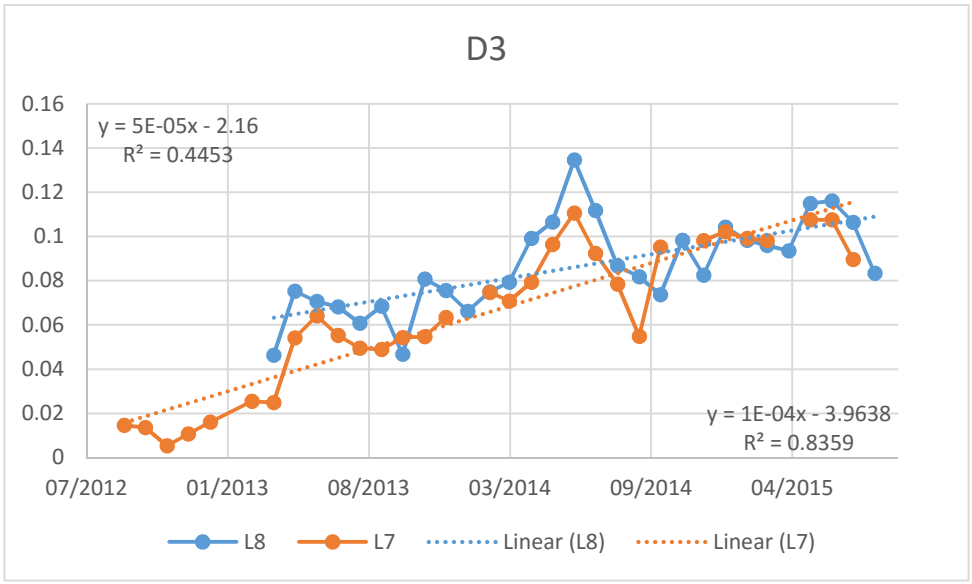

Figure 45: DVI regression slope D3

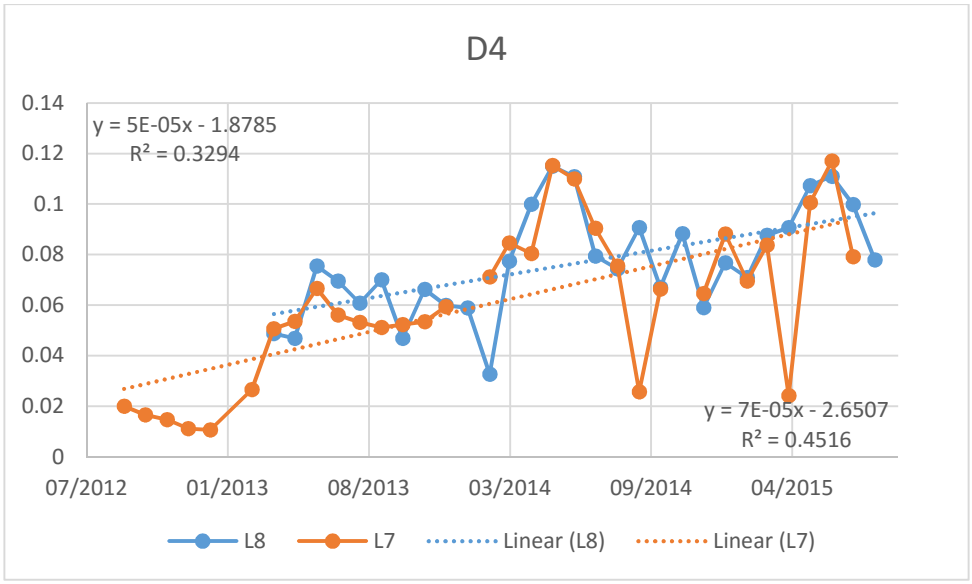

Figure 46: DVI regression slope D4

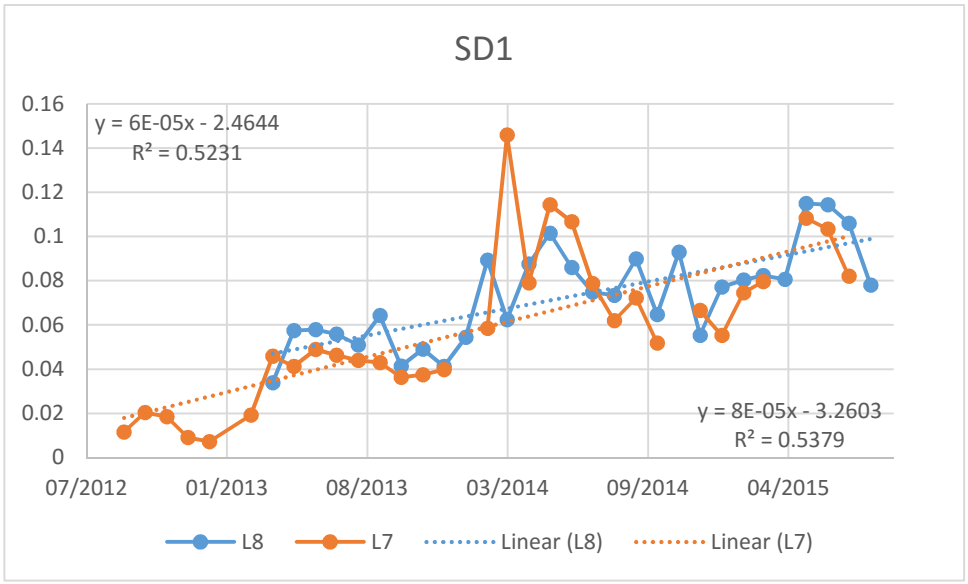

Figure 47: DVI regression slope SD1

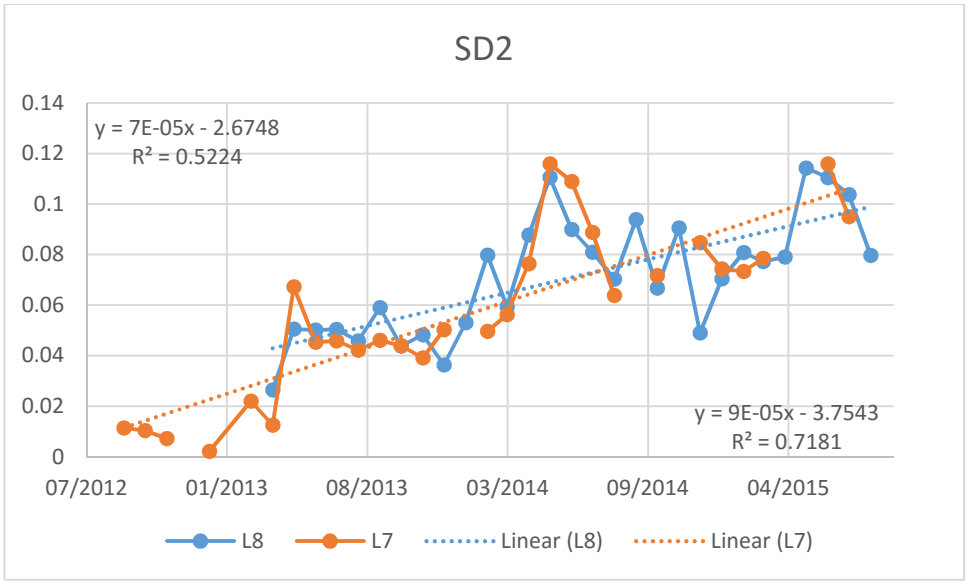

Figure 48: DVI regression slope SD2

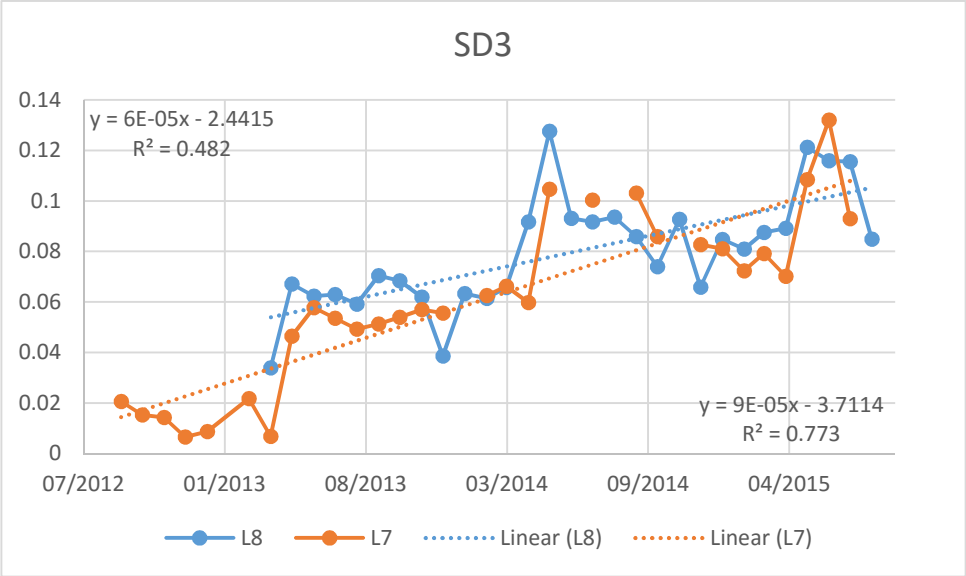

Figure 49: DVI regression slope SD3

11.2 SAVI

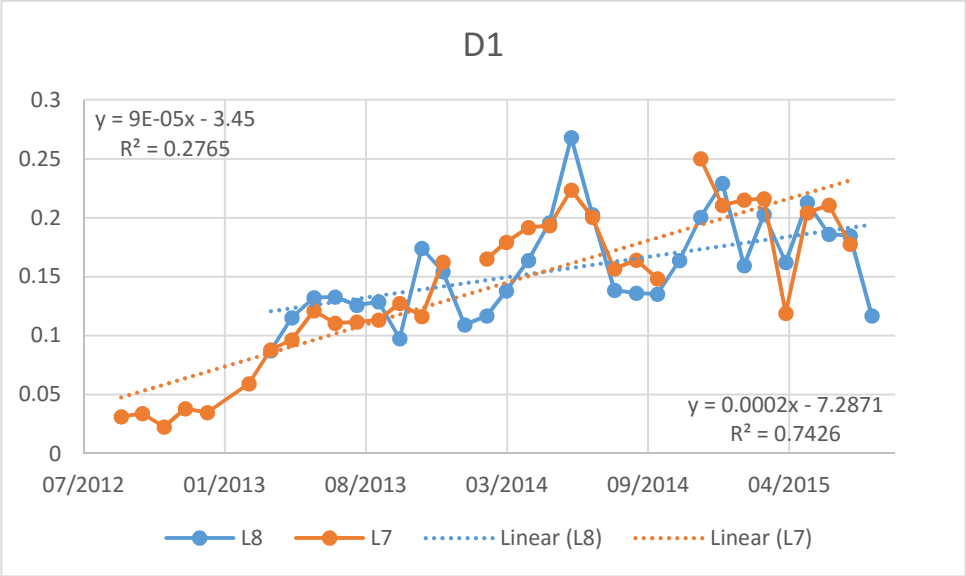

Figure 50: SAVI regression slope D1

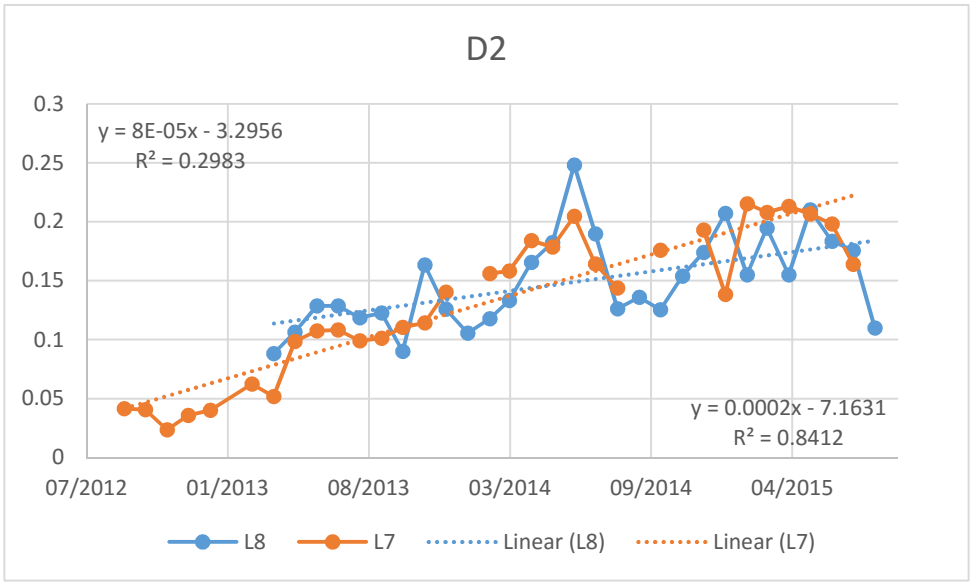

Figure 51: SAVI regression slope D2

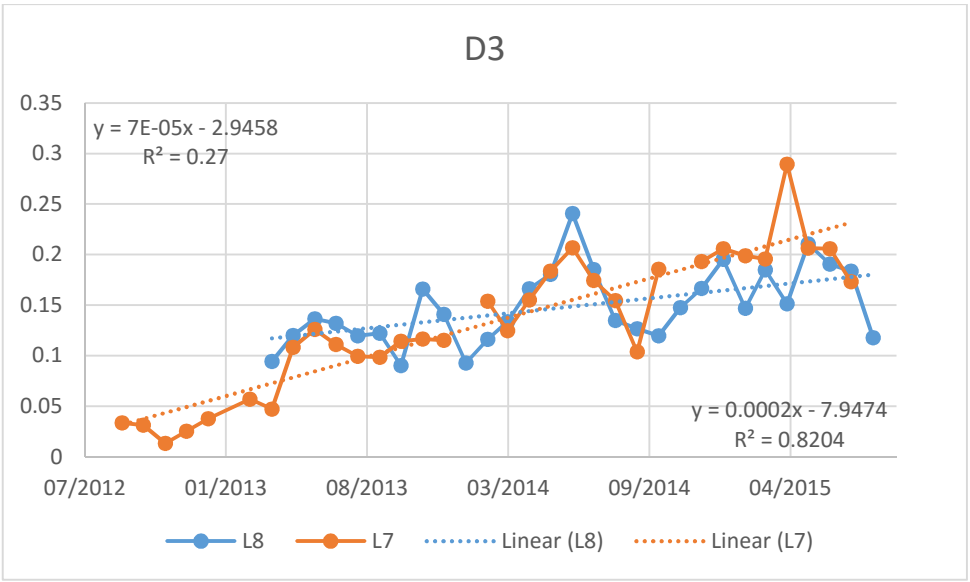

Figure 52: SAVI regression slope D3

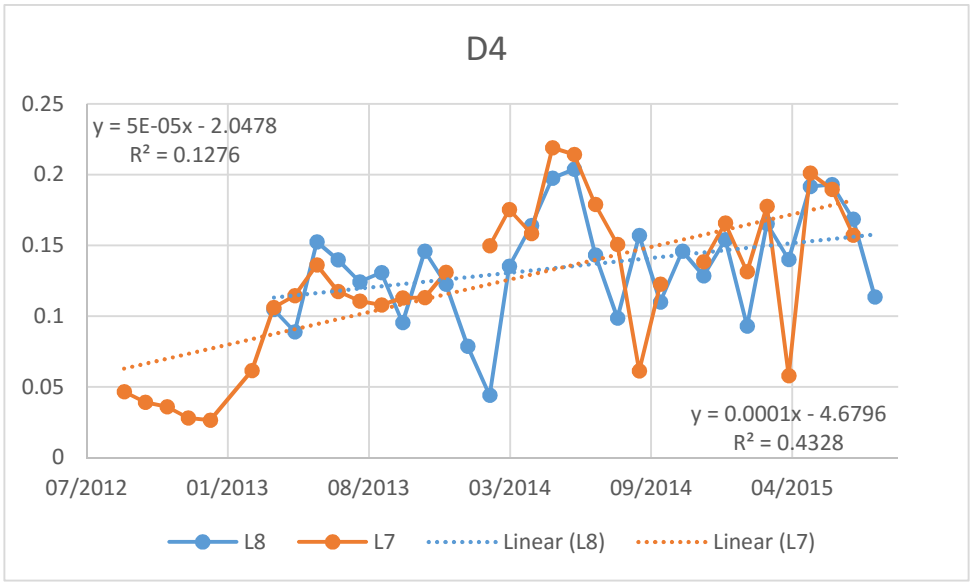

Figure 53: SAVI regression slope D4

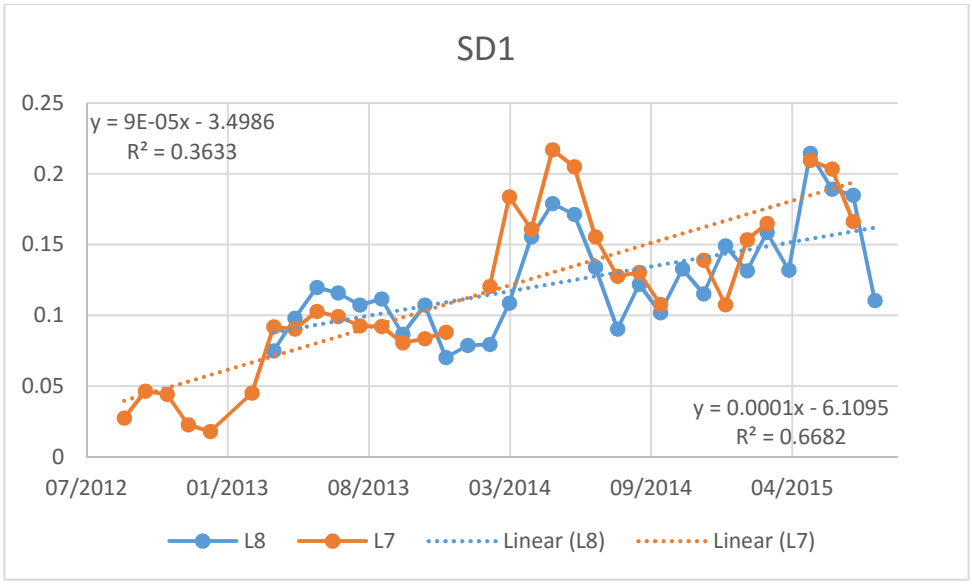

Figure 54: SAVI regression slope SD1

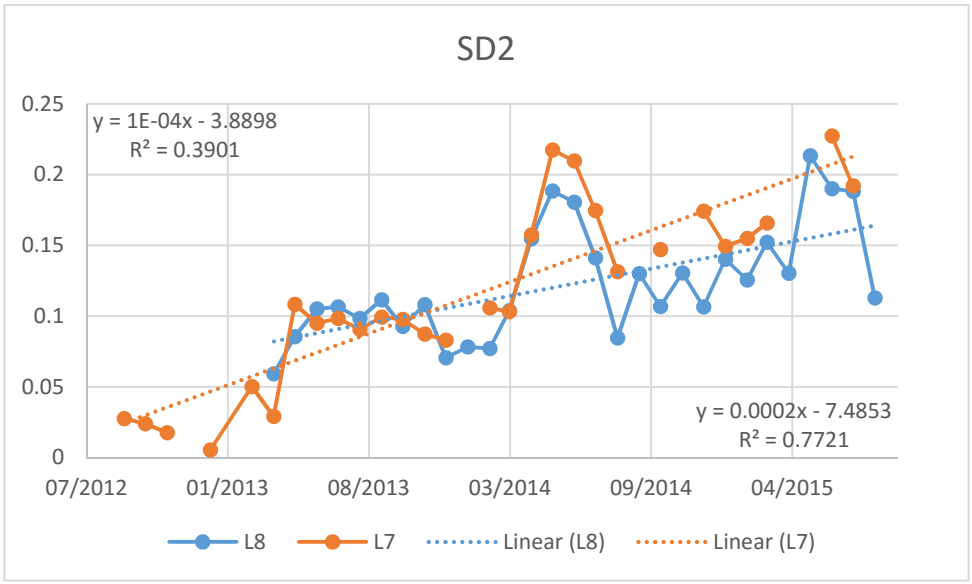

Figure 55: SAVI regression slope SD2

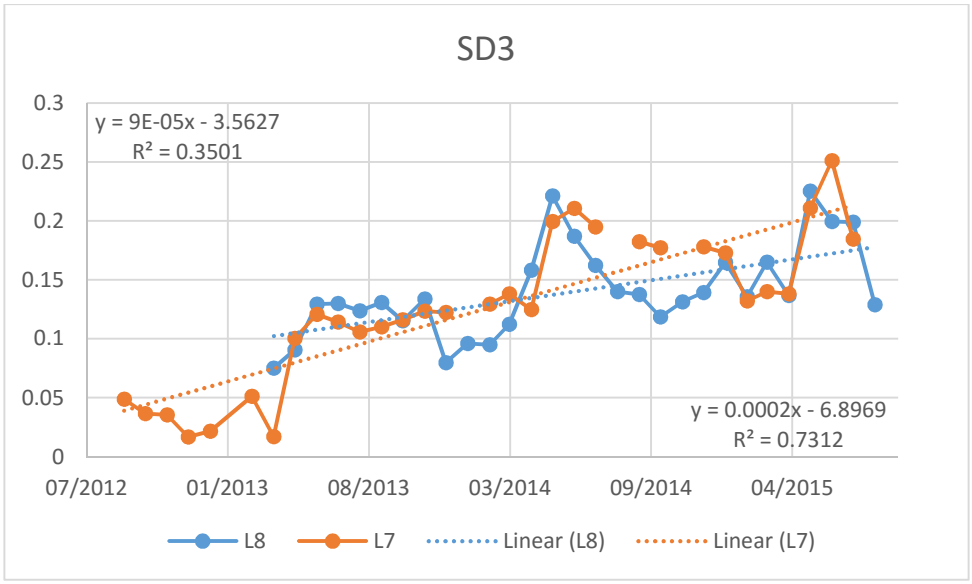

Figure 56: SAVI regression slope SD3

12. APPENDIX E: ORTHOPHOTO STATISTICS

Appendix D contains tables with statistics from the areas obtained with the orthophoto and Landsat 7 and 8 images for the comparison of the orthophoto and the satellite images.

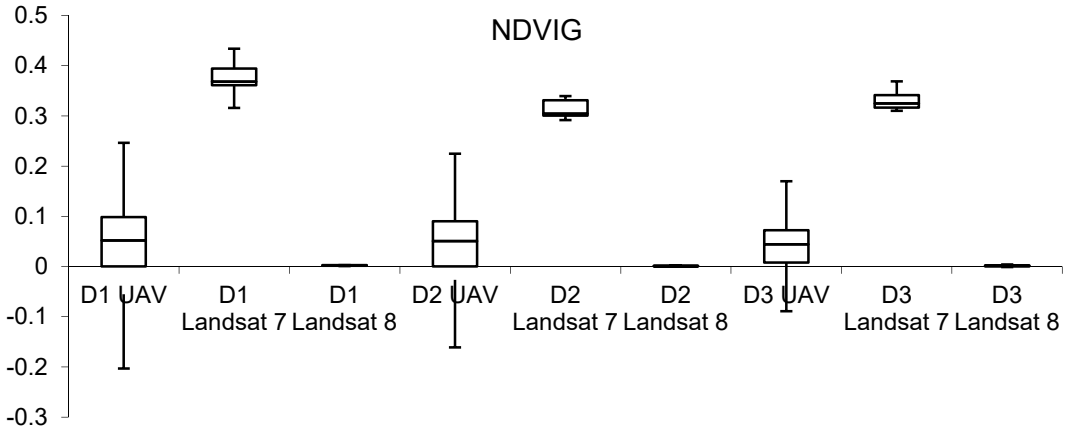

Figure 57: NDVIG boxplot comparison

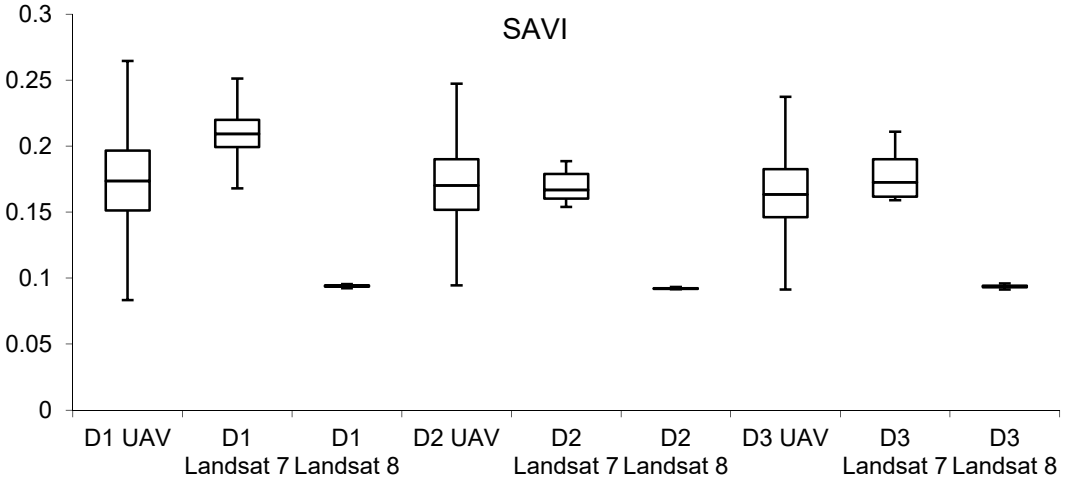

Figure 58: SAVI boxplot comparison

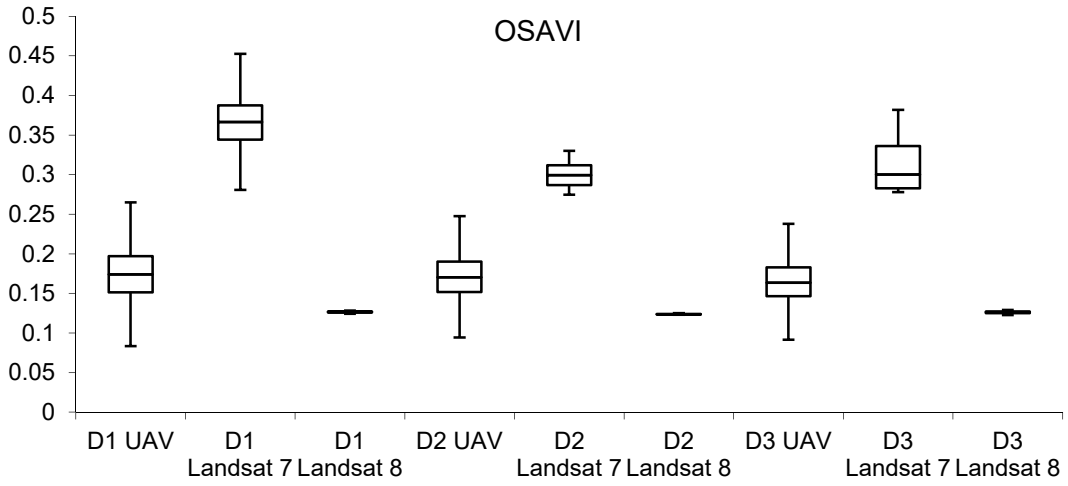

Figure 59: OSAVI boxplot comparison

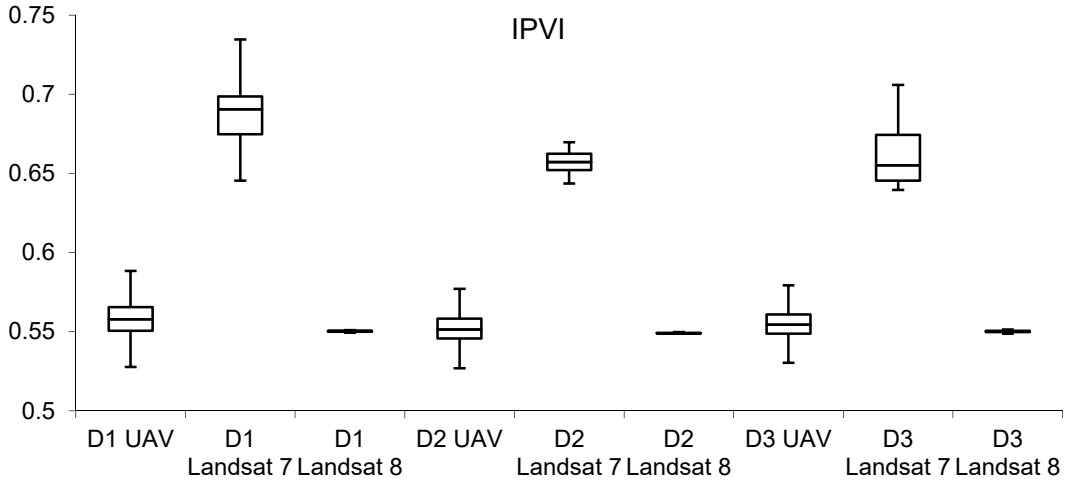

Figure 60: IPVI boxplot comparison

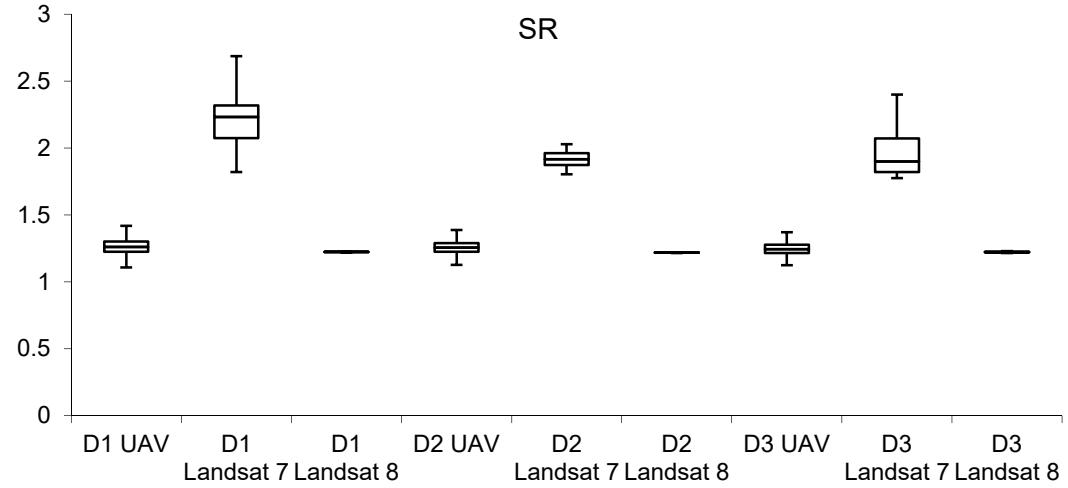

Figure 61: SR boxplot comparison

BIBLIOGRAPHY

ALATORRE, L. C., BEGUERÍA, S., & VICENTE-SERRANO, S. (2011). Evolution of vegetation activity on vegetated, eroded, and erosion risk areas in the central Spanish Pyrenees, using multitemporal Landsat imagery. *Earth Surface Processes and Landforms*, *36*(3), 309–319. http://doi.org/10.1002/esp.2038

ALEXANDRE, P. (2011). Analyzing the Resilience of Mediterranean Forest Systems to Wildfire Using Satellite Imagery. *Earthzine.org*, 1–9. Retrieved from http://www.earthzine.org/2011/03/24/analyzing-the-resilience-of-mediterranean-forest-systems-to-wildfire-using-satellite-imagery/

BARET, F., & GUYOT, G. (1991). Potentials and limits of vegetation indices for LAI and APAR assessment. *Remote Sensing of Environment*. http://doi.org/10.1016/0034-4257(91)90009-U

BARET, F., GUYOT, G., & Major, D. J. (1989). TSAVI: A Vegetation Index Which Minimizes Soil Brightness Effects On LAI And APAR Estimation. *12th Canadian Symposium on Remote Sensing Geoscience and Remote Sensing Symposium, 3*(AUGUST 1989). http://doi.org/10.1109/IGARSS.1989.576128

BARET, F., JACQUEMOUD, S., & HANOCQ, J. F. (1993). The soil line concept in remote sensing. *Remote Sensing Reviews*, *7*(1), 65–82. http://doi.org/10.1080/02757259309532166

BARRY, K. M., STONE, C., & MOHAMMED, C. L. (2008). Crown-scale evaluation of spectral indices for defoliated and discoloured eucalypts. *International Journal of Remote Sensing*, *29*(1), 47–69. http://doi.org/10.1080/01431160701281056

BAUGH, W. M., & GROENEVELD, D. P. (2006). Broadband vegetation index performance evaluated for a low□cover environment. *International Journal of Remote Sensing*, *27*(February 2015), 4715–4730. http://doi.org/10.1080/01431160600758543

BERJÓN, A. J., CACHORRO, V. E., ZARCO-TEJADA, P. J., & FRUTOS, A. (2013). Retrieval of biophysical vegetation parameters using simultaneous inversion of high resolution remote sensing imagery constrained by a vegetation index. *Precision Agriculture*, *14*(5), 541–557. http://doi.org/10.1007/s11119-013-9315-8

BIRTH, G. S., & MCVEY, G. R. (1968). Measuring the Color of Growing Turf with a Reflectance Spectrophotometer1. *Agronomy Journal*, *60*(6), 640. http://doi.org/10.2134/agronj1968.00021962006000060016x

BIVAND, R. S., PEBESMA, E. J., & GÓMEZ-RUBIO, V. (2008). *Applied Spatial Data Analysis with R*. *Use R* (Vol. 1). New York, NY: Springer New York. http://doi.org/10.1007/978-0-387-78171-6

BRIMBLECOMBE, P., & DAVIES, T. D. (1978). Detection of air pollution from Landsat 1. *Weather*, *33*(1), 19–27. http://doi.org/10.1002/j.1477-8696.1978.tb04601.x

BROOK, R. K., & KENKEL, N. C. (2002). A multivariate approach to vegetation mapping of Manitoba's Hudson Bay Lowlands. *International Journal of Remote Sensing*, *23*(21), 4761–4776. http://doi.org/10.1080/01431160110113917

CALDERÓN, R., MONTES-BORREGO, M., LANDA, B. B., NAVAS-CORTÉS, J. A., & ZARCO-TEJADA, P. J. (2014). Detection of downy mildew of opium poppy using high-resolution multi-spectral and thermal imagery acquired with an unmanned aerial vehicle. *Precision Agriculture*. http://doi.org/10.1007/s11119-014-9360-y

CALDERÓN, R., NAVAS-CORTÉS, J. A. A., LUCENA, C., & ZARCO-TEJADA, P. J. J. (2013). High-resolution airborne hyperspectral and thermal imagery for early detection of Verticillium wilt of olive using fluorescence, temperature and narrow-band spectral indices. *Remote Sensing of Environment*, *139*, 231–245. http://doi.org/10.1016/j.rse.2013.07.031

CAMMARANO, D., FITZGERALD, G., CASA, R., & BASSO, B. (2014). Assessing the Robustness of Vegetation Indices to Estimate Wheat N in Mediterranean Environments. *Remote Sensing*, *6*(4), 2827–2844. http://doi.org/10.3390/rs6042827

CASADY, G. M., & MARSH, S. E. (2010). Broad-scale environmental conditions responsible for post-fire vegetation dynamics. *Remote Sensing*, *2*(12), 2643–2664. http://doi.org/10.3390/rs2122643

CLEVERS, J. G. P. W. (1988). the application of the weigthed near-infrared - red vegetation index for estimating lai at the vegetative and generative stage of cereals. In *XVIth ISPRS Congress Technical Commission VII: Interpretation of Photographic and Remote Sensing Data* (pp. 98–107). Kyoto.

CLEVERS, J. G. P. W. (1989). Application of a weighted infrared-red vegetation index for estimating leaf Area Index by Correcting for Soil Moisture. *Remote Sensing of Environment*, *29*(1), 25–37. http://doi.org/10.1016/0034-4257(89)90076-X

CLEVERS, J. G. P. W. (1991). Application of the WDVI in estimating LAI at the generative stage of barley. *ISPRS Journal of Photogrammetry and Remote Sensing*, *46*(1), 37–47. http://doi.org/10.1016/0924-2716(91)90005-G

COCKE, A. E., FULÉ, P. Z., & CROUSE, J. E. (2005). Comparison of burn severity assessments using Differenced Normalized Burn Ratio and ground data. *International Journal of Wildland Fire*, *14*(2), 189. http://doi.org/10.1071/WF04010

COHEN, W. B., YANG, Z., & KENNEDY, R. (2010). Detecting trends in forest disturbance and recovery using yearly Landsat time series: 2. TimeSync — Tools for calibration and validation. *Remote Sensing of Environment*, *114*(12), 2911–2924. http://doi.org/10.1016/j.rse.2010.07.010

CRIPPEN, R. (1990). Calculating the vegetation index faster. *Remote Sensing of Environment*, *34*(1), 71–73. http://doi.org/10.1016/0034-4257(90)90085-Z

CUNDILL, S., VAN DER WERFF, H., & VAN DER MEIJDE, M. (2015). Adjusting Spectral Indices for Spectral Response Function Differences of Very High Spatial Resolution Sensors Simulated from Field Spectra. *Sensors*, *15*(3), 6221–6240. http://doi.org/10.3390/s150306221

DATT, B. (1998). Remote Sensing of Chlorophyll a, Chlorophyll b, Chlorophyll a+ b, and Total Carotenoid Content in Eucalyptus Leaves. *Remote Sensing of Environment*, *66*(2), 111–121. http://doi.org/10.1016/S0034-4257(98)00046-7

DATT, B. (1999). Visible/near infrared reflectance and chlorophyll content in Eucalyptus leaves. *International Journal of Remote Sensing*, *20*(14), 2741–2759. http://doi.org/10.1080/014311699211778

DEFRIES, R. S., HANSEN, M. C., TOWNSHEND, J. R. G., JANETOS, A. C., & LOVELAND, T. R. (2000). A new global 1-km dataset of percentage tree cover derived from remote sensing. *Global Change Biology*, *6*(2), 247–254. http://doi.org/10.1046/j.1365-2486.2000.00296.x

EDIRIWEERA, S., PATHIRANA, S., DANAHER, T., & NICHOLS, D. (2014). Estimating above-ground biomass by fusion of LiDAR and multispectral data in subtropical woody plant communities in topographically complex terrain in North-eastern Australia. *Journal of Forestry Research*. http://doi.org/10.1007/s11676-014-0485-7

ELVIDGE, C., & CHEN, Z. (1995). Comparison of broad-band and narrow-band red and near-infrared vegetation indices. *Remote Sensing of Environment*, *48*(June 1994), 38–48. Retrieved from http://www.sciencedirect.com/science/article/pii/003442579500132K

EPIPHANIO, J. C. N., & HUETE, A. R. (1992). Dependence of NDVI and SAVI on Sun / Sensor Geometry and Its Effect on fAPAR Relationships in Alfalfa, *4257*.

EPTING, J., VERBYLA, D., & SORBEL, B. (2005). Evaluation of remotely sensed indices for assessing burn severity in interior Alaska using Landsat TM and ETM+. *Remote Sensing of Environment*, *96*(3-4), 328–339. http://doi.org/10.1016/j.rse.2005.03.002

ESCUIN, S., NAVARRO, R., & FERNÁNDEZ, P. (2008). Fire severity assessment by using NBR (Normalized Burn Ratio) and NDVI (Normalized Difference Vegetation Index) derived from LANDSAT TM/ETM images. *International Journal of Remote Sensing*, *29*(4), 1053–1073. http://doi.org/10.1080/01431160701281072

FAN, H., FU, X., ZHANG, Z., & WU, Q. (2015). Phenology-Based Vegetation Index Differencing for Mapping of Rubber Plantations Using Landsat OLI Data. *Remote Sensing*, *7*(5), 6041–6058. http://doi.org/10.3390/rs70506041

FAO. (2001). Global forest fire assessment 1990-2000. *Forest Resources Assessment Programme*, 494 pp.

FERREIRA, A. J. D., COELHO, C. O. A., BOULET, A. K., & LOPES, F. P. (2005). Temporal patterns of solute loss following wildfires in Central Portugal. *International Journal of Wildland Fire*, *14*(4), 401–412. http://doi.org/10.1071/WF05043

FOWLER, M. J. F. (2013). Declassified Intelligence Satellite Photographs. In *Archaeology from Historical Aerial and Satellite Archives* (pp. 47–66). New York, NY: Springer New York. http://doi.org/10.1007/978-1-4614-4505-0_4

GALVÃO, L. S., FORMAGGIO, A. R., & TISOT, D. A. (2005). Discrimination of sugarcane varieties in Southeastern Brazil with EO-1 Hyperion data. *Remote Sensing of Environment*, *94*(4), 523–534. http://doi.org/10.1016/j.rse.2004.11.012

GAO, B.-C. (1996). NDWI—A normalized difference water index for remote sensing of vegetation liquid water from space. *Remote Sensing of Environment*, *58*(3), 257–266. http://doi.org/10.1016/S0034-4257(96)00067-3

GARCÍA, M. J. L., & CASELLES, V. (1991). Mapping burns and natural reforestation using thematic Mapper data. *Geocarto International*, *6*(1), 31–37. http://doi.org/10.1080/10106049109354290

GITELSON, A. A. (2004). Wide Dynamic Range Vegetation Index for remote quantification of biophysical characteristics of vegetation. *Journal of Plant Physiology*, *161*(2), 165–73. http://doi.org/10.1078/0176-1617-01176

GITELSON, A. A., KAUFMAN, Y. J., STARK, R., & RUNDQUIST, D. (2002). Novel algorithms for remote estimation of vegetation fraction. *Remote Sensing of Environment*, *80*, 76–87.

GU, Y., BROWN, J. F., VERDIN, J. P., & WARDLOW, B. (2007). A five-year analysis of MODIS NDVI and NDWI for grassland drought assessment over the central Great Plains of the United States. *Geophysical Research Letters*, *34*(6), 1–6. http://doi.org/10.1029/2006GL029127

HABOUDANE, D., MILLER, J. R., PATTEY, E., ZARCO-TEJADA, P. J., & STRACHAN, I. B. (2004). Hyperspectral vegetation indices and novel algorithms for predicting green LAI of crop canopies: Modeling and validation in the context of precision agriculture. *Remote Sensing of Environment*, *90*(3), 337–352. http://doi.org/10.1016/j.rse.2003.12.013

HABOUDANE, D., MILLER, J. R., TREMBLAY, N., ZARCO-TEJADA, P. J., & DEXTRAZE, L. (2002). Integrated narrow-band vegetation indices for prediction of crop chlorophyll content for application to precision agriculture. *Remote Sensing of Environment*, *81*(2-3), 416–426. http://doi.org/10.1016/S0034-4257(02)00018-4

HUETE, A., DIDAN, K., MIURA, T., RODRIGUEZ, E. P., GAO, X., & FERREIRA, L. G. (2002). Overview of the radiometric and biophysical performance of the MODIS vegetation indices, *83*, 195–213.

HUETE, A. R. (1988). A soil-adjusted vegetation index (SAVI). *Remote Sensing of Environment*, *25*(3), 295–309. http://doi.org/10.1016/0034-4257(88)90106-X

IRELAND, G., & PETROPOULOS, G. P. (2015). Exploring the relationships between post-fire vegetation regeneration dynamics, topography and burn severity: A case study from the Montane Cordillera Ecozones of Western Canada. *Applied Geography*, *56*, 232–248. http://doi.org/10.1016/j.apgeog.2014.11.016

IRISH, R. R., BARKER, J. L., GOWARD, S. N., & ARVIDSON, T. (2006). Characterization of the Landsat-7 ETM+ Automated Cloud-Cover Assessment (ACCA) Algorithm. *Photogrammetric Engineering & Remote Sensing*, *72*(10), 1179–1188. http://doi.org/10.14358/PERS.72.10.1179

KAUFMAN, Y. J., & TANRE, D. (1992). Atmospherically resistant vegetation index (ARVI) for EOS-MODIS. *IEEE Transactions on Geoscience and Remote Sensing*, *30*(2), 261–270. http://doi.org/10.1109/36.134076

KAUFMAN, Y. J., & TANRÉ, D. (1994). Direct and indirect methods for correcting the aerosol effect on remote sensing. *Remote Sensing of Environment*, *4257*(95), 65–79. http://doi.org/10.1016/0034-4257(95)00193-X

KEVIN C. RUFFNER. (1995). Corona- America´s First Satellite Program, 362.

LEMAIRE, G., FRANCOIS, C., SOUDANI, K., BERVEILLER, D., PONTAILLER, J., BREDA, N., … DUFRENE, E. (2008). Calibration and validation of hyperspectral indices for the estimation of broadleaved forest leaf chlorophyll content, leaf mass per area, leaf area index and leaf canopy biomass. *Remote Sensing of Environment*, *112*(10), 3846–3864. http://doi.org/10.1016/j.rse.2008.06.005

LENTILE, L. B., HOLDEN, Z. A., SMITH, A. M. S., FALKOWSKI, M. J., HUDAK, A. T., MORGAN, P., … BENSON, N. C. (2006). Remote sensing techniques to assess active fire characteristics and post-fire effects. *International Journal of Wildland Fire*, *15*(3), 319. http://doi.org/10.1071/WF05097

LIU, L.-Y., HUANG, W.-J., PU, R.-L., & WANG, J.-H. (2014). Detection of Internal Leaf Structure Deterioration Using a New Spectral Ratio Index in the Near-Infrared Shoulder Region. *Journal of Integrative Agriculture*, *13*(4), 760–769. http://doi.org/10.1016/S2095-3119(13)60385-8

MALVAR, M. C., PRATS, S. A., NUNES, J. P., & KEIZER, J. J. (2011). Post-fire overland flow generation and inter-rill erosion under simulated rainfall in two eucalypt stands in north-central Portugal. *Environmental Research*, *111*(2), 222–236. http://doi.org/10.1016/j.envres.2010.09.003

MORENO, A., MASELLI, F., CHIESI, M., GENESIO, L., VACCARI, F., SEUFERT, G., & GILABERT, M. A. (2014). Monitoring water stress in Mediterranean semi-natural vegetation with satellite and meteorological data. *International Journal of Applied Earth Observation and Geoinformation*, *26*, 246–255. http://doi.org/10.1016/j.jag.2013.08.003

MOUSIVAND, A., MENENTI, M., GORTE, B., & VERHOEF, W. (2015). Remote Sensing of Environment Multi-temporal , multi-sensor retrieval of terrestrial vegetation properties from spectral – directional radiometric data. *Remote Sensing of Environment*, *158*, 311–330. http://doi.org/10.1016/j.rse.2014.10.030

NASA. (2014). Landsat 7 Handbook. Retrieved October 5, 2015, from http://landsathandbook.gsfc.nasa.gov/data_prod/prog_sect11_3.html

NASA. (2015). Landsat 8 (L8) data users handbook Version 1.0 June 2015, *8*(June).

NAVEH, Z. (1990). Chapter 3 Fire in the Mediterranean – a Landscape Ecological Perspective . *Fire in Ecosystem Dynamics*, (May 1989), 1–20.

NUMATA, I., ROBERTS, D. A., CHADWICK, O. A., SCHIMEL, J., SAMPAIO, F. R., LEONIDAS, F. C., & SOARES, J. V. (2007). Characterization of pasture biophysical properties and the impact of grazing intensity using remotely sensed data. *Remote Sensing of Environment*, *109*(3), 314–327. http://doi.org/10.1016/j.rse.2007.01.013

O'CONNELL, J. L., BYRD, K. B., & KELLY, M. (2014). Remotely-sensed indicators of N-related biomass allocation in Schoenoplectus acutus. *PloS One*, *9*(3), e90870. http://doi.org/10.1371/journal.pone.0090870

PEREIRA, J. M. C., CARREIRAS, J. M. B., SILVA, J. M. N., & VASCONCELOS, M. J. (2006). Alguns Conceitos Básicos sobre os Fogos Rurais em Portugal. *Incêndios Florestais Em Portugal: Caracterização, Impactes E Prevenção*, (September), 133–161.

PETTORELLI, N., VIK, J. O., MYSTERUD, A., GAILLARD, J.-M., TUCKER, C. J., STENSETH, N. C., & LYON, C. B. (2005). Using the satellite-derived NDVI to assess ecological responses to environmental change, *20*(9). http://doi.org/10.1016/j.tree.2005.05.011

PIMSTEIN, A., KARNIELI, A., BANSAL, S. K., & BONFIL, D. J. (2011). Exploring remotely sensed technologies for monitoring wheat potassium and phosphorus using field spectroscopy. *Field Crops Research*, *121*(1), 125–135. http://doi.org/10.1016/j.fcr.2010.12.001

PINTY, B., & VERSTRAETE, M. M. (1992). GEMI: a non-linear index to monitoring global vegetation from satellite. *Vegetation*, *101*(2), 15–20.

QI, J., CHEHBOUNI, A., HUETE, A. R., KERR, Y. H., & SOROOSHIAN, S. (1994). A modified soil adjusted vegetation index. *Remote Sensing of Environment*, *48*(2), 119–126. http://doi.org/10.1016/0034-4257(94)90134-1

QUIRING, S. M., & GANESH, S. (2010). Evaluating the utility of the Vegetation Condition Index (VCI) for monitoring meteorological drought in Texas. *Agricultural and Forest Meteorology*, *150*(3), 330–339. http://doi.org/10.1016/j.agrformet.2009.11.015

RAMA RAO, N., GARG, P. K., GHOSH, S. K., & DADHWAL, V. K. (2007). Estimation of leaf total chlorophyll and nitrogen concentrations using hyperspectral satellite imagery. *The Journal of Agricultural Science*, *146*(01), 65–75. http://doi.org/10.1017/S0021859607007514

RAVI, S., BADDOCK, M. C., ZOBECK, T. M., & HARTMAN, J. (2012). Field evidence for differences in post-fire aeolian transport related to vegetation type in semi-arid grasslands. *Aeolian Research*, *7*, 3–10. http://doi.org/10.1016/j.aeolia.2011.12.002

RICHARDSON, A. J., & WEIGAND, C. L. (1977). Distinguishing vegetation from soil background information. *Photogrammetric Engineering & Remote Sensing*, *43*(12), 1541–52.

RONDEAUX, G., STEVEN, M., & BARET, F. (1996). Optimization of soil-adjusted vegetation indices. *Remote Sensing of Environment*, *55*(2), 95–107. http://doi.org/10.1016/0034-4257(95)00186-7

ROUSE, J. W., HAAS, R. H., SCHEEL, J. A., & DEERING, D. W. (1974). Monitoring Vegetation Systems in the Great Plains with ERTS. In *Proceedings, 3rd Earth Resource Technology Satellite (ERTS) Symposium* (pp. 48–62).

SAHU, R. K., & KHARE, D. (2015). Spatial and temporal analysis of rainfall trend for 30 districts of a coastal state (Odisha) of India. *International Journal of Geology, Earth & Environmental Sciences*, *5*(1), 40–53.

SCHABENBERGER, O., & GOTWAY, C. A. (2004). *Statistical Methods for Spatial Data Analysis*. Chapman and Hall/CRC.

SCHLERF, M., ATZBERGER, C., & HILL, J. (2005). Remote sensing of forest biophysical variables using HyMap imaging spectrometer data, *95*, 177–194. http://doi.org/10.1016/j.rse.2004.12.016

SENSEFLY A PARROT COMPANY. (2015). Retrieved November 11, 2015, from https://www.sensefly.com/drones/ebee.html

SHAKESBY, R. A. (2011). Post-wildfire soil erosion in the Mediterranean: Review and future research directions. *Earth-Science Reviews*, *105*(3-4), 71–100. http://doi.org/10.1016/j.earscirev.2011.01.001

SIMS, D. A., & GAMON, J. A. (2002). Relationships between leaf pigment content and spectral reflectance across a wide range of species, leaf structures and developmental stages. *Remote Sensing of Environment*, *81*(2-3), 337–354. http://doi.org/10.1016/S0034-4257(02)00010-X

TSIROS, E., DOMENIKIOTIS, C., SPILIOTOPOULOS, M., & DALEZIOS, N. R. (2004). Use of Noaa / Avhrr-Based Vegetation Condition Index (Vci) and Temperature Condition Index (Tci) for Drought Monitoring in Thessaly , Greece. In *EWRA Symposium on water resources management: risks and challenges for the 21st century* (pp. 1–10).

TURNER, D. P., RITTS, W. D., LAW, B. E., COHEN, W. B., YANG, Z., HUDIBURG, T., … DUANE, M. (2007). Scaling net ecosystem production and net biome production over a heterogeneous region in the western United States. *Biogeosciences Discussions*, *4*(2), 1093–1135. http://doi.org/10.5194/bgd-4-1093-2007

VAN LEEUWEN, W. J. D., CASADY, G. M., NEARY, D. G., BAUTISTA, S., ALLOZA, J. A., CARMEL, Y., … ORR, B. J. (2010). Monitoring post-wildfire vegetation response with remotely sensed time-series data in Spain, USA and Israel. *International Journal of Wildland Fire*, *19*(1), 75–93. http://doi.org/10.1071/WF08078

VAN WAGTENDONK, J. W., ROOT, R. R., & KEY, C. H. (2004). Comparison of AVIRIS and Landsat ETM+ detection capabilities for burn severity. *Remote Sensing of Environment*, *92*(3), 397–408. http://doi.org/10.1016/j.rse.2003.12.015

VERSTRAETE, M. M., PINTY, B., & MYNENI, R. B. (1996). Potential and limitations of information extraction on the terrestrial biosphere from satellite remote sensing. *Remote Sensing of Environment*, *58*(96), 201–214. http://doi.org/10.1016/S0034-4257(96)00069-7

VESCOVO, L., & GIANELLE, D. (2008). Using the MIR bands in vegetation indices for the estimation of grassland biophysical parameters from satellite remote sensing in the Alps region of Trentino (Italy). *Advances in Space Research*, *41*(11), 1764–1772. http://doi.org/10.1016/j.asr.2007.07.043

VINCINI, M., FRAZZI, E., & D'ALESSIO, P. (2006). Angular dependence of maize and sugar beet VIs from directional CHRIS/Proba data, 5–9. Retrieved from http://earth.esa.int/workshops/4th_chris_proba/posters/p09_Vincini.pdf

WANG, Q., ADIKU, S., & TENHUNEN, J. (2005). On the relationship of NDVI with leaf area index in a deciduous forest site, *94*, 244–255. http://doi.org/10.1016/j.rse.2004.10.006

WIEGAND, C. L., & RICHARDSON, A. J. (1982). Comparisons among a new soil index and other two- and four-dimensional vegetation indices. In *Technical papers of the American Society of Photogrammetry : 1982 ACSM-ASP Convention, March 14-20, Denver, Colorado*. Weslaco, Texas: American Society of Photogrammetry.

WILLIAMS JR., R. S., & CARTER, W. D. (1976). *ERTS-1, a new window on our planet* (-ed.). *Professional Paper*. Retrieved from http://pubs.er.usgs.gov/publication/pp929

WIMBERLY, M. C., & REILLY, M. J. (1997). Using Satellite Imagery To Map Fire Severity and Forest Community Change in the Southern Appalachians. *Distribution*, 1–4.

XIAO, Y., ZHAO, W., ZHOU, D., & GONG, H. (2014). Sensitivity Analysis of Vegetation Reflectance to Biochemical and Biophysical Variables at Leaf, Canopy, and Regional Scales. *IEEE Transactions on Geoscience and Remote Sensing*, *52*(7), 4014–4024. http://doi.org/10.1109/TGRS.2013.2278838

YAN, W. Y., MAHENDRARAJAH, P., SHAKER, A., FAISAL, K., LUONG, R., & AL-AHMAD, M. (2014). Analysis of multi-temporal landsat satellite images for monitoring land surface temperature of municipal solid waste disposal sites. *Environmental Monitoring and Assessment*, *186*(12), 8161–8173. http://doi.org/10.1007/s10661-014-3995-z

YANG, C. (2012). A high-resolution airborne four-camera imaging system for agricultural remote sensing. *Computers and Electronics in Agriculture*, *88*, 13–24. http://doi.org/10.1016/j.compag.2012.07.003

ZARCO-TEJADA, P. J., GONZÁLEZ-DUGO, V., WILLIAMS, L. E., SUÁREZ, L., BERNI, J. A. J., GOLDHAMER, D., & FERERES, E. (2013). A PRI-based water stress index combining structural and chlorophyll effects: Assessment using diurnal narrow-band airborne imagery and the CWSI thermal index. *Remote Sensing of Environment*, *138*, 38–50. http://doi.org/10.1016/j.rse.2013.07.024